UNIVERSITÉ DE FRIBOURG
UNIVERSITÄT FREIBURG

UNIT OF GEOGRAPHY
DEPARTMENT OF GEOSCIENCES

Dynamics of the Aget back-creeping push-moraine from 1998 to 2017

Master thesis

By

Julie Wee
Route Principale 167
1628 Vuadens

Supervised by

Prof. Reynald Delaloye

Fribourg, November 2018

Abstract

Glacier forefields within the belt of discontinuous permafrost are complex glaciological systems. Present-day landforms – such as push-moraines – existing in these systems are legacies of the interrelation between glacial and periglacial morphodynamics. The coexistence of glaciers and permafrost suggests that one can influence the other as a function of Holocene climate fluctuations. Knowledge of these interactions remains sparse. This study aims to gather elements contributing to the better understanding of these systems to help fill the knowledge gap.

Electrical resistivity measurements, which were carried out in 1998 to understand the impact of the advance of a small cirque glacier during the Little Ice Age (LIA) on pre-existing frozen debris, provided evidence for the frozen state of an active back-creeping push-moraine, morphologically similar to an active rock glacier. These measurements were repeated in 2017 to assess the evolution of permafrost in the push-moraine and its immediate surroundings. In combination with respectively 20-year and 15-year time series of surface temperature and displacement, data comparison indicates an overall permafrost degradation, which supposedly contributes to the decelerating behaviour of the push-moraine. The decrease of the creep rate of the Aget push-moraine is likely caused by a gradual geometrical readjustment and an advanced state of ice melt in some parts of the push-moraine, and consequently a change in friction at the shear horizon, hindering creep processes. Such observations reflect the influence of ice content on surface dynamics.

Key words: permafrost, push-moraine, glacier forefield, electrical resistivity, kinematics

Acknowledgements

I would like to take the opportunity to thank all the people who made this Master thesis possible.

First of all, my gratitude goes to Reynald Delaloye for encouraging me and trusting me to work on this challenging yet fascinating subject. His valuable insights and experience on permafrost and alpine geomorphology allowed me to learn a lot and to develop a certain enthusiasm and curiosity for exploring the research possibilities in the field of mountain permafrost. I would also like to thank him for his time and for steering me in the right direction whenever I needed it.

To all the field helpers who spent time in Aget – from the ones who set foot there in 1998 to the ones who were there last September: without the priceless work of all of these people who gathered geoelectrical data but also kinematics data and temperature loggers, this Master thesis would not have been possible. A special thanks to Armando Bodeo, Patrick Gabioud, Baptiste Ecoffey, Eliane Dohner, Hanne Hendricx, Alexander Nestler and Nicoletta Trabucchi for helping me out on the field last September. Your presence made this field campaign a successful one.

Furthermore, I would like to thank *Les Joyeux Périglacialistes Alpins* for their insights during our first meeting in Mont-sur-Rolle. Their feedback helped me improve certain aspects of this research.

Special thanks to Victoria and Elise, for the last technicalities of this work.

Last but certainly not least, *je tiens à remercier ma famille pour son soutien sans faille et pour toutes les belles choses que l'on partage*.

Par ces dernières lignes, je prends le temps d'arrêter le temps et de tourner mon regard vers le ciel pour dédier ce travail de Master et ces dernières années de vie à ma maman, à qui je dois tout.

Table of contents

Figures and tables

List of abbreviations

DEM	Digital elevation model
GNSS	Global navigation satellite system
dGPS	Differential global positioning system
ERT	Electrical resistivity tomography
GSB	Grand-Saint-Bernard
GST	Ground surface temperature
LIA	Little Ice Age
LiDAR	Light detection and ranging
MAAT	Mean annual air temperature
MAGST	Mean annual ground surface temperature
VES	Vertical electrical sounding

1 Introduction

This chapter aims to present the general state and context of research (1.1) in which this study inscribes itself. The historical view on the state of research (1.2) and the state of knowledge and definitions (1.3) will bring key notions on glacier-permafrost interrelations, which are essential to the understanding and interpretation of the results obtained within the scope of this research.

1.1 General state and context of research

Climate warming, initiated at the end of the Little Ice Age (LIA) has largely contributed to the alteration of alpine environments. The climatic sensitivity of glaciers reflects changes in climate conditions through time. Hence, their evolution serves as an indicator to assess temperature fluctuations over the past 150 years (Zemp et *al*., 2008). Indeed, since the LIA, a distinctive warming of 0.6 ± 0.2°C has been observed in the northern hemisphere (Zemp, 2006). Since the early 1980s, the warming experienced in the Alps exceeds 1.5°C causing “pronounced effects in the glacial and periglacial belts” (Beniston, 2005; Haeberli and Beniston,1998 : 258). Indeed, the rapid melt of glaciers in has become a symbol of the observed warming climatic trend. “For the Alps, glacier surface area is reported to have decreased from about 4500 km^2 at the end of the LIA in 1850 to 1800 km^2 in 2010, while glacier ice volume has decreased from about 300 km^3 to 80 ± 25 km^3 (Levermann et *al*., 2012 in Hilger, 2017). As a consequence of glacier shrinkage, new high-mountain environments such as glacier forefields have been exposed. Often, **these recently deglaciated areas express intense geomorphological activity**, which is “mainly due to their young age, their glaciation history and the (resulting) high topographic relief” (Otto and Schrott, 2010 in Hilger, 2017). Moreover, recent geomorphic processes constantly work as a response to **paraglacial readjustment and equilibrium reach**.

In the Alps, the shrinkage of small glaciers since the LIA has often occurred in areas located within the belt of discontinuous permafrost, that is above about 2600 ± 200 m.a.s.l. Permafrost conditions and ground ice – interstitial ice or buried ice – are

commonly encountered in the margins of these deglaciated areas, whereas they are often absent in the central zones. Such distribution dominantly reflects both the thermal and mechanical impacts of the LIA glacier advance over **pre-existing permafrost** terrain (Delaloye, 2004; Bosson et *al*., 2014). Indeed, the period that succeeded the last glaciation experienced reasonably small climatic oscillations, which infers that the lower limit of permafrost at the start of the LIA was not differing significantly from the actual one. Therefore, during the LIA, small glaciers advanced in permafrost environments thus partially or completely covering pre-existing frozen sediments (Delaloye, 2004). Such thermal and mechanical interactions between glaciers and permafrost modified the distribution of frozen debris in these glacier forefields.

Glacier forefields within the belt of discontinuous permafrost are complex glaciological systems. Present-day landforms existing in such systems are legacies of the **interrelation between glacial and periglacial morphodynamics**. The coexistence of glaciers and permafrost suggests that one can influence the other as a function of Holocene climate fluctuations (Etzelmüller and Hagen, 2005; Bosson, 2016). Indeed, repeated sequences of glacial and interglacial periods throughout the Holocene (Table 1) have strongly orchestrated the multi-phased geomorphic processes in glacier forefields and contributed to the morphology of present-day glacier forefields in permafrost environments (Scapozza, 2012; Ivy-Ochs et *al.*, 2009; Maisch et *al.*, 2003).

Table 1 : Main glacial and interglacial periods throughout the Holocene in the Swiss Alps (Scapozza, 2012).

Oscillation	Type	Age cal BP
Palü	Glacial	ca. 10’800
Schams	Glacial	ca. 9600 – 8900/8500
Misox	Glacial	ca. 8350 – 6850
Holocene Climatic Optimum	Interglacial	ca. 9500 – 6300
Piora I	Glacial	ca. 6100 – 5700
Piora II	Glacial	ca. 5500 – 4950
Löbben	Glacial	ca. 3750 – 3300
Göschenen I	Glacial	ca. 2900 – 2300
Roman Warm Period	Interglacial	*ca. 200 av. J.-C. – 400 AD*
Göschenen II	Glacial	ca. 1500 – 1150
Medial Warm Period	Interglacial	*ca. 800/900 – 1250/1300 AD*
Little Ice Age	Glacial	*ca. 1350 – 1850/1860 AD*

In the context of this study, the focus is attributed to the LIA (1350-1850/1860 AD), the last important glacial period, as it has a direct influence on today's morphodynamic processes in glacier forefields. Remnants of this cold phase are present in the Aget glacier forefield, where impacts of the Aget glacier on permafrost can be observed through dynamic geomorphic processes.

In general, these recently deglaciated forefields are **dynamic and rapidly changing as a result of intensive paraglacial readjustment** (Bosson et *al*., 2014). The glacier retreat has altered the thermal regime of glacier forefields within permafrost terrain. Indeed, the shrinkage of small glaciers provoked the modification of heat fluxes between the ground surface and the atmosphere. Ground cooling may be an expected outcome of this temperature-based variation, as the isolating effect of the glacier no longer hinders the influence of cold winter temperatures on the ground surface thermal regime (Delaloye, 2004). Nevertheless, the recent 30-year strong increase in air temperature – and consequently of ground surface temperature – could have counterbalanced this cooling effect. In glacier forefields where massive glacier ice was in some cases embedded into the ground during the LIA glacier advance, the thawing and downwasting of this in-depth buried massive glacier ice can lead to the development of subsidence features such as thermokarst, reflecting thermal and mechanical readjustments to glacier retreat. Moreover, purely morphodynamic readjustments such as the back-creeping of formerly displaced frozen sediments (push-moraines) as a response to glacial debuttressing, are likely to occur.

Observations made at the LIA Aget glacier forefield suggest the occurrence of an active back-creeping push-moraine system whose ice content was investigated by means of geoelectrical measurements in 1998 (Devaud, 1999). Ground ice was found in the active zone of the back-creeping push-moraine at larger depths, as well as in its margins, but not elsewhere in the proglacial area. Surface temperature and surface displacement have been monitored in this glacier forefield since 1998 and 2001, respectively.

For the last decade, displacement velocities of the push-moraine have decreased compared to the regional trend: in particular the 2012-16 peak activity was not observed on the push-moraine in contrast with the 2003-04 event (PERMOS, 2016). This behaviour suggests an ongoing and advanced permafrost degradation process. In such a context, **this study aims to gain further insight on the evolution of permafrost from 1998 to 2017 in the Aget glacier forefield**. To fulfil the main

objective of this study, field investigations were led according to three main research questions:

1. **What is the current thermal state of permafrost in some parts of the Aget glacier forefield?** The spatial distribution of permafrost has been the object of a field investigation in 1998 in which electrical resistivity measurements were carried out. To assess the current thermal state of permafrost, both the former vertical electrical soundings (VES) and resistivity mapping (Wenner profiling) were repeated in 2017.

2. **How has permafrost evolved in some parts of the Aget glacier forefield from 1998 to 2017?** To assess the evolution of permafrost in a context of changing climate, a comparative analysis of the results of the 1998 and 2017 geoelectrical field investigations has been made. Furthermore, the analysis of surface elevation changes provides insight concerning the processes involved in the evolution of permafrost. An integrative analysis between electrical resistivity measurements and surface displacement measurements is used in this study.

3. **What are the consequences of the evolution of permafrost on the dynamics of the Aget push-moraine?** Results from the current state of permafrost allow the consideration of processes involved in the evolution of the dynamics of the Aget push-moraine. Surface displacement measurements will allow the assessment of the occurrence of a shift in geomorphic processes.

1.2 Historical view on the state of research

Historically, research on glaciers and permafrost has evolved along separate lines, and processes and landforms related to glaciers and permafrost are often treated separately, despite their common belonging to the cryosphere. Glaciers and permafrost often co-exist, consequently having a potential for interaction. Knowledge of these interactions is fundamental for a better understanding of the processes involved when both glacial and periglacial spheres converge and influence one another (Haeberli, 2005; Etzelmüller and Hagen, 2005; Berthling et *al.*, 2013).

The early literature that discussed glacier-permafrost interactions (Haeberli, 1979, 1981) provided the first key elements for the understanding of the occurrences of temperate/polythermal/cold glaciers and sub-/peri- glacial permafrost as functions of topography and continentality of the climate. In regions with dry climatic conditions, the inferior limit of glacier can coincide with the inferior limit of discontinuous permafrost. Hence, “permafrost is intimately related to polythermal and cold glaciers in regions with dry continental-type climatic conditions” (Haeberli et *al*., 2013: 156; Figure 1).

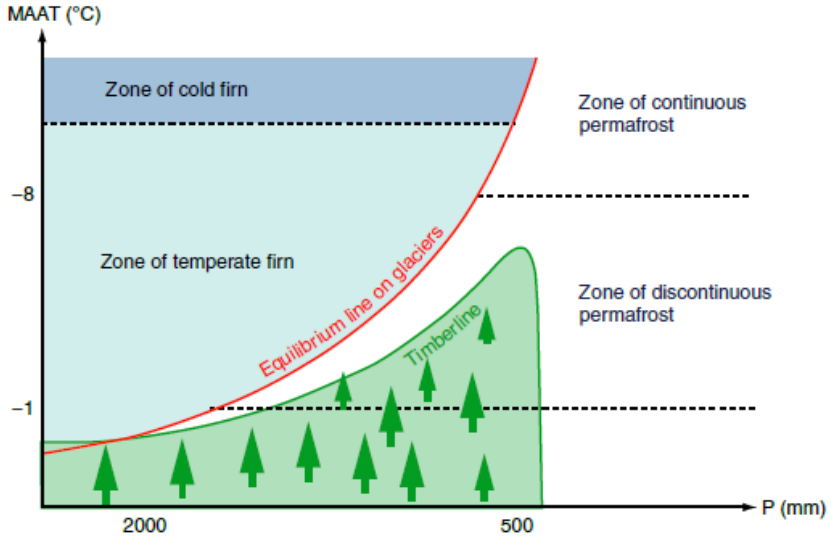

Figure 1: Cryosphere model that illustrates the spatial relations between glaciers and permafrost as a function of mean annual air temperature and annual precipitation (Haeberli et *al*., 2013).

Over the recent decades, interest for research in the domain of glacier-permafrost interactions has grown rapidly. Existing studies have mainly focused on investigating thermal conditions and permafrost occurrences in recently exposed glacier forefields located within the belt of discontinuous permafrost by using geomorphological mapping, ground surface measurements and geophysical soundings (Evin, 1992; Kneisel, 1998; Delaloye and Devaud, 2000; Delaloye, 2004; Lugon et *al*., 2004; Reynard et *al*., 2003). These methods were used in order to gain further insight on glacier-permafrost interrelations and on the dynamics of these complex systems. New insights on the process of creeping mountain permafrost in glacier forefields resulted from the combination of measured surface displacements with geophysical prospections of the subsurface, and these insights enabled the extension of earlier studies (Kneisel and Kääb, 2007; Lambiel and Delaloye, 2004). However, detailed

analyses of the evolution of the dynamics of post-LIA glacier-permafrost systems remain sparse, as “complete temporal and spatial analysis of proglacial areas in mountainous permafrost environment remains a challenging task” (Bosson et *al*., 2014: 667).

1.3 State of knowledge and definitions

This section explores glacier-permafrost interactions in scientific literature. Glaciers and permafrost have traditionally been studied as two separate entities. Indeed, the processes related to these interactions are rarely recognised and studied as a whole, as they sit astride the frontier of two historically distinct disciplines. However, in high mountain glacier systems glaciers and permafrost can sometimes co-exist. The intimate interrelation between glacial and periglacial systems affects the geomorphological processes taking place in these environments sitting at the boundary of one another. The distribution of permafrost within these glacier systems is a key element for understanding glacial and periglacial (geomorphologic) processes. Based on the existing literature, this state of knowledge tries to give the most complete overview of glacier – permafrost interactions.

1.3.1 Glaciers in permafrost environments

> *A permafrost environment will influence the glacier indirectly by providing cold and dry conditions that dictate its mass balance, thermal regime, glacial hydrology, and internal creep. Permafrost also influences glaciers directly by providing subglacial and lateral boundary conditions with respect to thermal and material properties that affect subglacial sliding and deformation, erosion and deposition, and associated landforms.*
>
> (Berthling et *al*., 2013: 488)

Glaciers confined within permafrost environments form in areas where specific ranges of temperatures and precipitations only allow the development of relatively small glaciers (Bosson, 2016). Wet maritime climate conditions induce significant amounts of snow, contributing to the development of glaciers bellow the periglacial belt (Pfeffer et *al*., 2014), whereas extremely dry conditions in continental climates hinder the development of glaciers in cold mountainous environments (Azócar and Brenning, 2010 in Bosson, 2016).

Permafrost is commonly defined in terms of thermal conditions, namely material that is continuously at or below 0°C for at least two consecutive years (Van Everdingen, 1989 in Berthling et *al*., 2013). The spatial distribution of mountain permafrost is very complex and heterogeneous, as the spatial variability of ground temperatures is especially marked in high mountain environments due to the complexity of the micro-relief and ground characteristics (Bosson, 2016), but also to the impact of glaciers on permafrost.

Most glaciers present in permafrost environments are either cold-based or polythermal (Etzelmüller and Hagen, 2005), as the temperature of glacier ice depends on the energy exchanges with climate and Earth surface (Cuffey and Paterson, 2010). Etzelmüller and Hagen (2005) identified three main spatial configurations of thermal regime for these glaciers: (1) In high altitude or cold and dry climatic conditions, all the ice is likely to be below the temperature of the pressure melting point, making the glacier cold (Figure 2a). Whereas polythermal glaciers occur in warmer and wetter area where summer melting occurs, therefore (2) the basal layer is temperate (temperature at the pressure melting point) due to latent heat release by meltwater refreezing (Figure 2b-c), or (3) the cold ice is present in the marginal glacier zones, while the central part is temperate (Figure 2d-e). Given the spatial distribution of permafrost in the LIA Aget glacier forefield, the glacier's thermal configuration is presumed to be of type d (cf. Figure 2). Indeed, permafrost occurs in the margins of the forefield and not in its central zone.

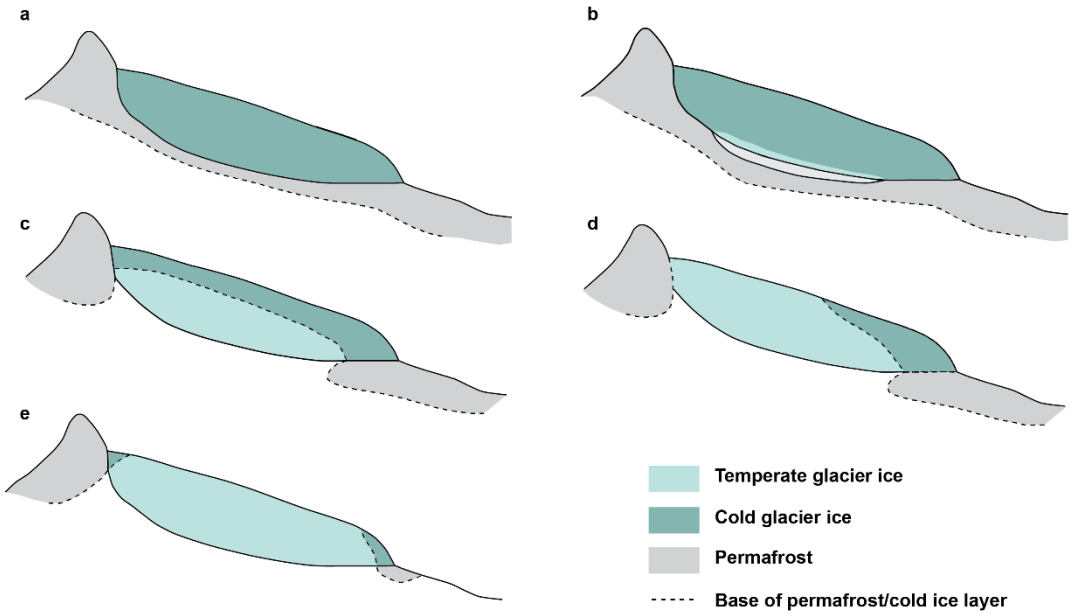

Figure 2: Schematic longitudinal profiles of glaciers showing the distinct thermal regimes that possibly occur under permafrost conditions. In the (a) situation, the glacier is entirely cold. For (b-c), temperate ice occurs at the glacier-ground interface, and for (d-e), cold ice is located at the margins of the glacier and temperate ice at its central part (modified after Etzelmüller and Hagen, 2005).

The thermal regime of a glacier is influenced by many different factors such as: the spatial and temporal variations of the snow cover thickness, the glacier thickness, the energy fluxes related to water circulation and phase changes, as well as geothermal heat fluxes (Cuffey and Paterson, 2010; Gilbert et *al*., 2012). In polythermal glaciers, one of the driving process behind the occurrence of temperate ice in the accumulation zone is the release of latent heat, caused by the refreezing of percolating meltwater in firn areas. Conversely, the presence of cold ice in the marginal zones is partly due to the more efficient cooling of the ice by air temperature in winter, as the snow covers the ablation zone sets on later in the season and is often thinner than in the accumulation zone thus diminishing its isolating effect. Moreover, englacial meltwater circulations, which contribute to the warming of ice are rare or absent in glacier margins (Cuffey and Paterson, 2010; Gilbert et *al*., 2012).

The thermal regime of a glacier has a significant influence on its mechanical and hydrological properties (Cuffey and Paterson, 2010). Hydrological processes are present in temperate ice, whereas they are rare or absent in cold ice, as the latter acts as an impermeable layer. The presence of water within a glacier has an important effect on the deformation properties of the ice and enhances the glacier's dynamics

(basal sliding). Conversely, cold ice is less subject to internal deformation as the cooling of ice increases its viscosity (Cuffey and Paterson, 2010).

1.3.2 Influences of glaciers in permafrost environments

Glacier forefields “illustrate the role of Holocene glaciers in the production, the transfer, the deposition and the reworking of sediments” which contribute to their development (Bosson, 2016: 66). Permafrost related landforms in proglacial areas are thereby inherited from the numerous glacial and interglacial variations throughout the Holocene. Present-day spatial distribution of permafrost and associated landforms in glacier forefields dominantly reflects the thermal and mechanical impacts of the most recent glaciation.

Sediment accumulations

The thermal structure and pressure of glaciers in developing permafrost environments enables the modification of the spatial distribution of pre-existing frozen landforms as well as their thermal state. Present-day permafrost-related landforms have been strongly influenced by their exposure to different glacial and interglacial fluctuations (Maisch et *al*., 2003; Ivy-Ochs et *al*., 2009). Glacier fluctuations at varying rates over time created conditions favourable to the continuous production of sediments within the glacier catchment. The sediment accumulated in glacier forefields within the belt of discontinuous permafrost are of multi-phased and complex origin. Indeed, they are the heritage of the sediment production and glacier fluctuations of the Holocene (Maisch et *al*., 2003; Delaloye, 2004; Bosson, 2016). However, the actual thermal state of sediment accumulations and their distribution within LIA glacier forefields is essentially a legacy of the last significant cold period: the LIA itself (Bosson, 2016).

Thermal and mechanical influences of glacier on permafrost

During the LIA, the advance of glaciers induced a thermal buffer effect between the atmosphere and the ground surface. Despite the cooling of the atmosphere during this cold period, warming of the overridden sub-glacial permafrost system occurred. The ice layer had both an insulating and warming effect due to the potential advective heat transport of ice masses and meltwater. Moreover, a temperate-based glacier provokes the warming of the underlying frozen layer due to the release of latent heat when

meltwater refreezes. However, a decrease in the ground temperature gradient slows the thermal response of permafrost to the presence of a glacier. Therefore, the longevity of permafrost can persevere even under a temperate-based glacier (Etzelmüller and Hagen, 2005).

Often present in the marginal zones of polythermal glaciers, cold ice allows the preservation of permafrost. The marginal distribution of the latter reflects the mechanical influence of advancing polythermal glacier on frozen terrain. Instead of overriding the frozen sediments, the cold ice found in the glacier's margins binds with the frozen material and the pressure exerted by the advancing glacier displaces the latter towards the margins of glacier forefields, consequently building push-moraines.

As a consequence of glacier shrinkage initiated at the end of the LIA, the thermal evolution of the subsurface becomes directly constrained by the heat transfers between the ground surface and the atmosphere. In response to these energy exchanges, the subsurface reaches a new thermal equilibrium. In zones deprived of permafrost, ground cooling may be expected to occur. Moreover, the cold glacier snouts would have allowed the formation of permafrost at the glacier's margins during its retreat (Reynard et al., 2003; Kneisel, 2003; Etzelmüller and Hagen, 2005). However, in a warming context, permafrost degradation is more likely than permafrost aggradation. Furthermore, the retreat of glaciers triggered morphodynamic readjustments of formerly confined frozen landforms, such as the back-creeping of push-moraines (Delaloye, 2004; Bosson et *al*., 2014).

1.3.3 Geomorphological indicators

Field observations allowed the identification of two main geomorphological indicators, which provide elements of answer regarding the influence of small LIA glaciers on frozen debris, and consequently the build-up of the Aget push-moraine system. The spatial distribution of these geomorphological indicators within proglacial areas allow the coherent interpretation of the glacier-permafrost related processes occurring in such environments.

Fluted moraines

Fluted moraines can be described as a set of low ridges formed on the basal moraine surface, parallel to the glacier's flow direction (Hoppe and Schytt, 1953; Figure 3; Figure 14). The formation of fluted moraines is essentially due to the compression exerted on a water-saturated basal moraine following a basal detachment of the glacier when surpassing an obstacle (large boulder, outcrop of bedrock) (Delaloye, 2004). The presence of such patterns indicate that "**the glacier rested on water-saturated sediments and, thus, was temperate at the base**" (Haeberli, 1979: 44). At a smaller scale, glacier stripes on boulders also indicate the glacier's thermal state and flow direction. Furthermore, the visibility of these stripes imply that the glacier was bare of sediments.

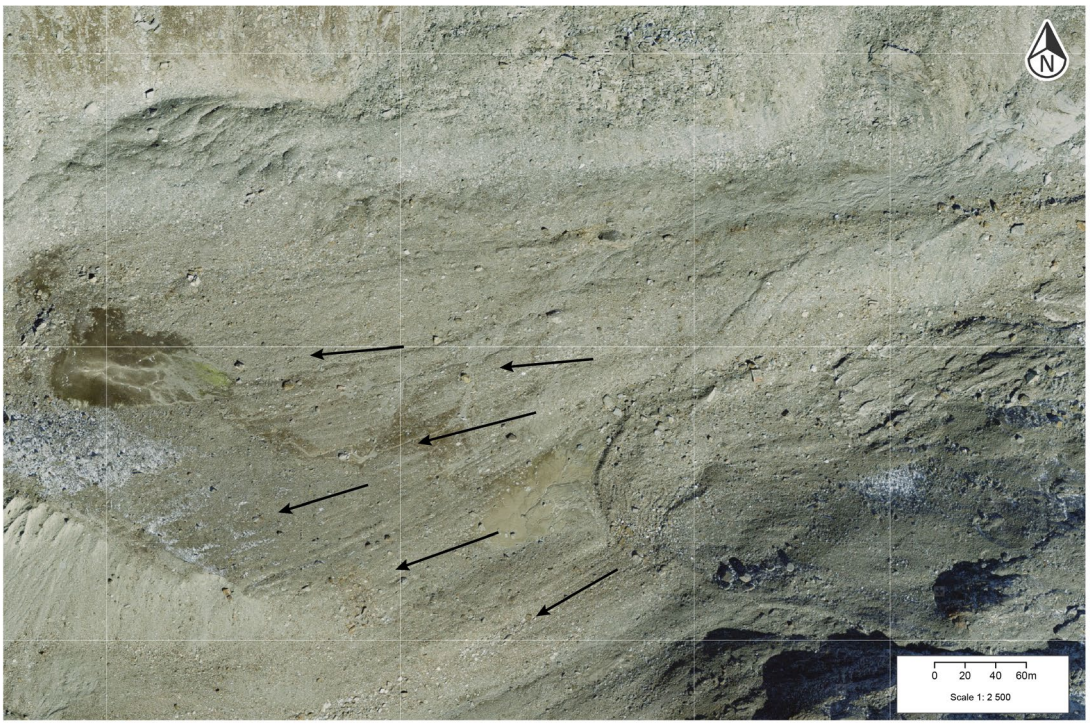

Figure 3: Example of fluted moraines observed at the Gruben glacier forefield (Saas valley, VS). The arrows indicate the glacier's flow direction, parallel to the fluted moraines pattern (basemap Swisstopo).

Push-moraines

Push-moraines are glacio-tectonically deformed and displaced pre-existing frozen sediments in front or at the side of an advancing glacier, which is frozen to its bed (at least at its margins) (Haeberli, 1979; Figure 4). Their formation is essentially due to the shearing of the frozen material caused by the pressure exerted by the glacier (Delaloye, 2004). Push-moraines are considered as “morphological expressions of the deformation of permafrost” and reveal the interactions between glaciers and permafrost in proglacial areas (Haeberli, 1979: 43). Moreover, in glacier forefields within the belt of discontinuous permafrost, their formation suggests that a transition from a rock glacier to a push-moraine “may exist in cases where a glacier was in contact with a rock glacier during Holocene glacier advances” (Haeberli, 1979: 46).

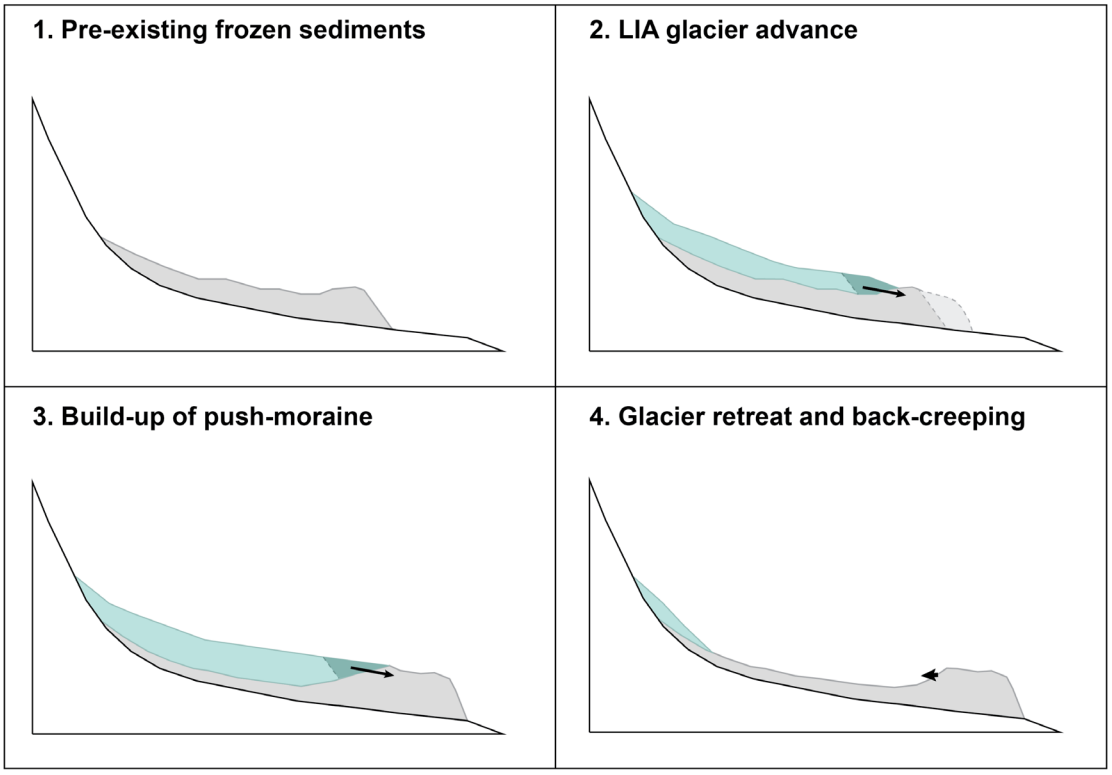

Figure 4: Schematic description of the formation of a push-moraine. Pre-existing frozen sediments (1) are displaced by the advance of the LIA glacier (2-3). Initiation of a back-creeping process after the glacier retreat (4). Dark blue = cold ice; light blue = temperate ice.

Push-moraines are complex systems (Figure 5) whose characterization is determined by:

1. **Their position within a glacier forefield system**. A push-moraine may or may not be overridden by a glacier. Internal push-moraine systems are found in the internal margins of a glacier forefield, suggesting the glacier's superimposition during its advance (as the extent is delimited by an external moraine and not by the push-moraine). Conversely, external push-moraines delimit the maximal extent of a glacier forefield, which implies that the body of frozen sediments was not covered by the glacier and only transported towards its margins.

2. **Their position in relation to the glacier**. Frontal push-moraines are built from the pressure exerted by the glacier's front onto a body of frozen material, whereas lateral push-moraines (Figure 6) are not only built by the glacier's pressure, but are also an expression of the lateral shearing of frozen sediments.

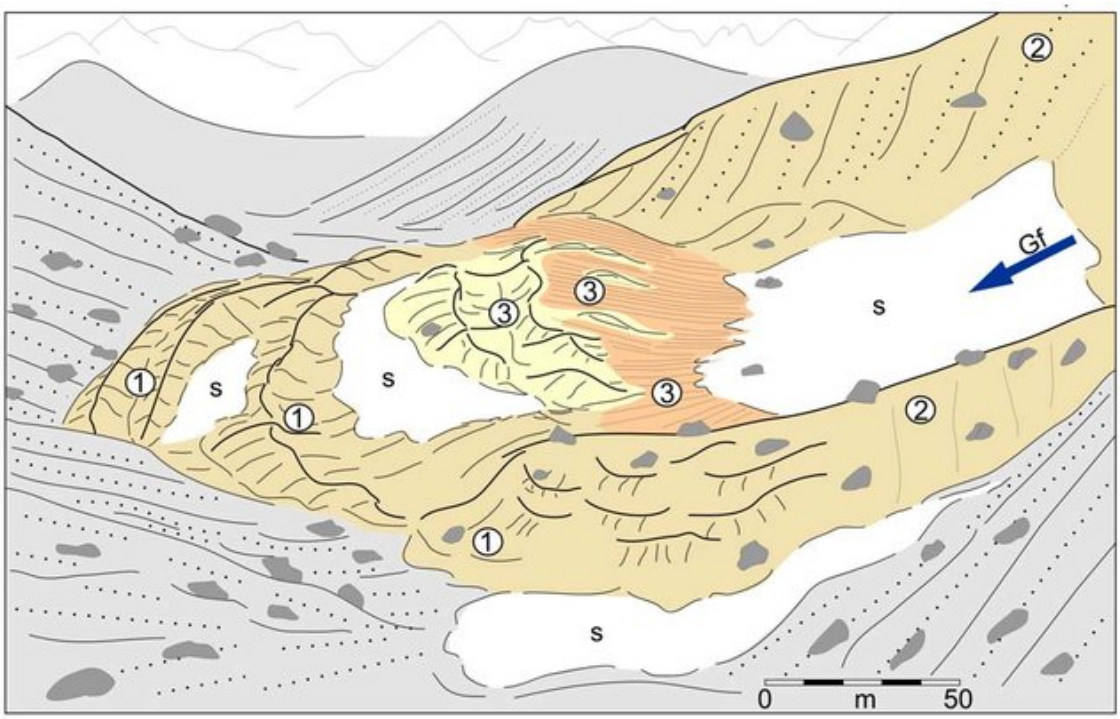

Figure 5: Illustration of the complexity of a push-moraine system. External frontal moraines (1) delimit the glacier's maximal extent. Lateral push-moraines indicate the lateral shearing of pre-existing frozen sediments (2). Internal push-moraines show that the body of frozen sediments was overridden by the glacier during its advance (3) (Serrano and Martín-Moreno, 2018).

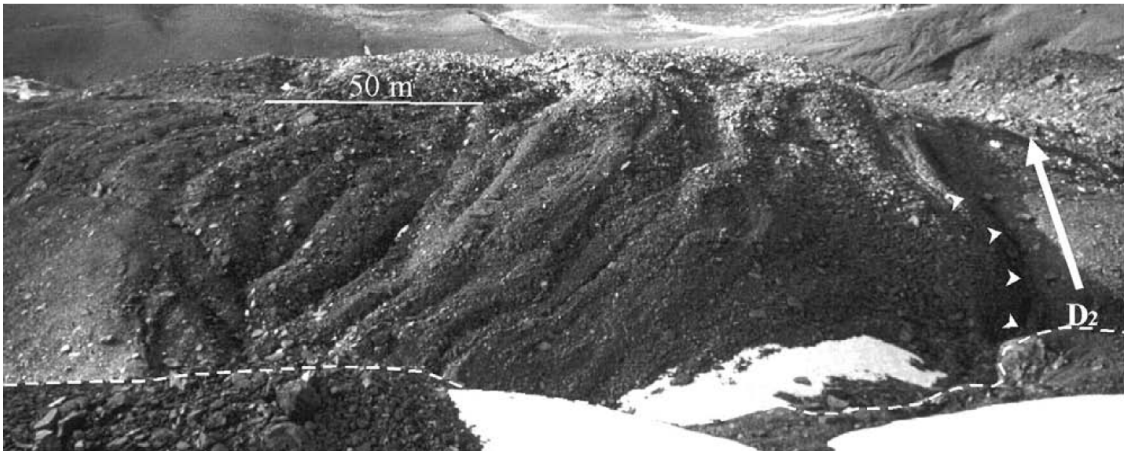

Figure 6: Lateral push-moraine system of the Becs-de-Bosson glacier-rock glacier complex. The arrowheads indicate the push-moraine's back-creep flow direction towards the depression (D2) (Delaloye, 2004).

During their development, push-moraines are often displaced towards a counter-slope. The glacier's retreat generates a debuttressing process, which causes a slope instability. To counterbalance this disequilibrium, the back-creeping of push-moraines is a common kinematic (and geometrical) response to glacier retreat, which also attests the frozen state of the landform. This paraglacial readjustment process often affects the internal flanks of lateral push-moraines (Delaloye, 2004). The Gruben push-moraine's kinematic behaviour illustrates relatively well this counter flow mechanism (Figure 7).

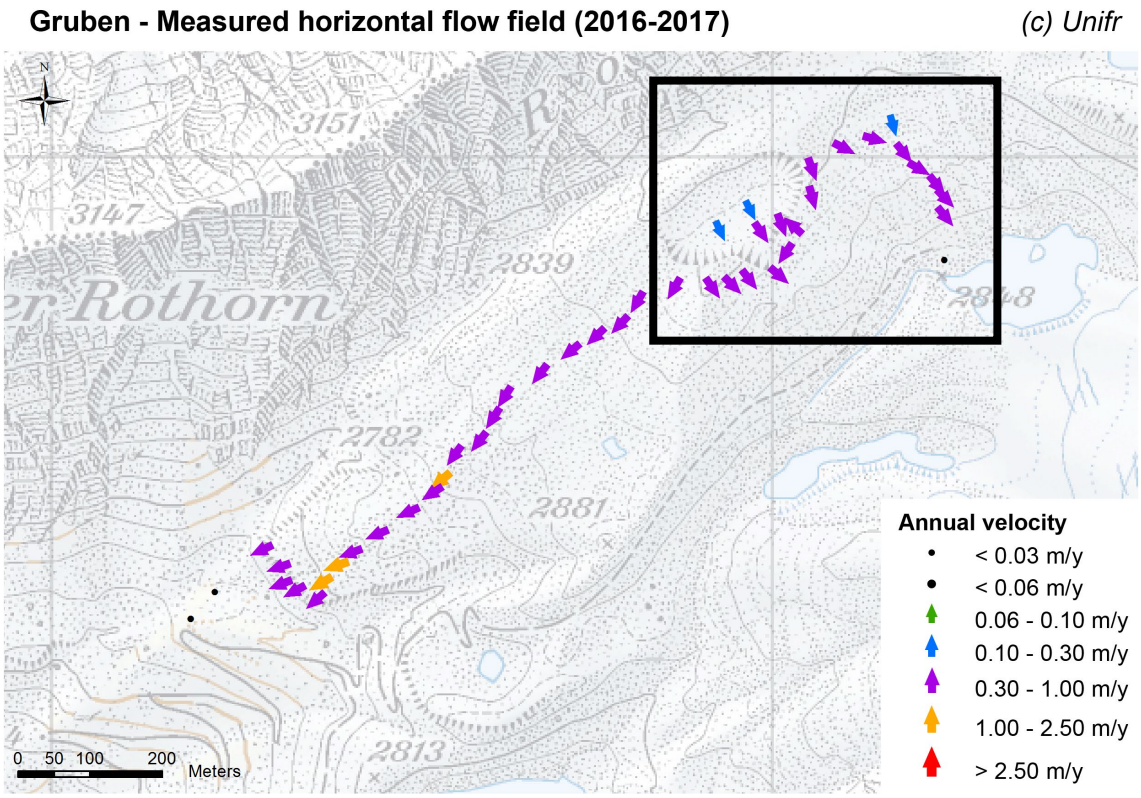

Figure 7: Gruben rock glacier and push-moraine complex where a counter flow (or back-creeping) mechanism can be observed (UniFR. 2017).

1.4 Synthesis and research objectives

The research objectives of this contribution are presented and synthetized in Figure 8. As shown in the previous sections, the development of knowledge on glacier-permafrost interactions is relatively recent as glaciers and permafrost were for a long time treated separately. An intensification of studies on this particular field of research has emerged in the past decades, however knowledge still remains sparse. Indeed, the complexity of the these systems sitting astride the glacial, paraglacial and periglacial frontier lead to confusions regarding the definition of the processes and dynamics involved in these systems. Moreover, insights on the response of these systems to the current climate warming are still lacking. Indeed, the assessment of the spatio-temporal evolution of permafrost in proglacial systems would allow a better understanding of their geomorphic activity.

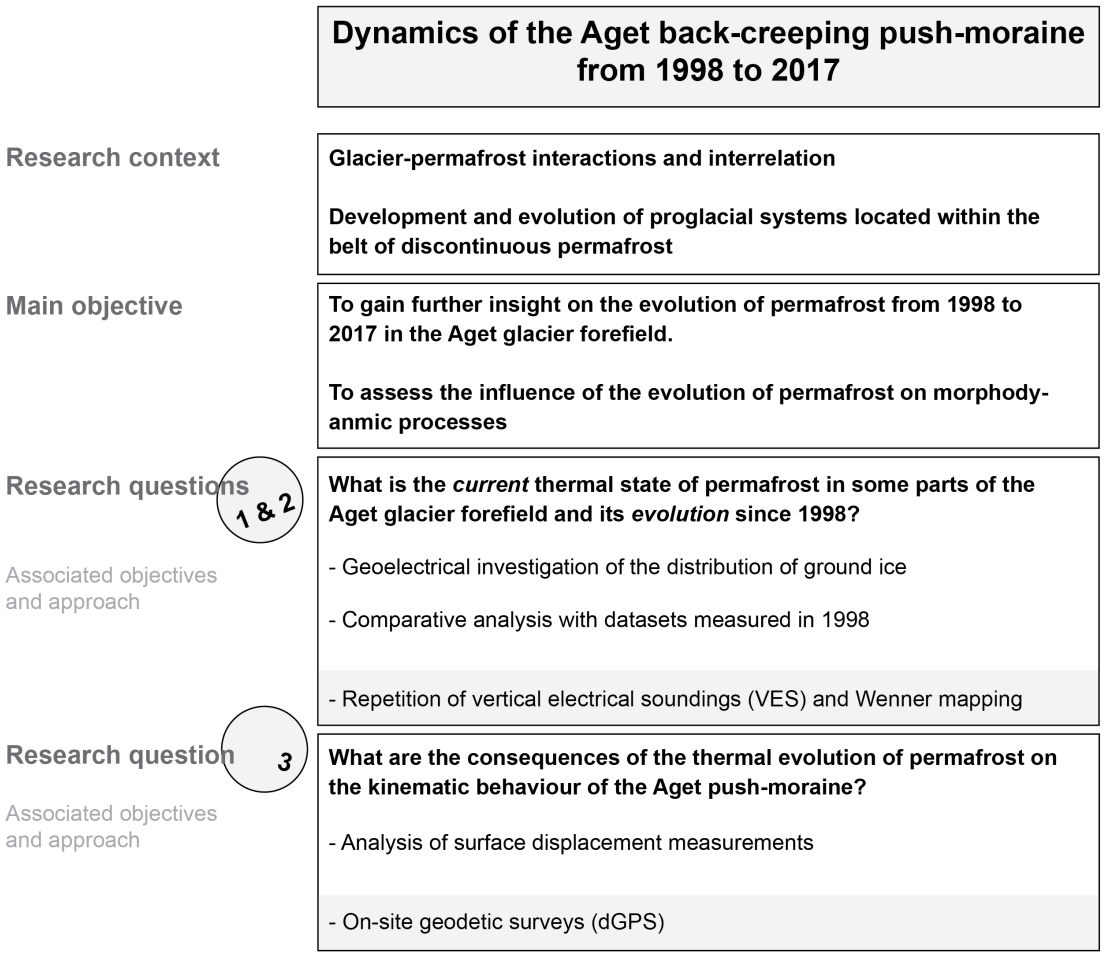

Figure 8: Synthesis of the research objectives.

2 Site description

The general situation (2.1) of the study site will be followed by a description of the key elements (2.2 and 2.3) that compose the Aget glacier forefield. The kinematic (2.4) and thermal state (2.5) of the Aget glacier forefield will be presented along with the climatic setting (2.6) in which this study site lies.

2.1 General situation

The Aget push-moraine complex (2760-2920 m.a.s.l.) is located in the south-western flank of the LIA Aget glacier forefield (2 584 620 / 1 095 225), in the Bagnes valley at about 10 km north of the Combin massif in the Valais Alps (Figure 9). Grand-Aget (3133 m.a.s.l.) and Mont Rogneux (3084 m.a.s.l.) summits enclose the uppermost zone of the study area, which extends down to a small proglacial lake (Goli d'Aget at 2760 m.a.s.l.) situated close but upstream of the LIA frontal moraine of the Aget glacier.

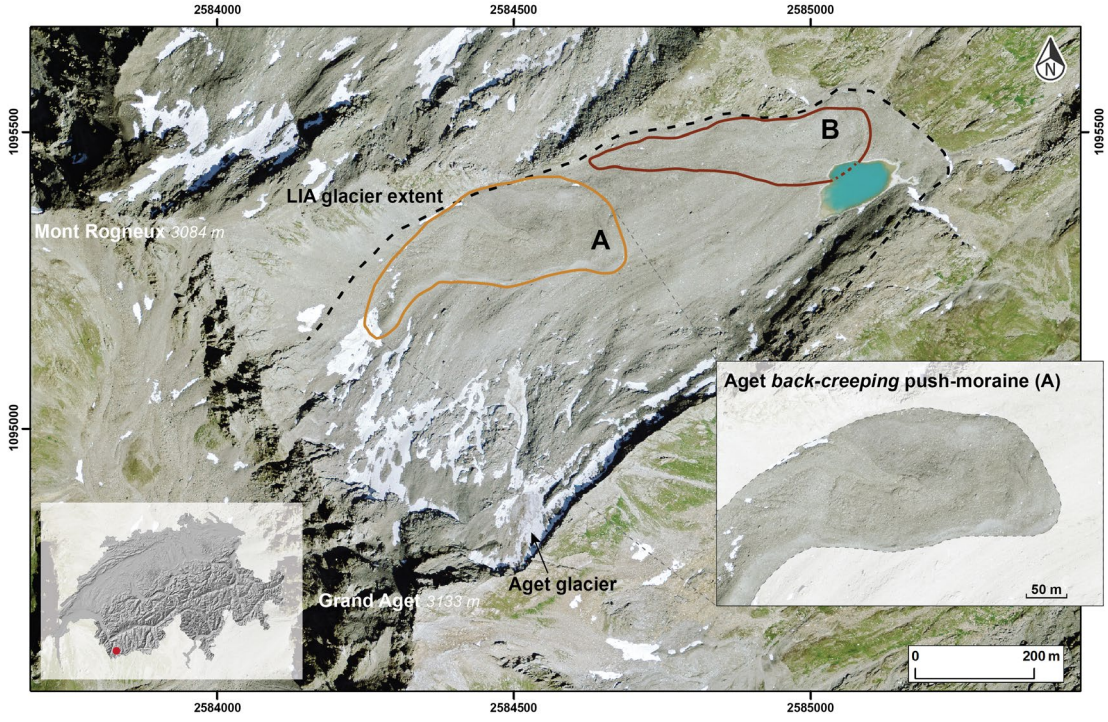

Figure 9: Location of the Aget push-moraine complex within the LIA glacier forefield. The active back-creeping push-moraine A (orange) and the non-active push-moraine B (red) (basemap Swisstopo).

The study area lies within the belt of the discontinuous permafrost (Devaud, 1999; Reynard et *al*., 2003; Delaloye, 2004). However, according to the map of potential permafrost distribution (empirical model) (Figure 10) the location of the Aget push-moraine systems (A and B) coincides with a non-favourable permafrost area (south facing), making permafrost degradation likely to occur independently of the current climate evolution.

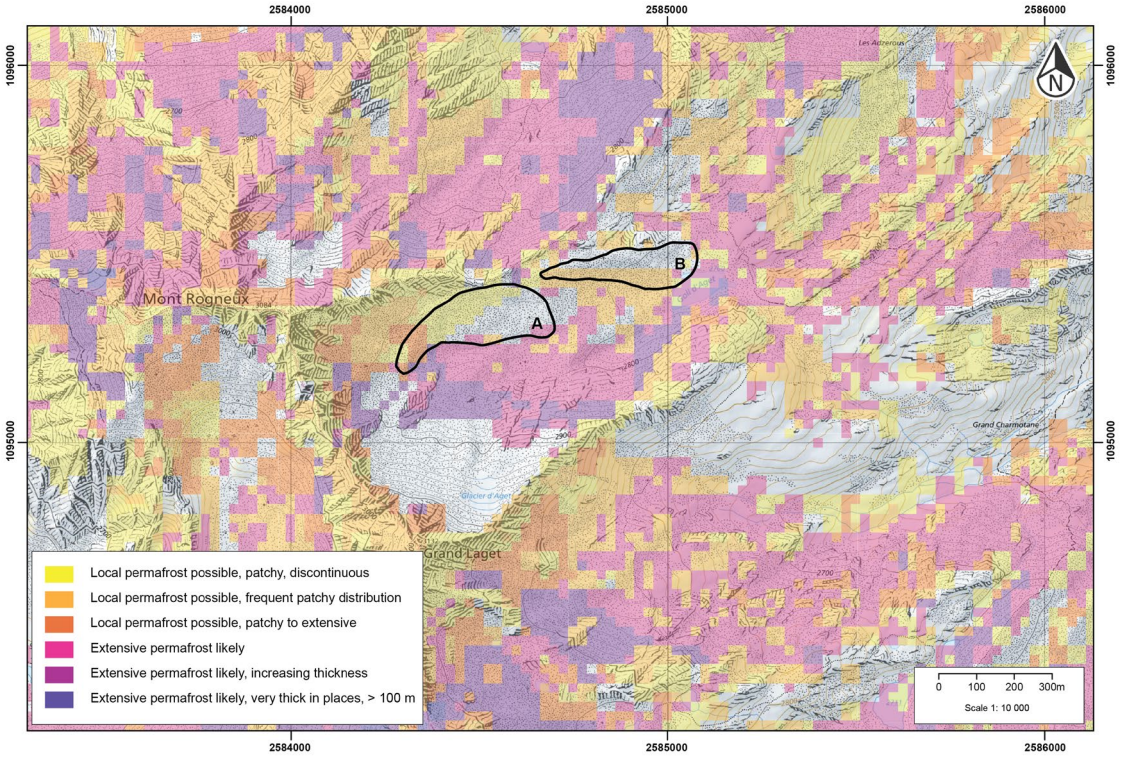

Figure 10: Map of potential permafrost distribution (Federal Office for the Environment – FOEN). This map depicts the complex and discontinuous spatial distribution of permafrost in mountainous alpine environments and highlights the location of the Aget push-moraines (A and B) (modified after Swisstopo).

2.2 Aget glacier

North-east of the Grand-Aget lies the feeble remains of the Aget glacier. To answer Devaud's (1999) question about the glacier's lifespan: the Aget glacier still subsists, but for *how long*? Its lifespan is expected to arrive soon at an end. According to Huss and Fischer (2016), the Aget glacier will disappear by 2030. Since 1999, it has lost about 90% of its surface area: from about 8 ha to 0.08 ha (Figure 11). During its LIA maximal extent, the glacier's surface area reached about 90 ha.

Figure 11: Surface change of the Aget glacier from 1999 to 2017. The white dashed line delimits the glacier's extent in 2017.

The direction of the glacier's flow is reflected by fluted moraines (Figure 12), whose presence indicate that the glacier's base was temperate and was essentially bare of debris. Indeed, the sedimentary deposits that occupy the thalweg originate from the erosion of the surrounding rock walls over several thousands of years. An important debris production during interglacial periods allowed the development of frozen landforms. It is presumed that prior to the LIA, a rock glacier (or a frozen landform) was present in the north-western flank of the Aget glacier forefield, and was then displaced (bulldozed and overridden) over 250-300 meters by the Aget glacier during its LIA advance, building-up a push-moraine.

2.3 Aget push-moraine complex

The morphology of the orographic left side of the Aget glacier forefield suggests the occurrence of a push-moraine complex (Figure 12). Geoelectrical measurement carried out in 1998 (Devaud, 1999) allowed the distinction of two separate systems. In the north-western part of the forefield, ground ice was found in the active (back-creeping) zone at larger depth of **push-moraine A** (Figure 13), as well as in its margins, which testifies to the existence of a displaced pre-existing frozen landform. Whereas, in the north-eastern part of the forefield, resistivity values revealed the absence of ground ice, which suggest the presence of a relict push-moraine (**push-moraine B**).

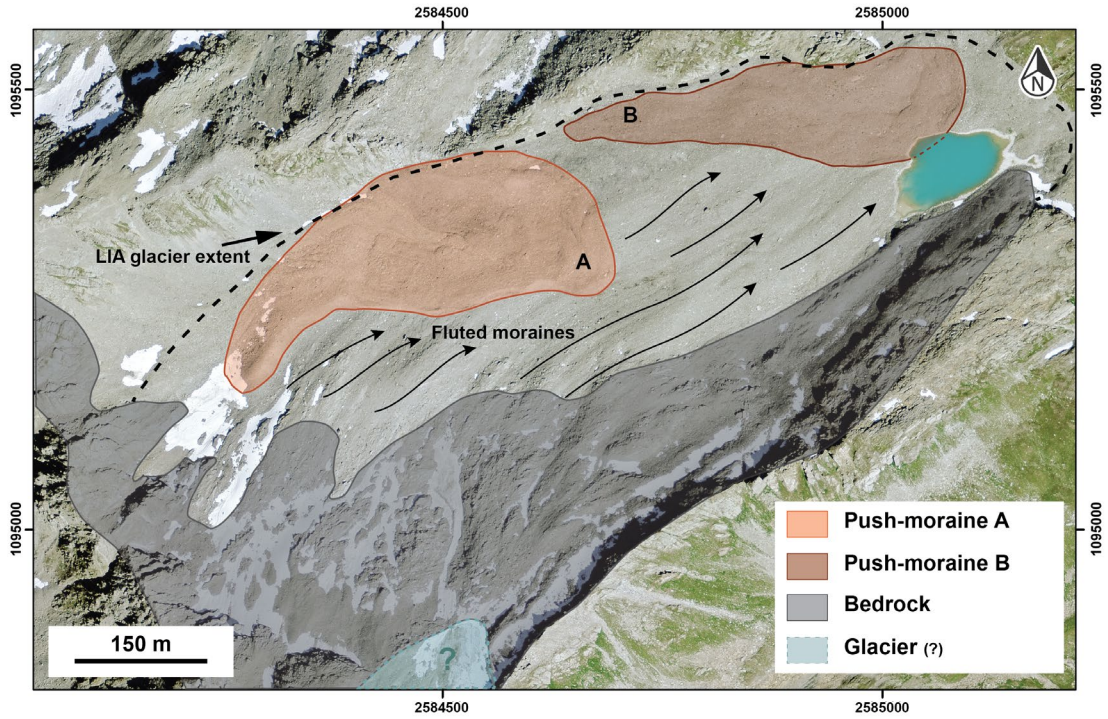

Figure 12: Aget push-moraine complex. The fluted moraines (arrows) indicate the glacier's flow direction (basemap Swisstopo).

Figure 13: Aget back-creeping push-moraine A (Google Earth).

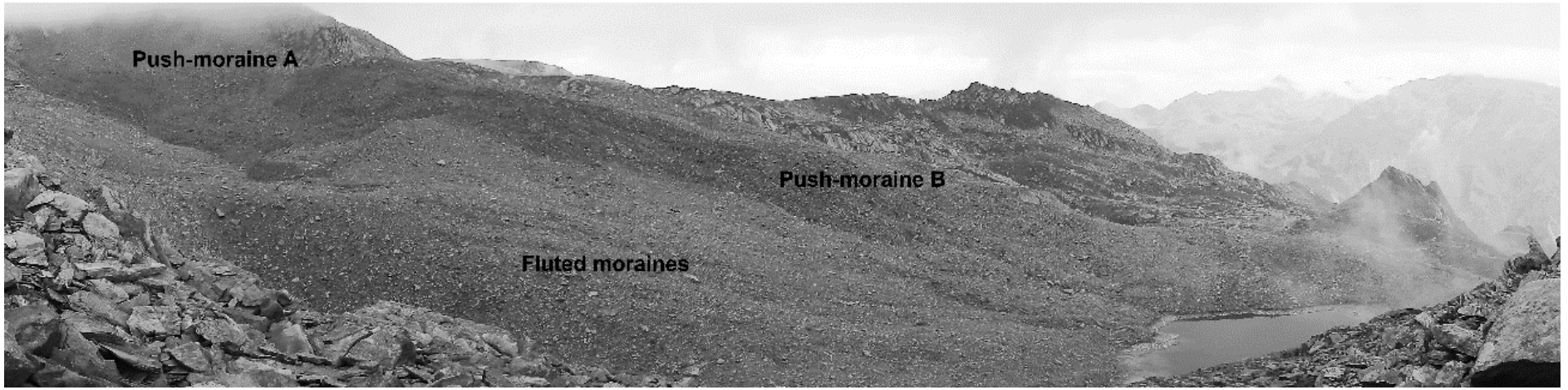

Figure 14: Panoramic photograph of the Aget glacier forefield where the different geomorphological features are illustrated (September 16, 2018).

2.4 Kinematics of the Aget back-creeping push-moraine

Surface displacements have been monitored since 2001 on the Aget push-moraine A. For the last decade, displacement velocities of the Aget back-creeping push-moraine have decreased compared to the regional trend: in particular the 2012-16 peak activity was not observed on the push-moraine in contrast with the 2003-04 event (PERMOS, 2016, Figure 15). This behavioural change can be explained either by a geometrical response or by an ongoing permafrost degradation process.

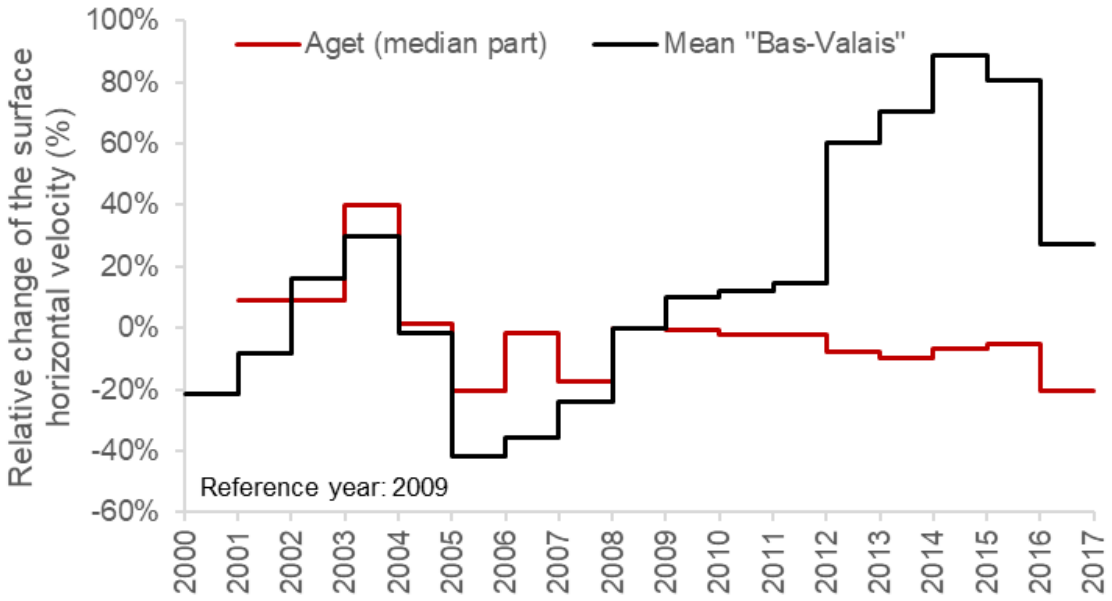

Figure 15: Relative change of the annual horizontal surface velocity (%) of the Aget push-moraine in comparison to the regional mean (mean Bas-Valais) behaviour of active rock glaciers (n=3-8 depending on year) (data from PERMOS).

2.5 Ground surface temperature

Ground surface temperatures (GST) at seven locations (Figure 16) in the Aget glacier forefield have been monitored since 1998. From these measurements, the mean annual ground surface temperature (MAGST), the ground freezing index (GFI) and ground thawing index (GTI), and the winter equilibrium temperature (WEqT) were calculated (Delaloye, 2004). These parameters provide "interesting and complementary information on the thermal state and on the possible occurrence of ice near the surface" (Bosson, 2016: 84).

> *Negative GST values indicate the influence of cold ground thermal regime and/or cold topoclimatic conditions. In this way, ground ice is more likely to exist and to persist under the coldest GST means. GFI estimates the "amount of cold" stored in the ground during the frozen days. Finally, WEqT is reached when a significant snow cover isolates the ground from atmospheric influence and temperature tends to an equilibrium controlled by the heat transfer from the upper ground layers. Cold WeqT values (some degree below 0°C) possibly indicate an influence of ground ice or permafrost conditions in the ground.*
>
> (Bosson, 2016: 84)

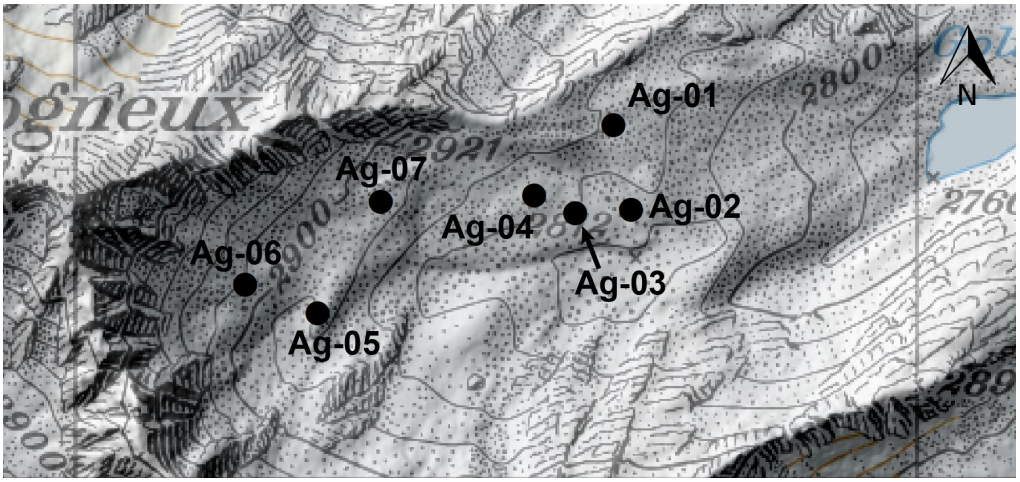

Figure 16: Position of the seven ground surface temperature measuring stations (basemap Swisstopo).

Over the past 20 years, the MAGST measured at Aget was +0.60 °C (Figure 17; Figure 18), increasing by 0.14°C per decade (Figure 19), essentially due to warmer summers. In comparison to other sites located in the Bas-Valais region, the MAGST measured at Aget is high, yet not exceptionally warm (Figure 18). The high MAGST likely contributes to the thermal degradation of ground ice in the Aget glacier forefield.

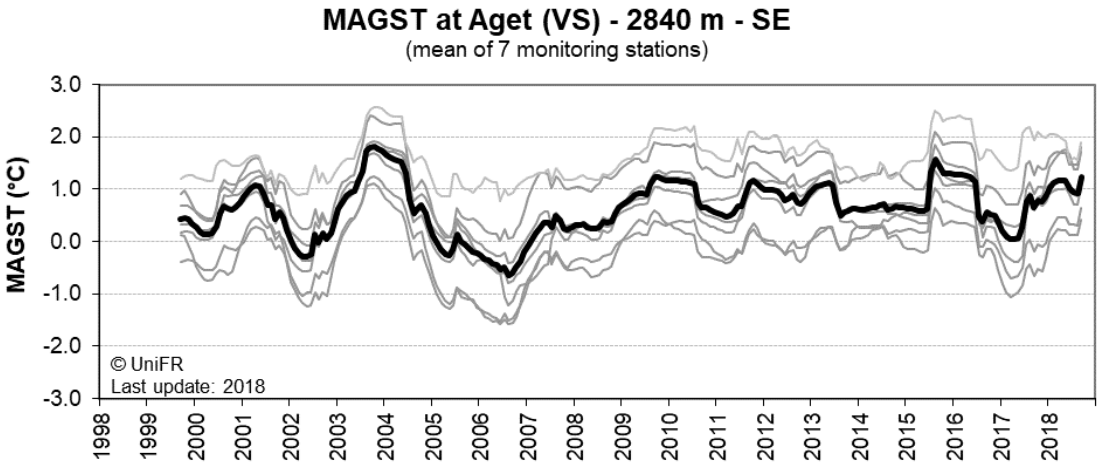

Figure 17: MAGST at Aget based on 7 monitoring stations (location cf. Figure 16).

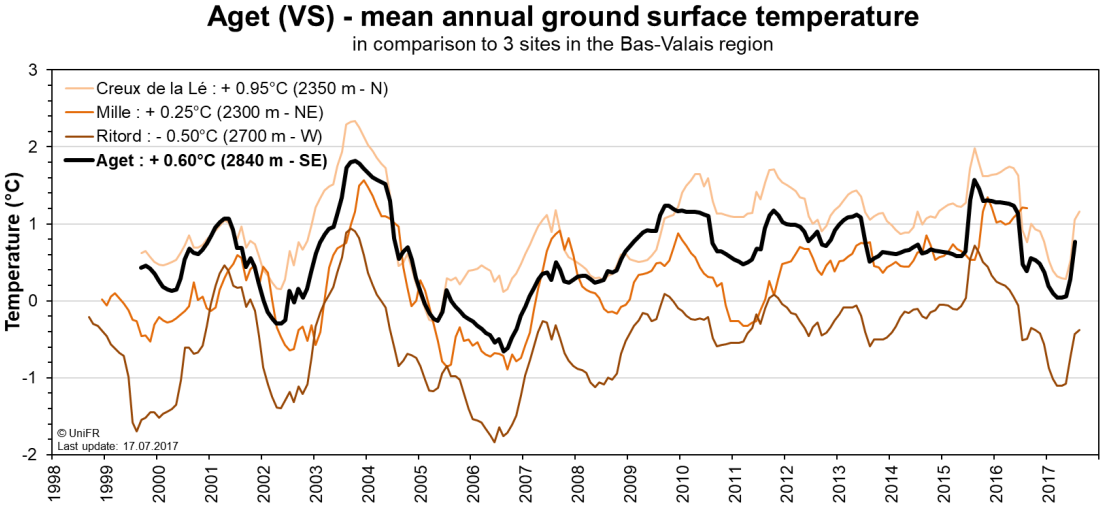

Figure 18: Mean annual ground surface temperature (MAGST) at Aget (n=7) in comparison to three sites in the Bas-Valais region: Ritord (n=15), Mille (n=10) and Creux de la Lé (n=7) (UniFR).

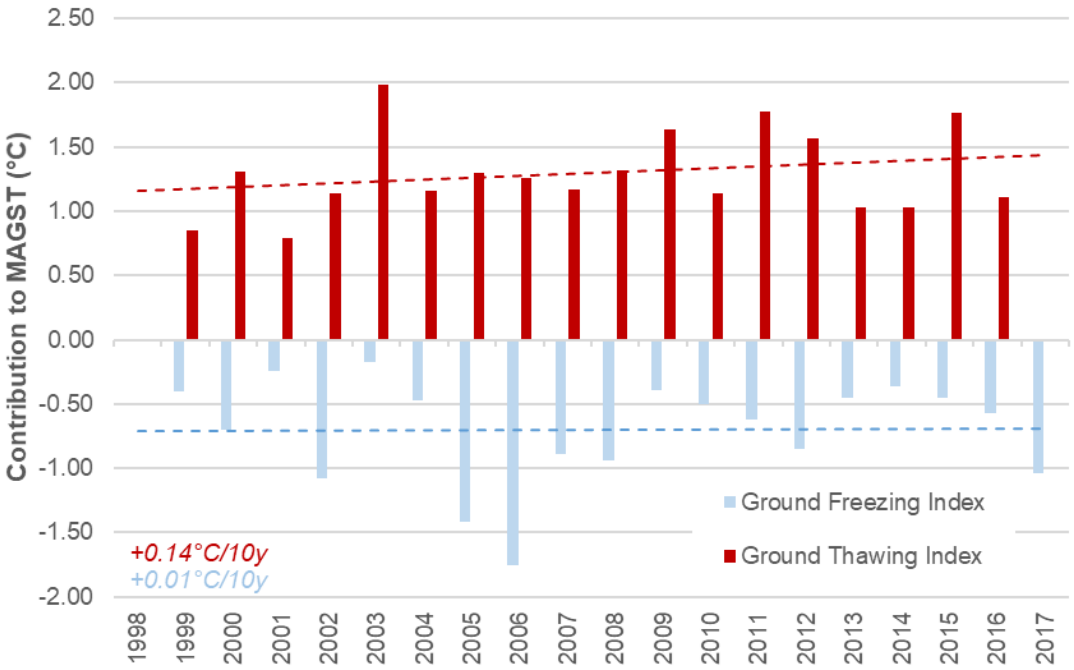

Figure 19: Contribution of the ground thawing and freezing index to the MAGST on the Aget push-moraine (mean of 7 monitoring stations).

2.6 Climatic setting

Between 1864 and 1980, air temperatures recorded at the Grand-Saint-Bernard (GSB) meteorological station since 1864 (cf. Figure 21) implied a **favourable climatic context for permafrost preservation**, as the mean annual air temperatures (MAAT) ranged between -2.86°C and -0.28°C at 2472 m.a.s.l. The Aget glacier forefield being 400 meters higher in altitude than the GSB meteorological station, it can be estimated (based on a 0.5°C loss for a gain of 100 m in elevation) that the air temperature on site ranged between -4.86°C and -2.28°C between 1864 and 1980. Such were the climatic conditions during the deglaciation of the Aget push-moraine complex, which began approximately in the 1940s (Figure 20), allowing the preservation of permafrost or the potential for the development of neo-permafrost, as suggested by Delaloye (2004).

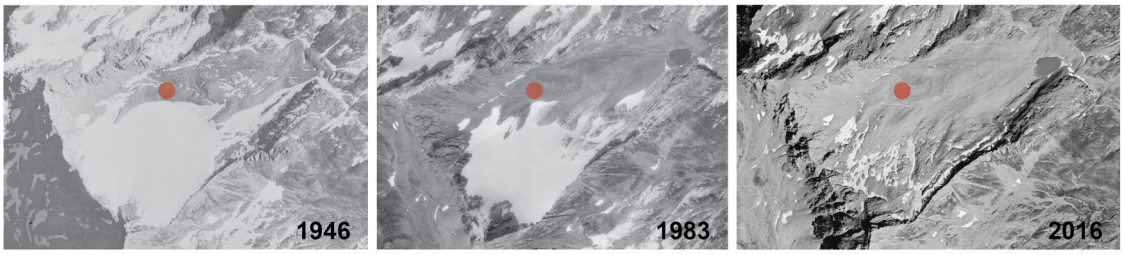

Figure 20: Evolution of the deglaciation of the Aget push-moraine complex and glacier forefield between 1946-1983-2016. The red dot marks the Aget push-moraine A (modified after Swisstopo).

However, as illustrated by Figure 21 an important increase in air temperatures has been recorded in the Alps since the 1980s, favouring the downwasting of frozen material. Indeed, the temperatures recorded at the GSB meteorological station since the 1980s reached its peak in 2015 with a MAAT of 1°C. In such climatic context, the degradation of permafrost is an expected response to increasing air temperatures.

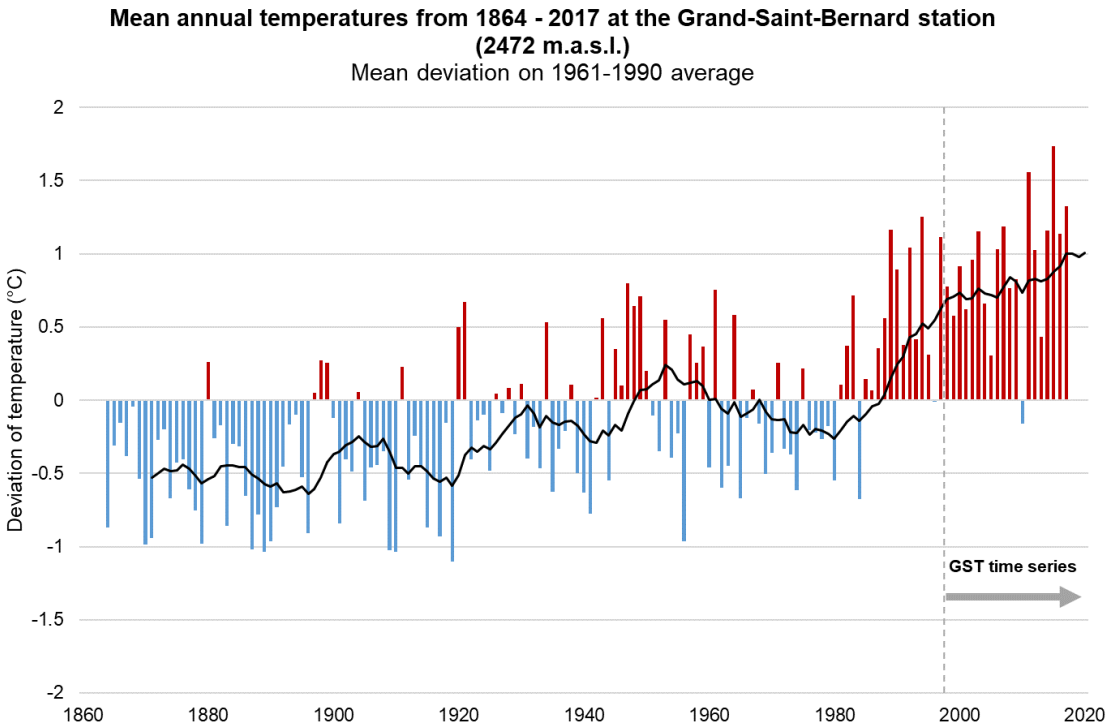

Figure 21: Deviation of mean annual temperatures from 1864 to 2017 at the Grand-Saint-Bernard meteorological station (2472 m.a.s.l.) from the reference of 1961-1990. Temperatures above the 1961-1990 mean are in red and temperatures below the 1961-1990 mean are in blue. The black line represents the annual running mean (homogenised data: MétéoSuisse).

3 Methods

The following chapter details the methodology applied to study the Aget push-moraine complex. **Electrical resistivity measurements** (3.1) were performed to investigate the spatial distribution of ground ice in some parts of the Aget glacier forefield and the evolution of its thermal state since 1998. To complete the understanding of the dynamics of the Aget push-moraine complex**, surface displacements** (3.2) have been measured on a regular basis since 2001 by geodetic surveys (Lambiel and Delaloye, 2004). These two complementary approaches used in the frame of this study provided the data presented and analysed in chapter 4.

3.1 Electrical resistivity measurements

3.1.1 Principles

The principle behind geoelectrical prospection of the subsurface is the contrast between the electrical properties of materials, such as water and ice (Table 2; Figure 22). Indeed, geoelectrical measurements of the subsurface are based on the difference of the electrical resistivity between materials. “Due to the great sensitivity of electrical resistivity to the transition from frozen to unfrozen materials, electrical resistivity measurements constitute one of the standard geophysical methods that is widely used in permafrost investigation” (Kneisel et *al.*, 2008: 159).

Table 2 : Range of resistivities for different materials (Kneisel, 1999).

Material	Range of resistivity (Ω m)
Groundwater	10 – 300
Sand	100 – 5 × 10^3
Granite	5 × 10^3 – 10^6
Gneiss	100 – 10^3
Schist	100 – 10^4
Frozen sediments, ground ice, mountain permafrost	1 × 10^3 - 10^6
Glacier ice (temperate)	10^6 – 10^8
Air	Infinity

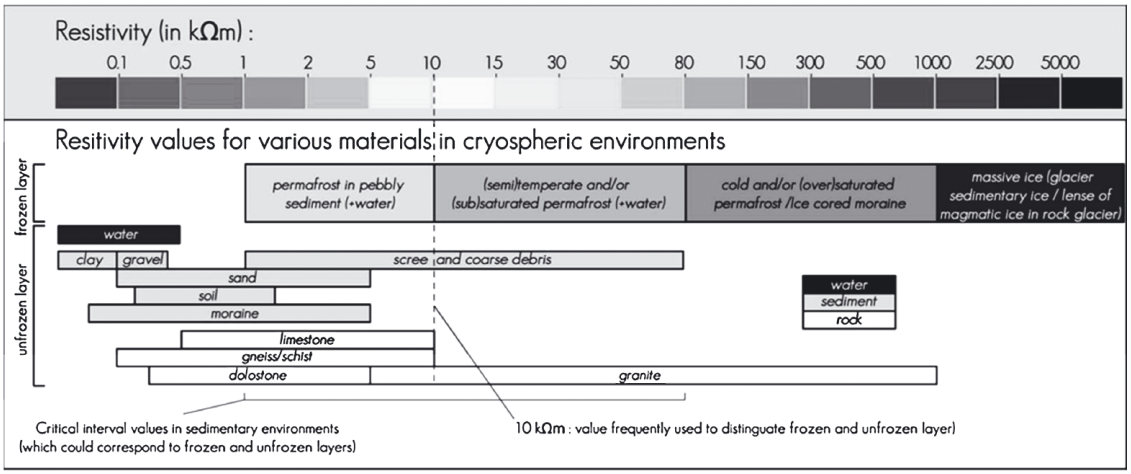

Figure 22: Resistivity values of various materials (Bosson et *al*., 2014).

During the LIA, small glaciers advanced within permafrost areas in the Alps, consequently provoking mechanical and thermal disturbances of the pre-existing frozen sediments. LIA glacier forefields located within the belt of discontinuous permafrost are complex geomorphic systems in which different types of ground ice can be found (for example buried glacier ice or interstitial ice), and in which the spatial distribution of frozen sediments is heterogeneous (Delaloye and Lambiel in Kneisel and Hauck, 2008: 101). In this context, geoelectrical measurements are particularly well adapted to map the ground ice distribution in these post-LIA glacier forefields.

Geoelectrical surveys are conducted by generating a continuous current of intensity I [mA] into the ground via two current electrodes (A and B). Two potential electrodes (M and N) allow the measurement of the potential different [ΔV] (Figure 23). From the

current I [mA] and potential difference values [ΔV] the electrical resistivity [Ω] of the subsurface can be determined. However, the final expression that is calculated considers the geometry of the electrode configuration, which is known as the geometric factor K. In fact, the subsurface consists of a heterogeneous medium, thus the resistivity calculated is known as the ***apparent resistivity*** (ρ_a):

$$\rho_a = (\Delta V/I) \cdot k$$

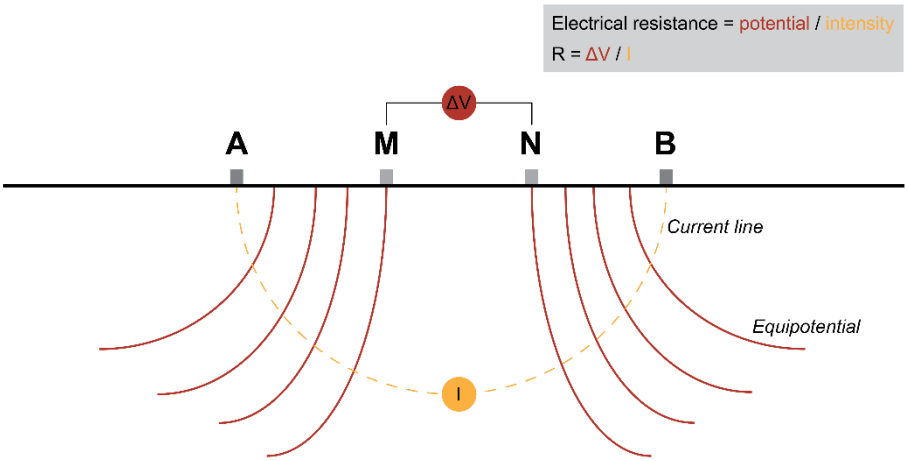

Figure 23: Current lines and equipotential surface.

3.1.2 Electrode arrays

Three types of arrays were applied in this study to obtain different types of measurements: vertical soundings and horizontal mapping. **Vertical soundings** were carried out by applying the Schlumberger and Hummel arrays, which allow the vertical prospection of the variation of resistivity directly beneath the centre of the sounding. This method allows the distinction of different layers of the subsurface. The Wenner array was applied for **horizontal mapping**, which allows the characterization of the lateral heterogeneity of the subsurface at a chosen pseudo-depth.

Schlumberger array

The **Schlumberger array** is known as the symmetrical configuration where the distances between the electrodes AM and NB are equal and multiples of the electrodes MN, where $k = \pi \cdot AM \cdot AN/MN$. This configuration is used when **vertical electrical soundings** (VES) are performed to characterize the electrical resistance of the subsurface. In Schlumberger surveys, the spacing between the outer current electrodes is increased logarithmically to increase the penetration depth of the current (Reynolds, 2011; Figure 24). To avoid too small values of the potential difference, the spacing between M and N is gradually increased.

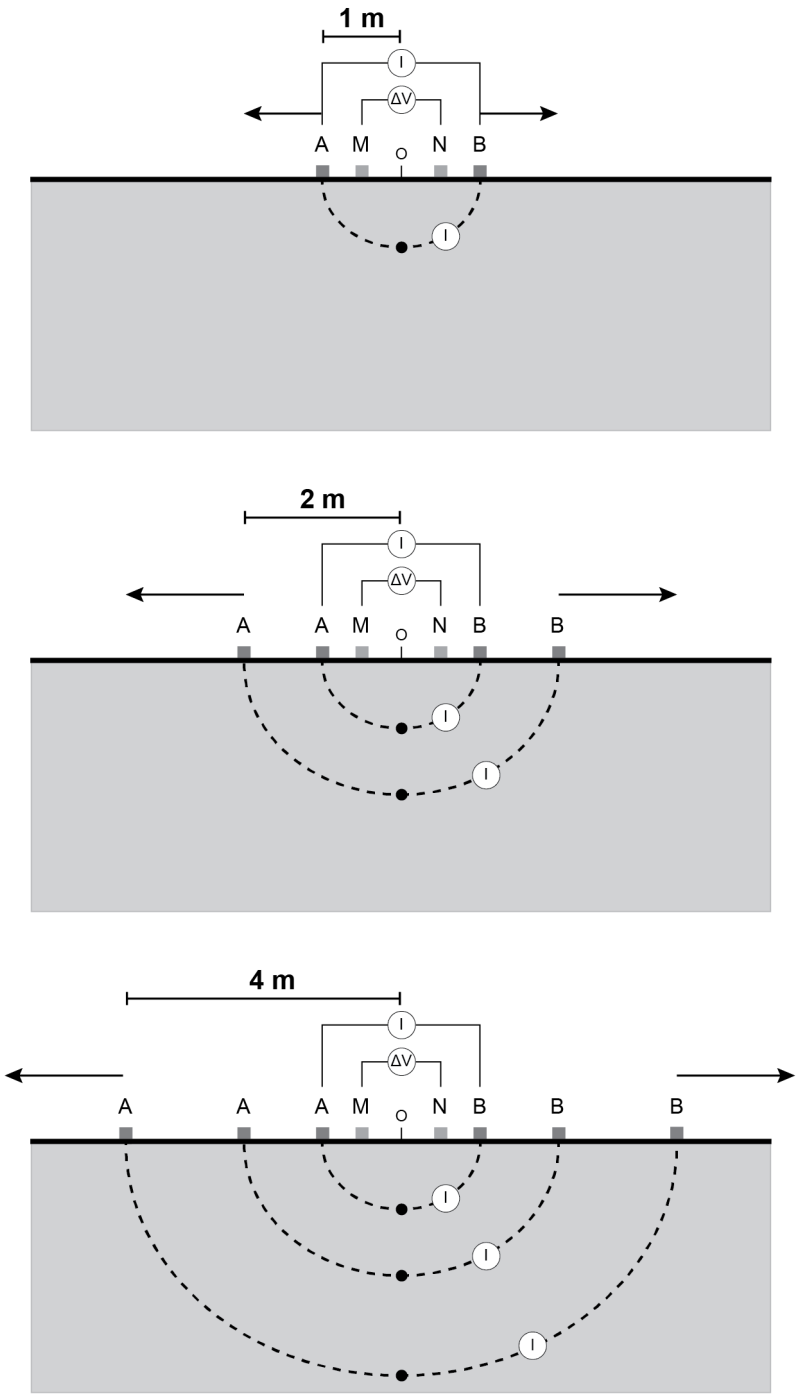

Figure 24: Scheme of a Schlumberger array with a gradual increase of electrode spacing, consequently increasing the depth of investigation (modified after Devaud, 1999).

Hummel array

The **Hummel array** is known as the dissymmetrical configuration or the semi-Schlumberger. A fixed current electrode C, which replaces the electrode A or B when measuring the resistivity of the upward or downward branch of the sounding, is placed perpendicularly to the AMNB electrode configuration at an “infinite” distance, meaning at a distance at least equal to the distance between the electrodes A and B. This electrode configuration allows the **horizontal heterogeneity** of the subsurface to be exposed (Figure 25).

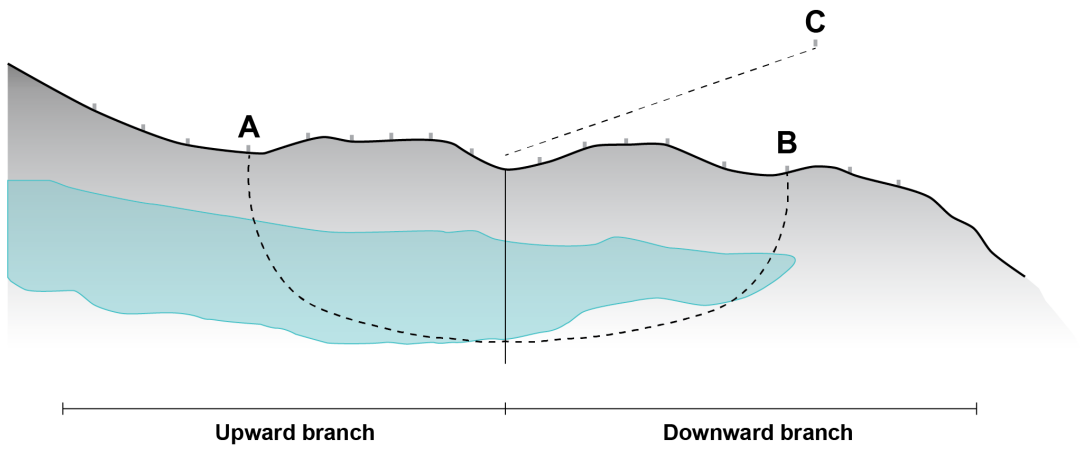

Figure 25: Hummel array electrode configuration.

Wenner array

The **Wenner array** has been applied for resistivity profiling (or Wenner mapping). This method is used for the visualisation of **lateral changes** in the subsurface apparent resistivity at a chosen pseudo-depth. The spacing between the electrodes remains fixed, but all four electrodes are moved simultaneously for each measurements (Hauck and Kneisel, 2008; Figure 26).

Results obtained from Wenner profiles translate to the resistivity of the subsurface. With the presence of a conductive superficial layer, the values of the apparent resistivity of layers of frozen sediments are generally two to ten times smaller than the specific resistivity values calculated from vertical electrical soundings (Delaloye, 2004).

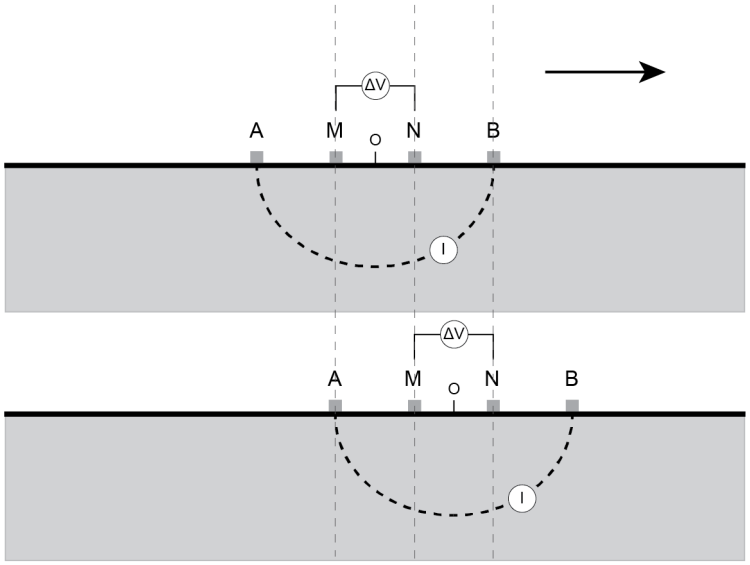

Figure 26: Wenner array. The spacing between all four electrodes remains the same throughout the entire profile while the electrodes are moved simultaneously (modified after Devaud, 1999).

3.1.3 Repetition of geoelectrical measurements

An initial geoelectrical campaign was conducted in September 1998 in the Aget glacier forefield to investigate its ice content and distribution, in which nine VES and nine Wenner profiles were carried out (Devaud, 1999). In late-August 2017, six of the VES and all nine Wenner profiles were repeated, using the same methods, electrode configurations and material (resistivity meter – McOhm 2115 A). Both the

Schlumberger and Hummel arrays were applied to all the soundings (VES) carried out in 1998 and 2017. In both campaigns (1998 and 2017), the Wenner profiles were carried out with the same spacing of 17.5 m between each electrode. By repeating the surveys with the same measuring parameters (electrode array and spacing), comparable results can be obtained (Figure 27). Nevertheless, it is important to consider the different field and measuring conditions of both campaigns. Even with a thorough effort of positing the profiles as they were in 1998 (with the help of cairns and coordinates), the terrain's creep behaviour (modification of the micro-topography) and configuration (irregular and coarse-blocky surface) made this a challenging task. Consequently, this should be considered as being part of the margin of error between both field campaigns.

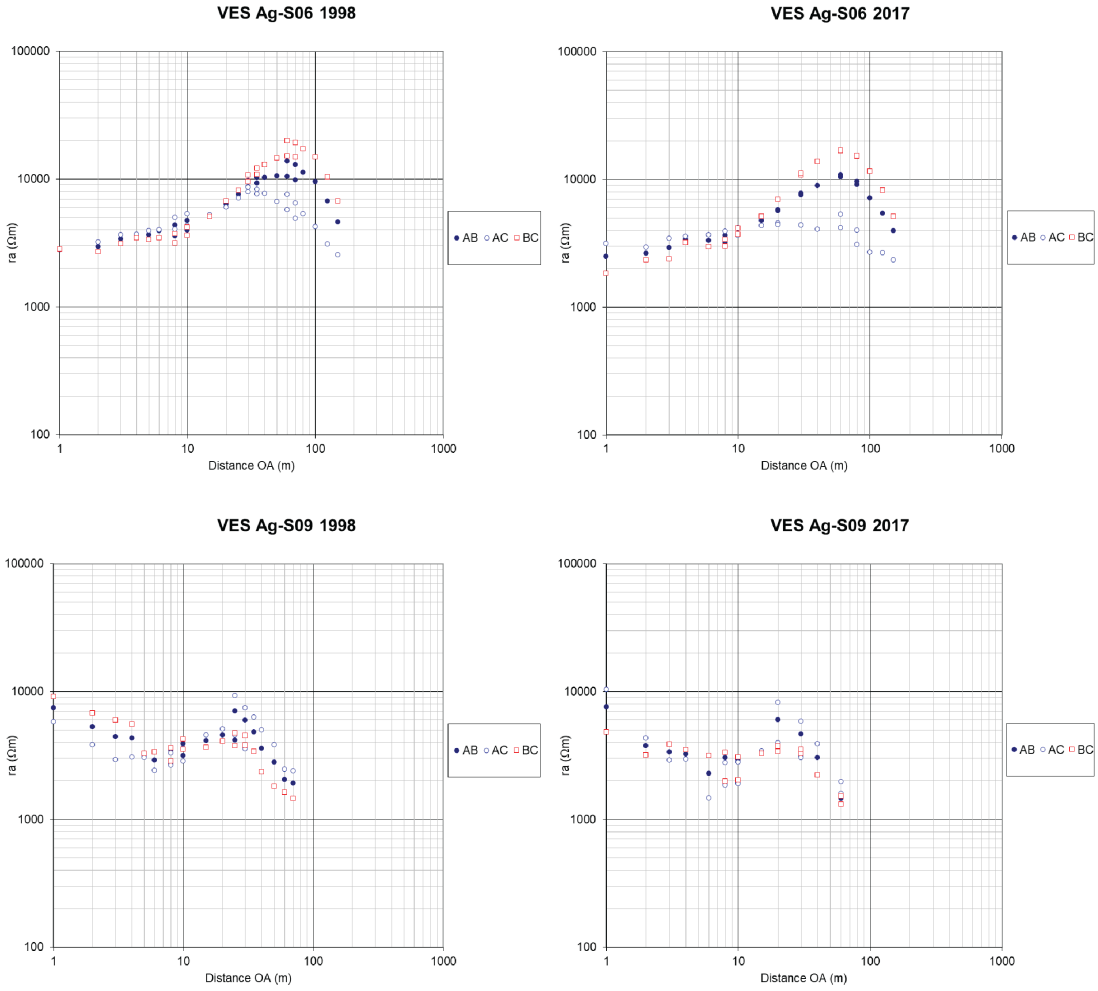

Figure 27: Comparable raw data (VES Ag-S06 and Ag-S09) obtained from the 1998 and 2017 measurement campaigns.

3.1.4 Data calibration: pre-processing

Hummel and **Schlumberger** arrays require a gradual increase of spacing between electrodes M and N at two to three intervals as the spacing between the current electrodes increases. This configuration generates three to four segments, where each segment corresponds to the measurements carried out with the given spacing of MN. Shifting between the segments often occurs in this process. To determine the importance of the shift between two segments, two measurements with the first electrode spacing of MN are systematically repeated with the new electrode spacing of MN. The segments are corrected and adjusted (logarithmic translation) to a fixed segment (Figure 28).

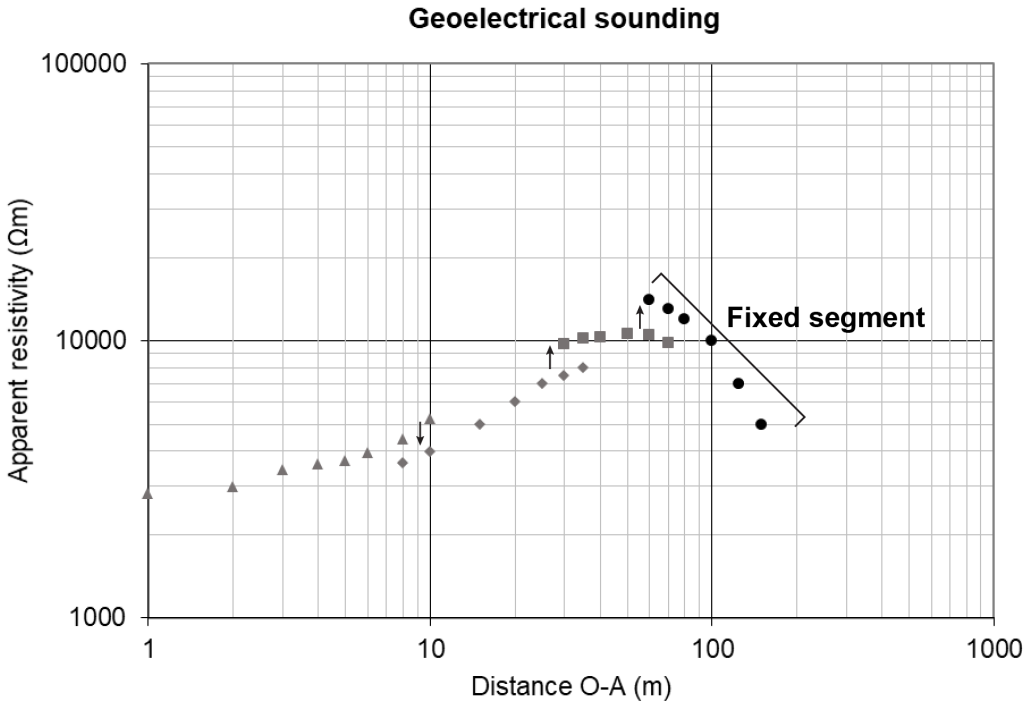

Figure 28: Proportional adjustment of the segments (1-2-3) on the fixed segment (4). Each marker-type corresponds to a different segment.

To determine the fixed segment, the segments were once adjusted to the second segment (fixed), as suggested by Vonder Mühll (1993) and repeated by Delaloye and Devaud (2004; 1999), and were also adjusted to the last (third or fourth) segment (fixed), as the margin of error caused by the electrode configuration is potentially smaller with an increased electrode spacing. The values obtained from the adjustment

of the segments on the second (fixed) and on the last (fixed) segment were compared to each other in order to determine the amplitude of the shift between an adjustment on the second segment or on the last segment. The amplitude between the different adjustments (shift of all segments on the second fixed segment or on the last (third or fourth) segment) varied from one sounding to another (Figure 29). This can be explained by the different amplitude ranges of the shifts between each segment, which is partly controlled by the measurement conditions (electrode configuration, terrain's configuration – roughness, irregularity, conductivity, etc.).

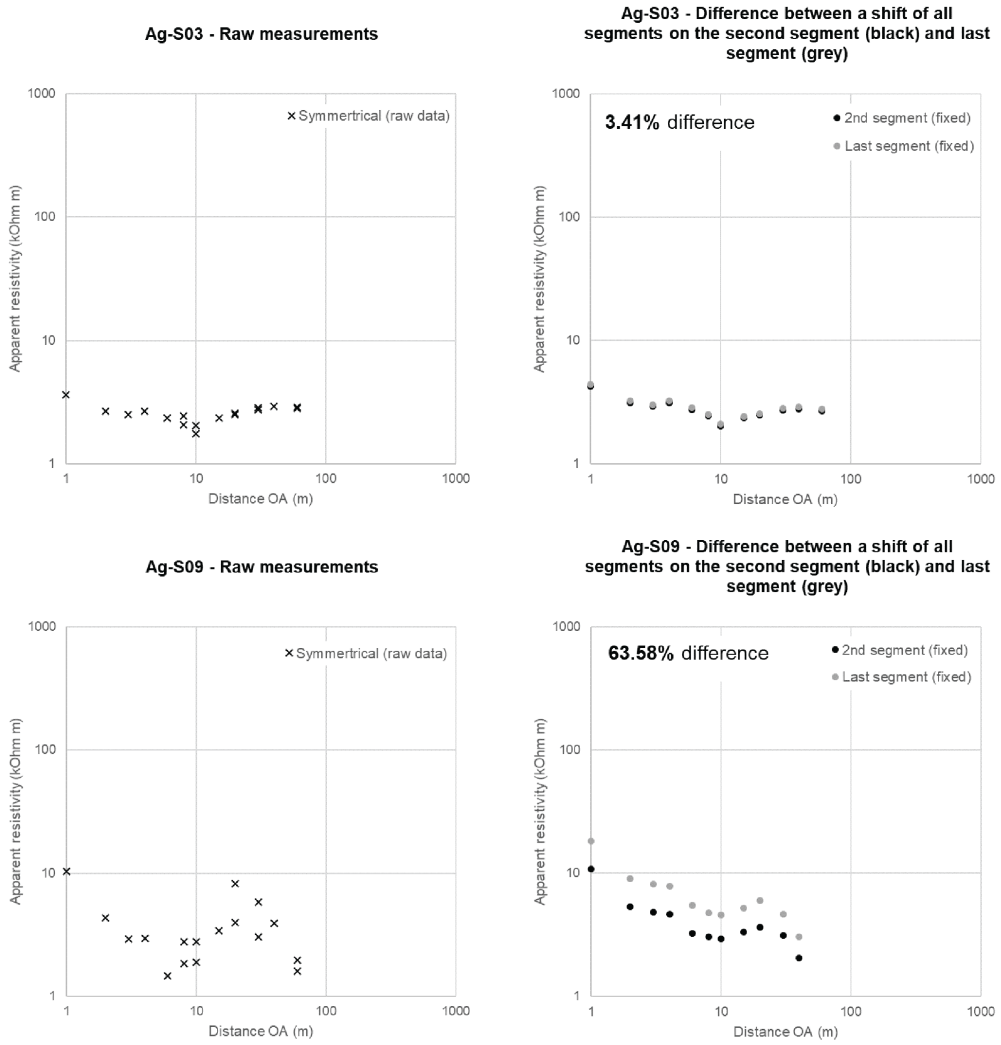

Figure 29: Variability of shifts' amplitude depending on the difference of amplitude between each segment.

3.1.5 Inversion processing

To grasp the heterogeneity of the subsurface, the ***specific resistivity*** of each layer can be obtained by interpretation methods, such as inversion models. **For vertical electrical soundings**, the programme SCHLUMY[1], a semi-automatic procedure that allows the user to manually define the thickness and the specific resistivity of superposed parallel layers was used to model the subsurface. A stratigraphic model of three to four layers was generated in most cases, according to the geomorphological context. However, the principle of equivalence constrains the interpretation processes, as variations inversely proportional of the thickness and resistivity of an intermediate layer provide similar results. Indeed, for certain relations of the parameters of a three or four-layer section, the nature of a layer under a very resistive intermediate layer cannot be distinguished. In such cases, it is hardly possible to make a distinction between two different intermediate layers, and errors of interpretation may occur (Bhattacharya and Patra, 1968; Delaloye, 2004).

3.2 Surface displacement measurements

3.2.1 Data acquisition principles: Real-Time Kinematic GNSS

Differential GNSS (dGNSS) makes use of two receivers in order to improve the accuracy of single measurements that are disturbed by the atmosphere. A reference receiver, set up at a fixed location that is assumed to be motionless, receives in permanence the satellite signals. This signal is used to calculate the satellite positions, and to determine the difference between the satellite location and the receiver's fixed coordinates. A second receiver, called the rover, is mobile and placed successfully on the points that need to be positioned. In real-time kinematic (RTK) mode the two receivers, reference and rover, are in a permanent state of communication, and the correction values are directly sent by radio from the reference to the rover. The main advantage of this mode in comparison to the triangulation technique is that visibility between the stations is not necessary. Therefore, it is not required to move the reference station once it is installed. However the topographic horizon can drastically limit the number of available satellites in a certain area. This technique allows a rapid

[1] Developed by Aquaphys, Geneva

acquisition of data once marking of points has been performed during the first campaign. In order to gain control of the measurement accuracy, the receiver is left calculating its position of ~10 s, and the average value of five to ten measurements is retained. The standard deviation of the measurement positioning during this time lapse is usually less than 1 cm in the horizontal component and less than 2 cm in the vertical one, by experience almost the same as in the absolute positioning. By adding the position errors, a total error up to 3 cm can be reached when comparing two sets of data (Lambiel and Delaloye, 2004).

3.2.2 Surface displacements

The surface displacement of the Aget push-moraine has been monitored on a yearly basis since 2001 and bi-annually from 2004 to 2013. This long-term monitoring provides an exceptional dataset to assess the temporal evolution of the surface movements of this back-creeping push-moraine.

Real-time kinematic GNSS allows the determination of surface displacements through comparing the position of the measurement points between two campaigns of measurements. Surface displacements of less than 3 cm are considered as non-significant, as it is in the same range as the position error. The total displacement is determined by its horizontal and vertical components. The horizontal velocity and direction of a moving point is given by the horizontal component, and the change in elevation is given by the vertical component. At least three different processes can influence the change in elevation of a point, making the interpretation a challenging task.

1. **Loss in elevation due to the downslope movement**. The direction of a moving mass usually follows the slope topography or at least the shear surface. Therefore, the amplitude of the slope angle determines the decrease in elevation relative to the horizontal displacement.
2. **Decrease or increase in elevation due to extending or compressing flow**. According to Lambiel and Delaloye (2004), a 1% extension of reference surface induces a subsidence of 10 cm for a layer of 10 m thick.
3. **Change in elevation in response to melting or aggradation of ice lenses** (or massive ice layers) in the ground (Lambiel and Delaloye, 2004).

3.2.3 Compression and extension zones

According to Lambiel and Delaloye (2004), compression and extension zones can be determined by establishing a net of triangles between a well-distributed set of points over a given area (Figure 30). The evolution of the area of a triangle between two measurement campaigns allows the quantification of either a compressing (decrease in the area) or extending (increase in the area) flow.

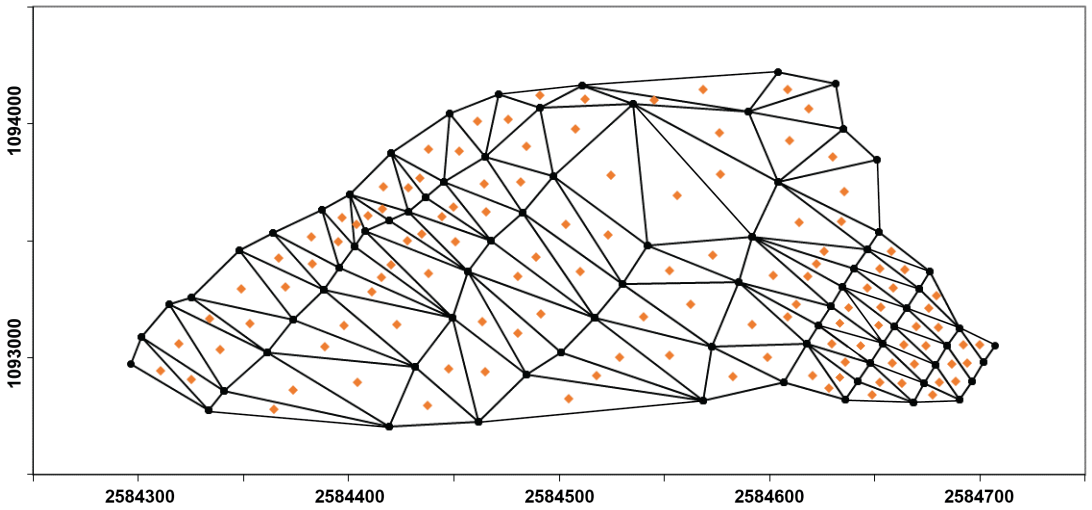

Figure 30: Net of triangles established to quantify an extending or compressing flow pattern (based on Lambiel and Delaloye's approach, 2004).

3.2.4 Thickness variation

> *The vertical component of surface movement results from the effects of slope angle, compression and extension strain rate and ice aggradation or thaw settlement. The first two parameters are related to the horizontal velocity, whereas the latter mainly depends on permafrost thermal regime.*
>
> (Lambiel and Delaloye, 2004: 233)

To estimate the thickness variation of a mass in movement between two series of measurements, the topographical slope and the slope angle of the motion of a measured block have to be considered. If the slope angle of the block motion is greater than the surface topography, a loss in thickness has occurred. Whereas if the

inclination of the topography is greater than the slope angle of the surface displacement, then a gain in thickness has occurred. This can be represented for a series of points along a longitudinal profile (Lambiel and Delaloye, 2004; Figure 31).

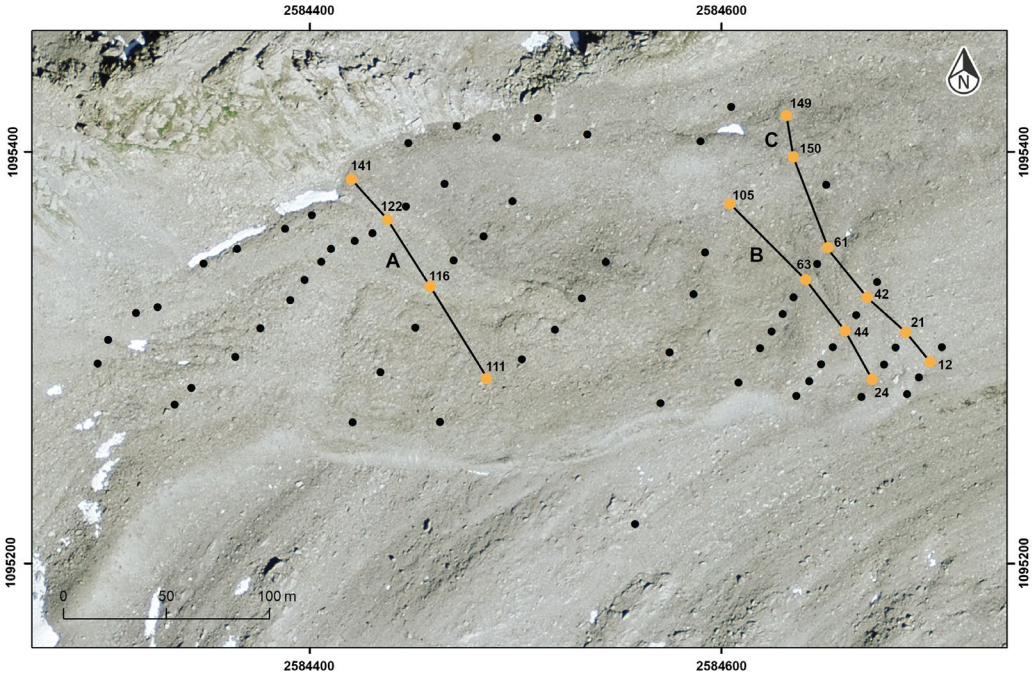

Figure 31: Selected longitudinal profiles on the Aget site along which a comparison between the topographical slope and movement of single blocks will be made (modified after Lambiel and Delaloye, 2004).

4 Results and interpretation

Geoelectrical surveys and surface displacement measurements yielded the main datasets that will be presented in the following chapter. The presentation and the comparison of the results obtained from the 1998- and the 2017-geoelectrical surveys will be established in the first two subchapters (4.1.1 and 4.1.2). The subchapters 4.2 and 4.2.2 will consist in the presentation and interpretation of data obtained from geodetic surveys carried out on an annual (bi-annual for some years) basis. Finally, a synthesis of the results (4.3) will conclude this section.

4.1 Resistivity changes

Electrical resistivity “is very sensitive to water and temperature changes around the melting point and particularly suitable to monitor changes in warm and degrading mountain permafrost” (Staub, 2015: 82). The change in resistivity of a frozen layer serves as a proxy to assess its thermal evolution. As illustrated by Figure 32, the seasonal evolution of the apparent resistivity appears to react closely to temperature changes. Therefore, in a context of increasing GST over the past two decades, a decrease in resistivity is expected to be observed between the results of the 1998 and 2017 geoelectrical surveys.

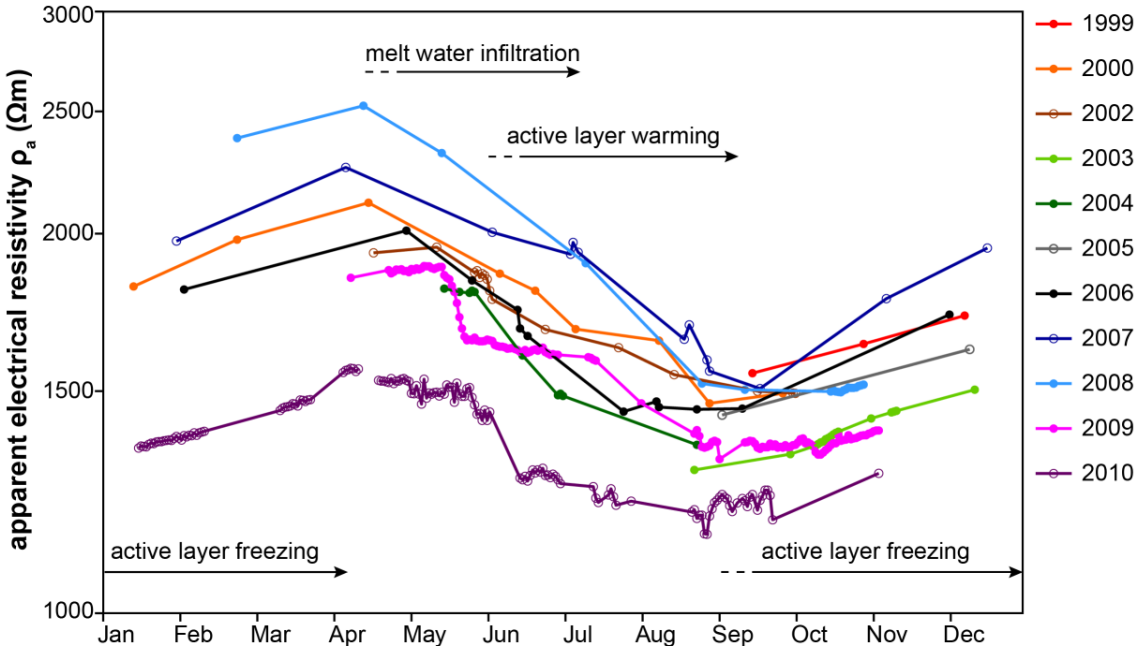

Figure 32: Seasonal pattern of mean apparent electrical resistivity measured at the Schilthorn measurement site expressing a sensitivity to temperature changes (Staub, 2015).

4.1.1 Repetition of vertical electrical soundings

Geoelectrical soundings were carried out for the first time in September 1998 to characterize the spatial distribution of ground ice in the Aget glacier forefield, and were repeated in late-August 2017 to assess the evolution of permafrost. Four VES extend from the uppermost outer limit of the LIA extent to the front of the push-moraine. In 1998, ground ice was found in the active zone at larger depth (Ag-S06 and Ag-S08), as well as in its margins (Ag-S07 and Ag-S09). Whereas in the lower zone of the glacier forefield, the two VES carried out on the push-moraine B (Ag-S03) and on the fluted moraines (Ag-S04) revealed the absence of frozen ground sediments (Devaud, 1999; Delaloye, 2004; Figure 33).

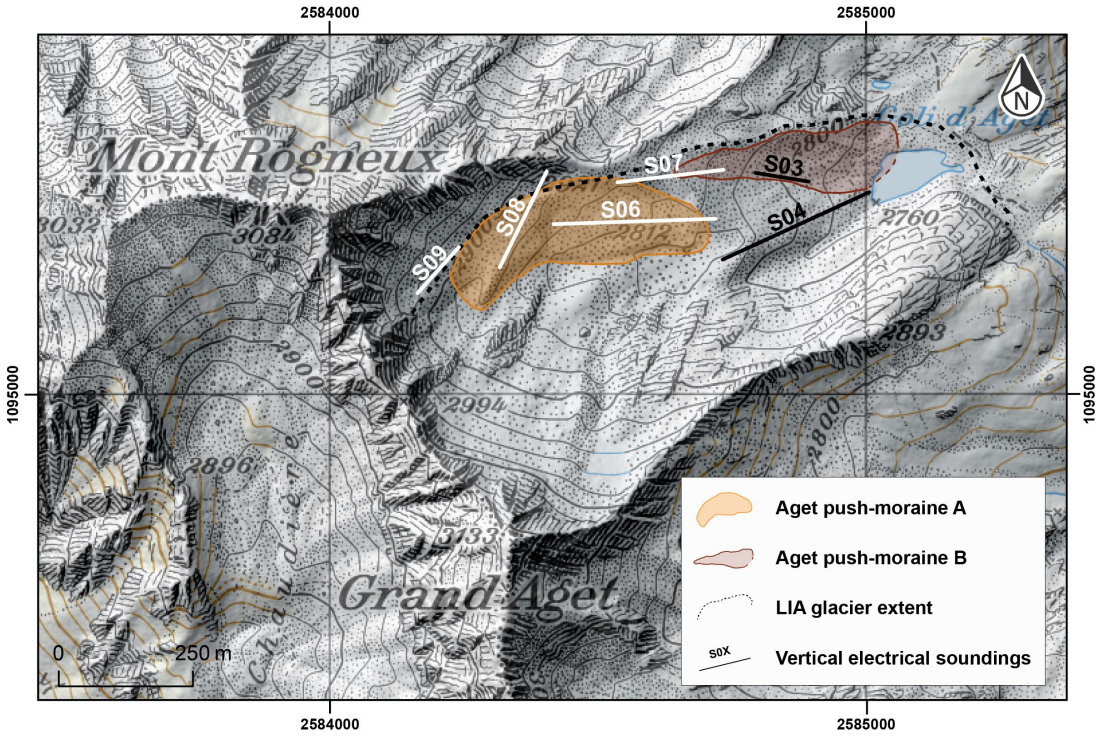

Figure 33: Location of the Aget push-moraine complex within the LIA glacier forefield and the repeated vertical electrical soundings (white: permafrost; black: no permafrost) (basemap Swisstopo).

The repetition of VES has successfully showed similar structures in 1998 and 2017 on all permafrost sites. However a significant decrease of the maximal apparent resistivity of roughly 20% has been systematically observed in the zones containing ground ice (Figure 34).

Close to the surface, a clear discrepancy of resistivity can be observed between the values measured in 1998 and 2017 for the soundings Ag-S08, Ag-S03 and Ag-S04 (Figure 34), which is most likely caused by the measuring conditions (placing and connectivity of electrodes, wetness of the terrain, etc.). Whereas at greater depth, the values of both years remain more or less unchanged, especially for the soundings (Ag-S03 and Ag-S04) carried out in the zone deprived of permafrost. From this observation, it can be assessed that large discrepancies of resistivity values in the uppermost layer (near surface changes) do not affect the resistivity of deeper layers.

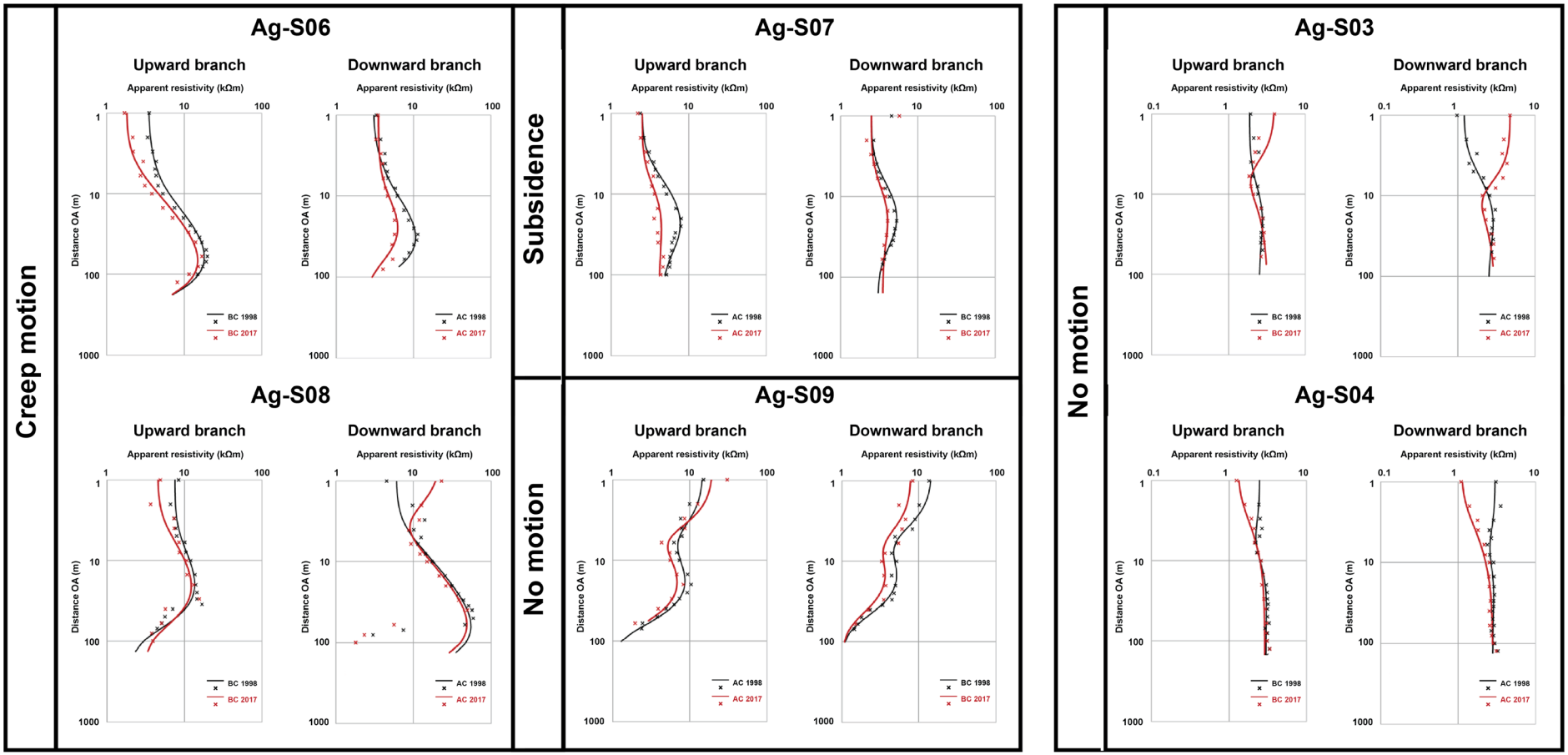

Figure 34: Overview of the comparison between the 1998 (black) and 2017 (red) vertical electrical sounding (Hummel) profiles.

Ag-S06 and Ag-S08: active zone of the push-moraine

The profiles **Ag-S06** and **Ag-S08** were carried out on the actively back-creeping part of the push-moraine A. The results obtained from the surveys performed using the Hummel array showed a clear **horizontal heterogeneity** of the subsurface for both soundings, which makes the presentation of the soundings carried out with the Schlumberger array not relevant for the spatial analysis of ground ice distribution in this zone. Consequently, the analysis will focus on the data measured with the Hummel array for both soundings Ag-S06 and Ag-S08. According to Delaloye (2004), the type of VES curves observed for the both downward and upward profiles indicates the presence of **cold** or **(over)saturated permafrost** under a layer of approximately 5 m thick of unfrozen sediments or of permafrost **undergoing a thawing process**.

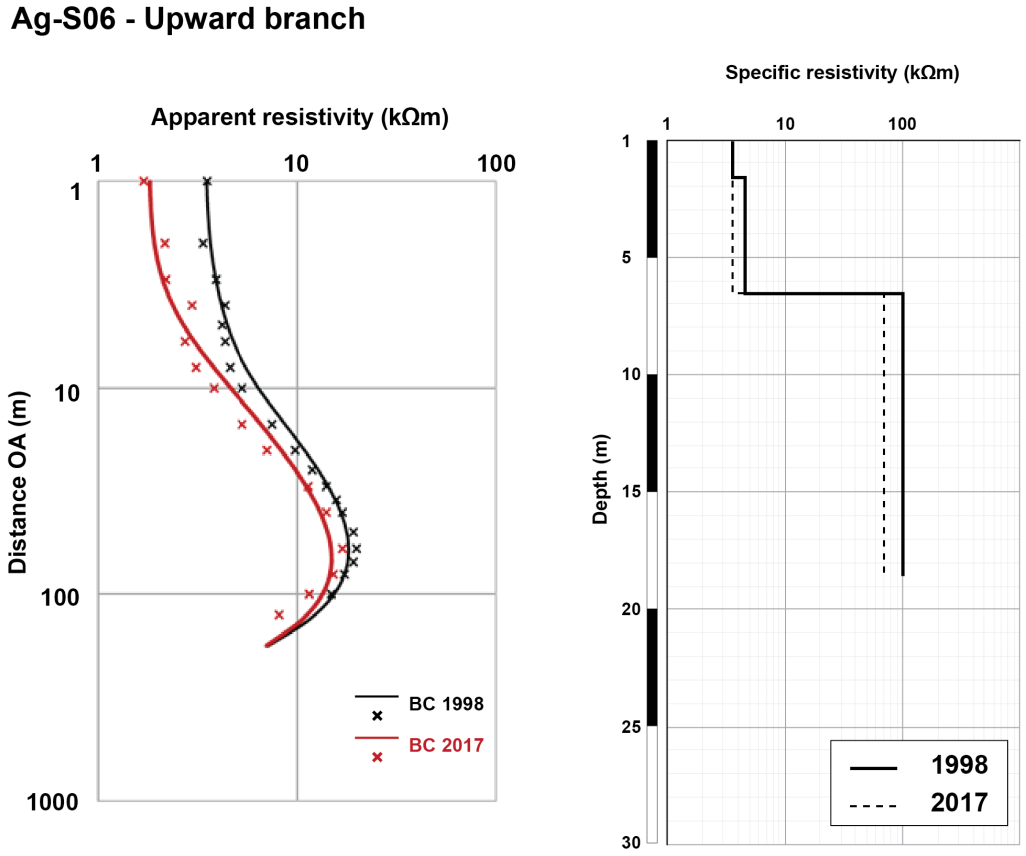

Figure 35: Apparent resistivity measured in 1998 and 2017 (left) and the modelled specific resistivity for 1998 and 2017 (right) of Ag-S06 upward branch (BC).

For the upward branch (NW) of the 1998 sounding Ag-S06, Devaud (1999) identified at a depth of 6 to 8 meters, a 10-meter thick layer of frozen sediments with a specific resistivity ranging between 80 and 140 kΩm. The modelled specific resistivity profile based on the apparent resistivity profile of 1998 fixed on the last segment (cf. chapter 3.1.4) yielded values similar to Devaud's interpretation. The presence of a resistive layer with a specific resistivity reaching up to **100 kΩm** was observed under a 6 to 8-meter layer of less resistive sediments. The data from the sounding carried out in 2017 revealed that the specific resistivity of this layer decreased down to **70 kΩm**, which corresponds to a **decrease of 21%** of the mean apparent resistivity (Figure 35; Table 3).

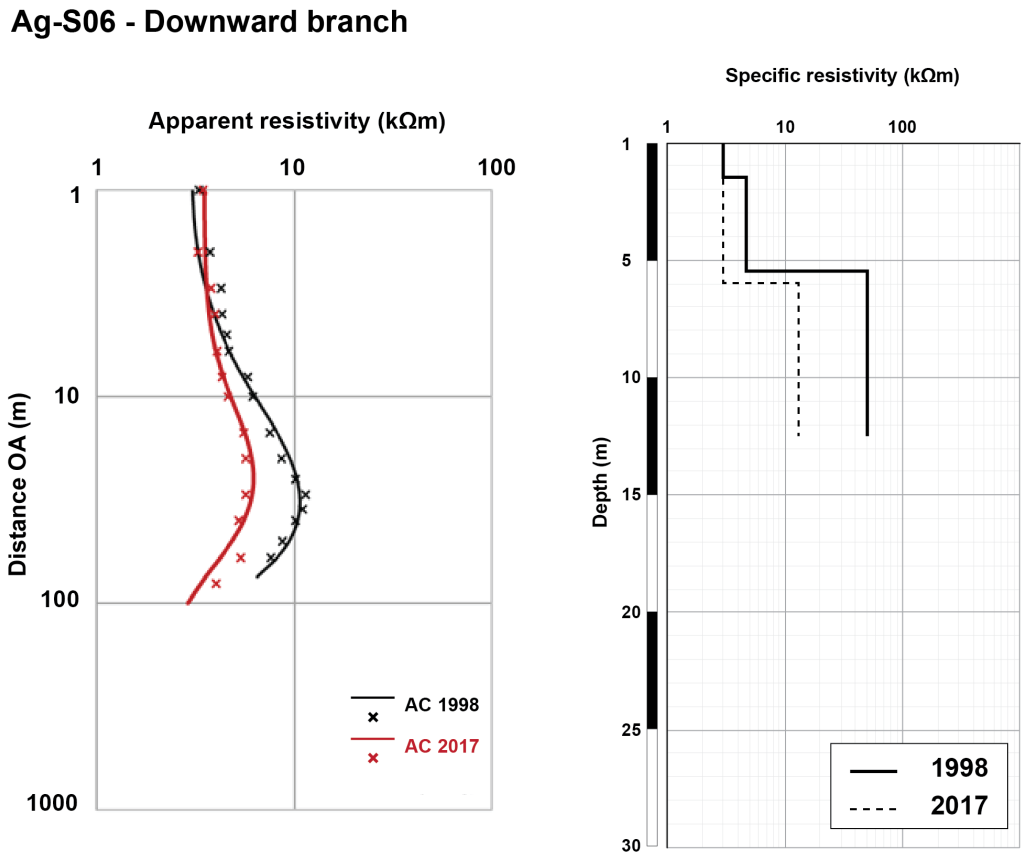

Figure 36: Apparent resistivity measured in 1998 and 2017 (left) and the modelled specific resistivity for 1998 and 2017 (right) of Ag-S06 downward branch (AC).

In comparison to the values obtained from the NW (upward) branch, the VES of the SE (downward) branch of Ag-S06 revealed a less resistive and thinner layer of frozen sediments at a similar depth (6 to 8 meters). From the data obtained in 1998, Devaud (1999) attributed to this layer of frozen ground a specific resistivity ranging from 30 to 80 kΩm, which corresponds to the values obtained from the inversion model based on the apparent resistivity profile of 1998 fixed on the last segment. Between 1998 and 2017, the specific resistivity of this frozen layer decreased from **50 to 15 kΩm**, corresponding to a **decrease of 34%** of the mean apparent resistivity of the downward branch (Figure 36; Table 3).

An ongoing process of thermal degradation has been observed for both profiles of the sounding Ag-S06. The resistivity values measured in the SE part (downward branch) of the profile in 1998 and 2017, revealed a greater decrease in resistivity than in the NW (upward) branch, which can be explained by the different properties of each layer. The less resistive values measured in the SE layer (downward branch) suggest the presence of a permafrost layer with higher relative water to ice content ratio. Whereas the more resistive properties of the NW layer (upward branch) suggest the presence of ice-rich conditions with small interstices, limiting the liquid water content.

Table 3 : Change in % of the apparent resistivity between 1998 and 2017 of the profile Ag-S06.

		Upward	Downward	Symmetrical
OA (m)		BC (kΩm)	AC (kΩm)	AB (kΩm)
10	1998	5.32	6.18	5.80
	2017	3.82	4.63	3.91
	1998-2017 change (%)	**-28.22**	**-25.02**	**-32.58**
15	1998	7.47	7.51	7.58
	2017	5.31	5.53	5.04
	1998-2017 change (%)	**-28.91**	**-26.34**	**-33.51**
20	1998	9.83	8.61	9.27
	2017	7.07	5.70	5.98
	1998-2017 change (%)	**-28.09**	**-33.81**	**-35.47**
30	1998	14.08	11.39	12.81
	2017	11.37	5.67	8.19
	1998-2017 change (%)	**-19.25**	**-50.20**	**-36.02**
40	1998	16.89	10.14	13.57
	2017	14.01	5.23	9.37
	1998-2017 change (%)	**-17.03**	**-48.41**	**-30.96**
60	1998	19.96	7.59	13.77
	2017	16.94	5.33	10.88
	1998-2017 change (%)	**-15.12**	**-29.77**	**-20.98**
80	1998	17.22	n/a	12.89
	2017	15.27	3.99	9.61
	1998-2017 change (%)	**-11.33**	**n/a**	**-25.44**

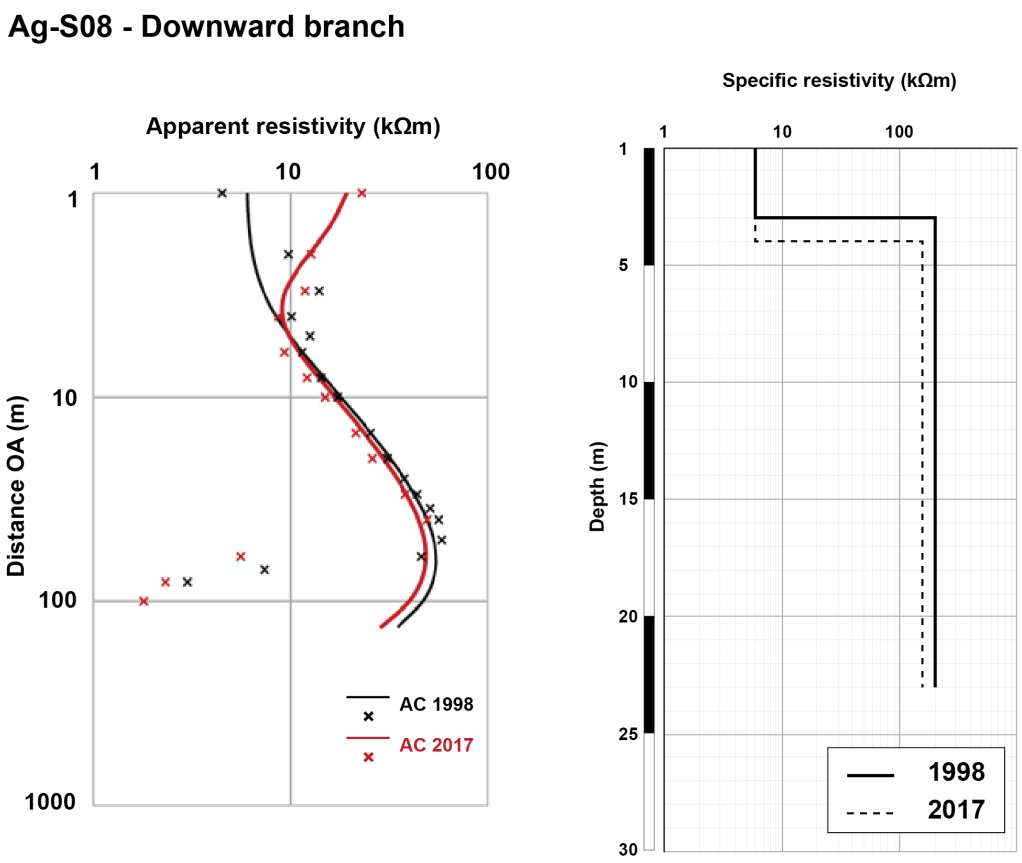

Figure 37: Apparent resistivity measured in 1998 and 2017 (left) and the modelled specific resistivity for 1998 and 2017 (right) of Ag-S08 downward branch (AC).

In 1998, Devaud (1999) identified for the NE branch Ag-S08 (downward) an 8 to 25 meters thick layer of frozen sediments at a depth of 3 to 6 meters, reaching specific resistivity values up to 350 kΩm (values ranged between 150 to 350 kΩm). The inversion model based on the 1998 values shifted on the last segment provided a specific resistivity of 200 kΩm for the same layer. The specific resistivity of this very resistive layer decreased to 170 kΩm in 2017, which corresponds to a **decrease of 16%** of the apparent resistivity between 1998 and 2017 (Figure 37;

Table 4). Similarly to the NW branch of the sounding Ag-S06, the high resistivity of this frozen layer and the mean WEqT of **-1.7°C** measured in 2017 in this zone expresses **cold and/or oversaturated permafrost conditions**. Moreover, in such conditions, the pore space is extremely limited, which **hinders the increase of liquid water content to ice ratio**.

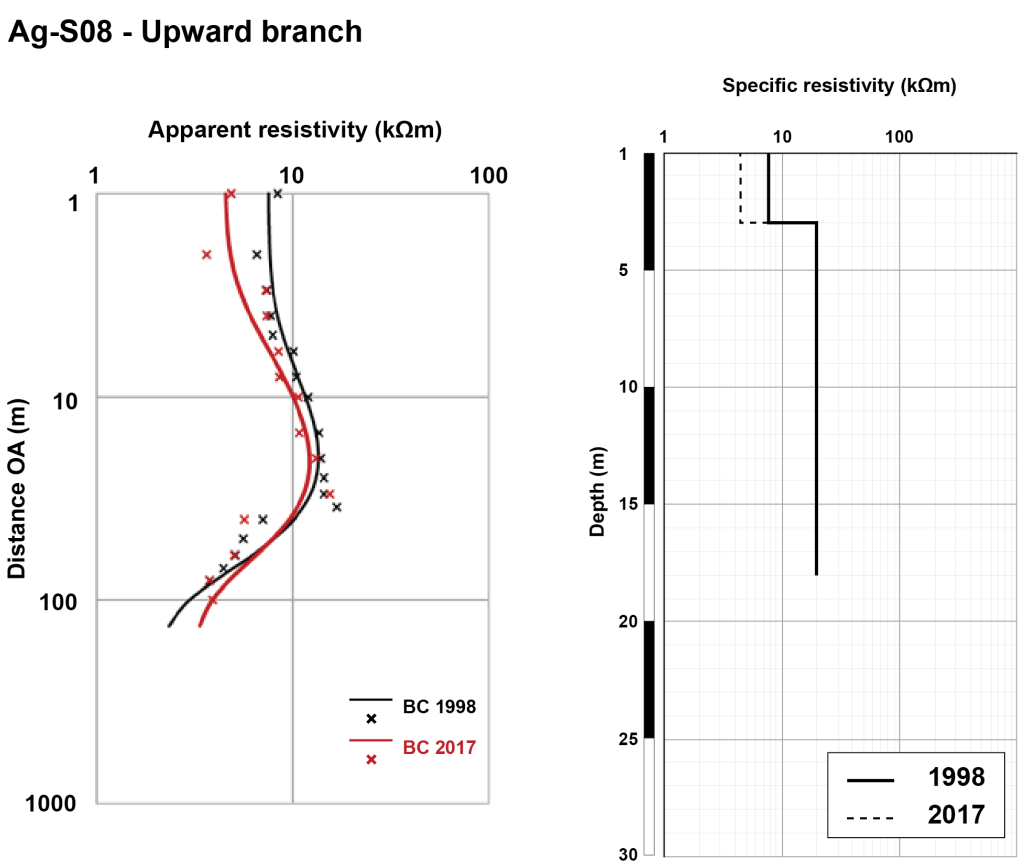

Figure 38: Apparent resistivity measured in 1998 and 2017 (left) and the modelled specific resistivity for 1998 and 2017 (right) of Ag-S08 upward branch (BC).

The SW facing (upward) branch, whose specific resistivity reached 20 kΩm in 1998, remained more or less the same in 2017 (Figure 38). Indeed, the apparent resistivity of the **upward branch decreased by 7%**. Two parameters can explain this meagre change in resistivity values: the **properties of the frozen layer** and the **topographical configuration of the ground surface** (topo-climatic conditions). The latter is a controlling parameter of the heat and energy exchanges between the atmosphere and the ground surface (surface energy balance) that contribute to the thermal evolution of the subsurface (Figure 39). The exposure of a surface to solar radiation or wind is controlled by its topography and orientation, which in turn also influences the snow cover, hence the energy fluxes. The negative MAGST (-0.13°C) measured near sounding Ag-S08 suggests a limited exposure to incoming solar radiation that can be partly explained by the flatness of the terrain. Consequently, less energy is available to melt the underlying frozen layer. Furthermore, the lower resistivity values of this branch (upward) suggest a thermal state of a **permafrost layer closer to 0°C** in comparison to the resistivity measured from the downward branch, which indicates colder

permafrost conditions. Despite a warmer thermal state, the change in resistivity suggest that the presence of an (over)saturated permafrost layer, which limits pore-space (leaving less space for water accumulation).

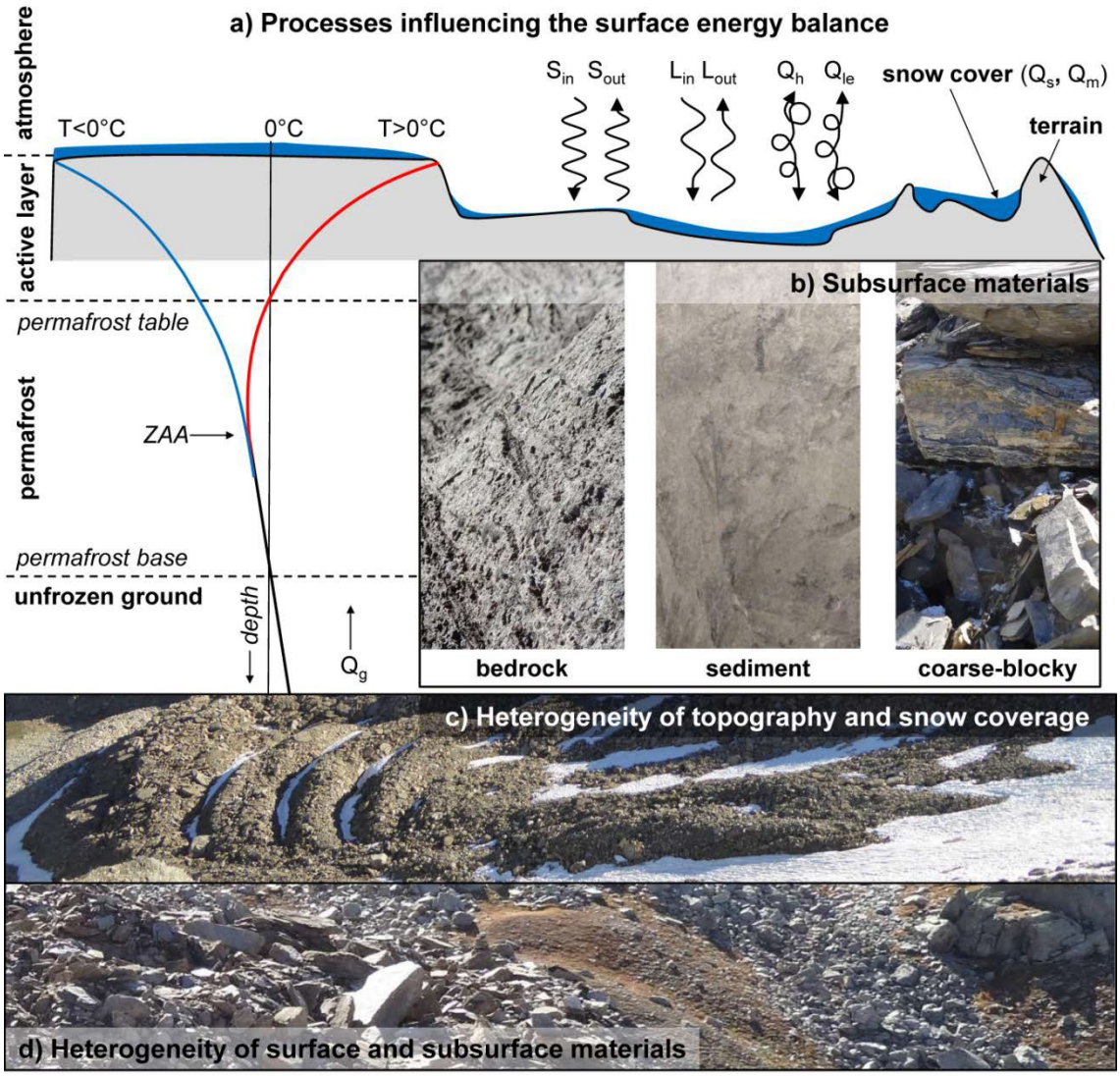

Figure 39: Processes of heat and energy exchange at the ground surface and typical characteristics of mountain permafrost (Staub, 2015).

Table 4 : Change in % of the apparent resistivity between 1998 and 2017 of the profile Ag-S08.

		Upward	Downward	Symmetrical
OA (m)		BC (kΩm)	AC (kΩm)	AB (kΩm)
10	1998	12.05	17.36	16.96
	2017	10.73	14.96	12.49
	1998-2017 change (%)	**-10.95**	**-13.80**	**-26.35**
15	1998	13.69	25.53	21.95
	2017	10.91	21.46	15.15
	1998-2017 change (%)	**-20.25**	**-15.95**	**-30.98**
20	1998	13.98	31.16	25.06
	2017	13.21	26.30	18.56
	1998-2017 change (%)	**-5.57**	**-15.62**	**-25.94**
30	1998	14.58	44.07	31.82
	2017	15.54	38.39	25.04
	1998-2017 change (%)	**6.61**	**-12.89**	**-21.31**
40	1998	7.03	57.00	31.74
	2017	5.67	49.52	24.12
	1998-2017 change (%)	**-19.37**	**-13.12**	**-23.99**
60	1998	5.13	46.02	25.51
	2017	5.03	5.63	5.33
	1998-2017 change (%)	**-2.01**	***-87.77***	***-79.11***
80	1998	3.77	3.01	3.40
	2017	3.77	2.33	3.02
	1998-2017 change (%)	**-0.14**	**-22.62**	**-11.28**

Ag-S07 and Ag-S09: permafrost in the margins of the push-moraine

The profiles **Ag-S07** and **Ag-S09** were carried out in the margins of the push-moraine A, where no creep process is involved. The resistivity profiles obtained by using the Hummel configuration illustrated similar structures, expressing a certain lateral homogeneity of the subsurface. Nevertheless, the upward and downward branches of both profiles expressed slight differences in resistivity values.

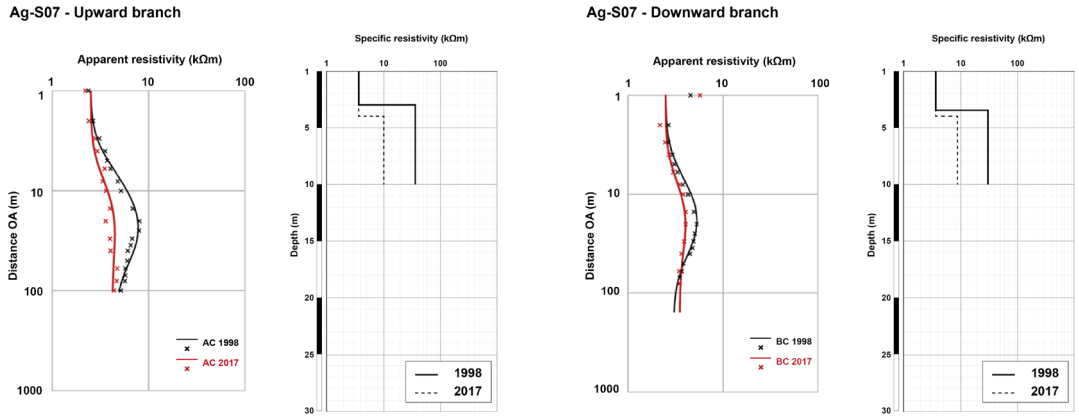

Figure 40: Apparent resistivity measured in 1998 and 2017 (left) and the modelled specific resistivity for 1998 and 2017 (right) of Ag-S07 upward branch (AC) and downward branch (BC).

Both the upward and downward branches of the profile **Ag-S07** show a similar structure (Figure 40). The bell shaped resistivity profile suggests the occurrence of frozen sediments even though the maximal apparent resistivity value is relatively small (8 kΩm in 1998). Such resistivity values suggest the presence of a **(semi)temperate permafrost layer**. The properties of this frozen layer allow important phase changes as illustrated by a **decrease in resistivity**, due to an increase in relative liquid water content to ice ratio. The specific resistivity of both soundings **decreased from 30 to more or less 10 kΩm**, which translates into a 20-30% change of the mean apparent resistivity (cf Appendix Table 6).

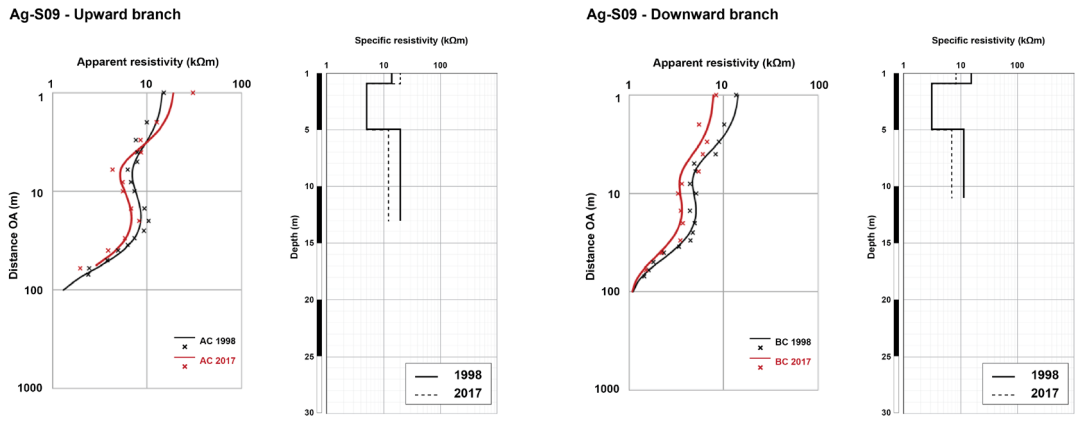

Figure 41: Apparent resistivity measured in 1998 and 2017 (left) and the modelled specific resistivity for 1998 and 2017 (right) of Ag-S09 upward branch (AC) and downward branch (BC).

The high apparent resistivity values observed in the uppermost layer of both (upward and downward) resistivity profiles of **Ag-S09** indicate the presence of a 5-meter thick coarse blocky layer bare of fine sediments, which is explained by the absence of the glacier in this zone during the LIA. The second bell curve indicates the presence of a frozen layer (intact permafrost) whose specific resistivity reached 20 kΩm in the upward branch and 15 kΩm in the downward branch in 1998, and decreased to 15 and 7 kΩm, respectively in 2017 (Figure 41). The VES performed in this intact zone (where the LIA Aget glacier did not extend to) revealed a **decrease by 20%** in apparent resistivity between 1998 and 2017 (cf Appendix Table 7).

Ag-S03 and Ag-S04: no permafrost zone

The data obtained from the sounding **Ag-S03** performed on the push-moraine B revealed the **absence of ground ice**, (despite a morphology expressing post-LIA creep motion) suggesting the fossil state of the push-moraine. The low resistivity values yielded from the sounding **Ag-S04** (zone of fluted moraines) allowed Devaud (1999) to identify a **zone deprived of frozen sediments**, and consequently bringing evidence of the temperate state of the glacier in this zone.

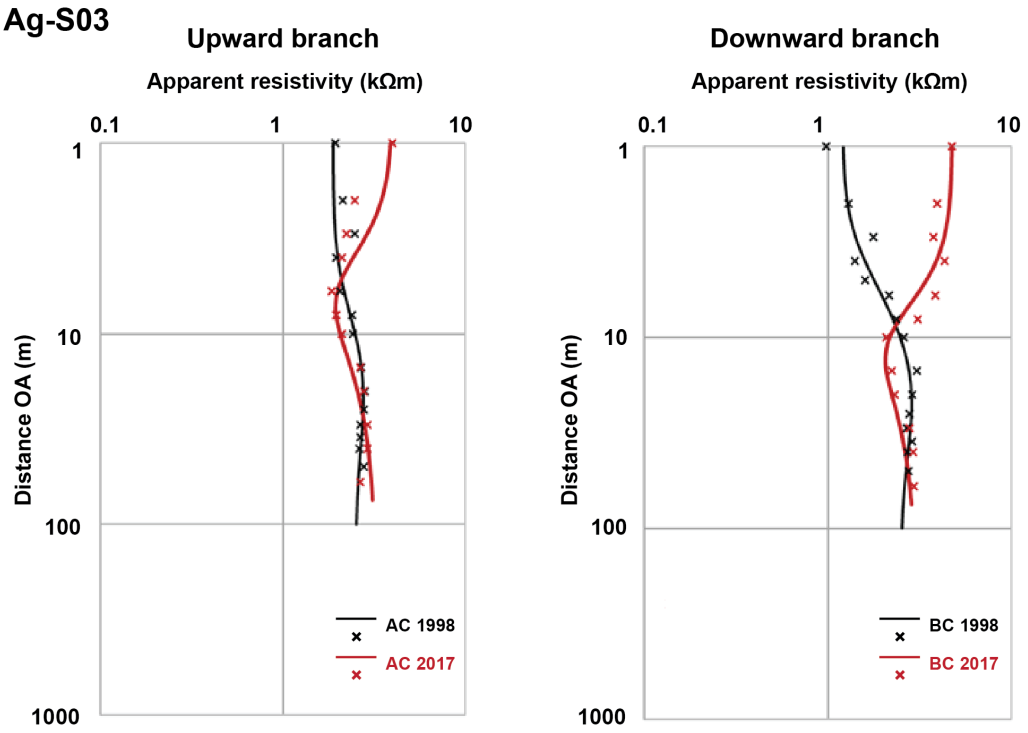

Figure 42: Apparent resistivity measured in 1998 (black) and 2017 (red) for the upward (right) and downward (left) branch of sounding Ag-S03.

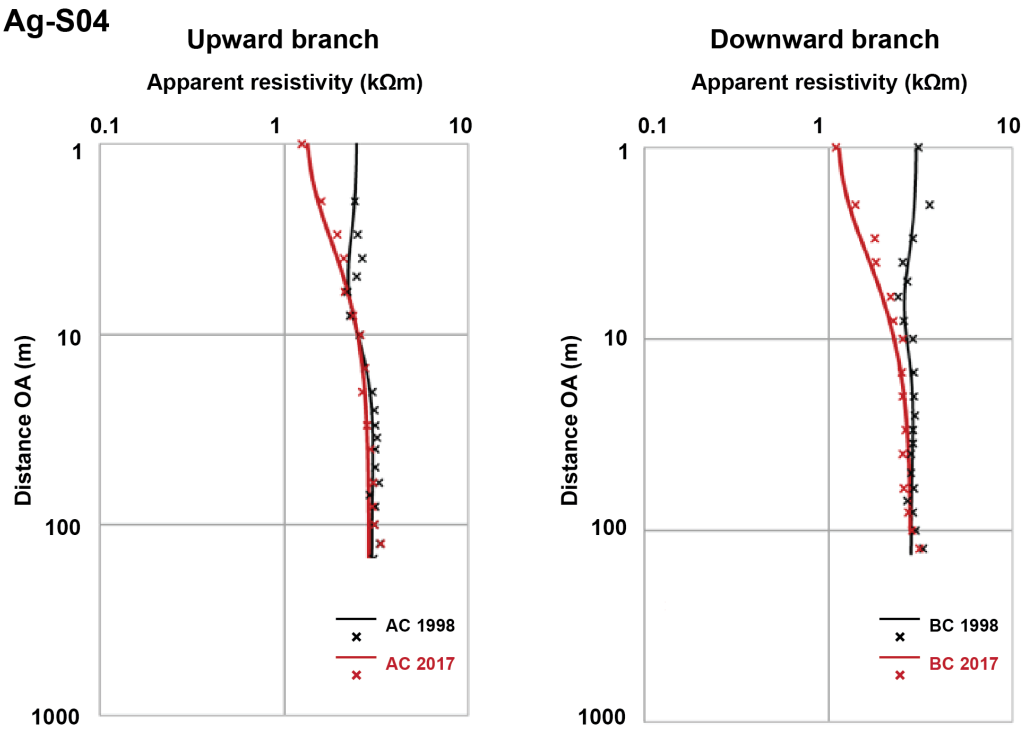

Figure 43: Apparent resistivity measured in 1998 (black) and 2017 (red) for the upward (right) and downward (left) branch of sounding Ag-S04.

The repeated resistivity surveys of the soundings Ag-S03 and Ag-S04 (Figure 42 and Figure 43) **confirmed the absence of permafrost** that was first observed by Devaud (1999) on the push-moraine B and on the zone of fluted moraine. Moreover, the MAGST measured in this zone (Ag-01, cf. localisation of temperature logger Figure 16) is of 0.70°C, which is not favourable for permafrost preservation.

4.1.2 Repetition of Wenner profiles (resistivity mapping)

The repetition of the nine Wenner profiles (Figure 44) has successfully provided **similar structures** in 1998 and 2017 on all permafrost sites, but a significant **decrease of the apparent resistivity** has been systematically observed (Figure 45). Minor geometrical irregularities between the structures of the 1998 and 2017 profiles indicate small inaccuracies regarding the geometrical configuration of the profiles and the position of the electrodes on the blocky terrain.

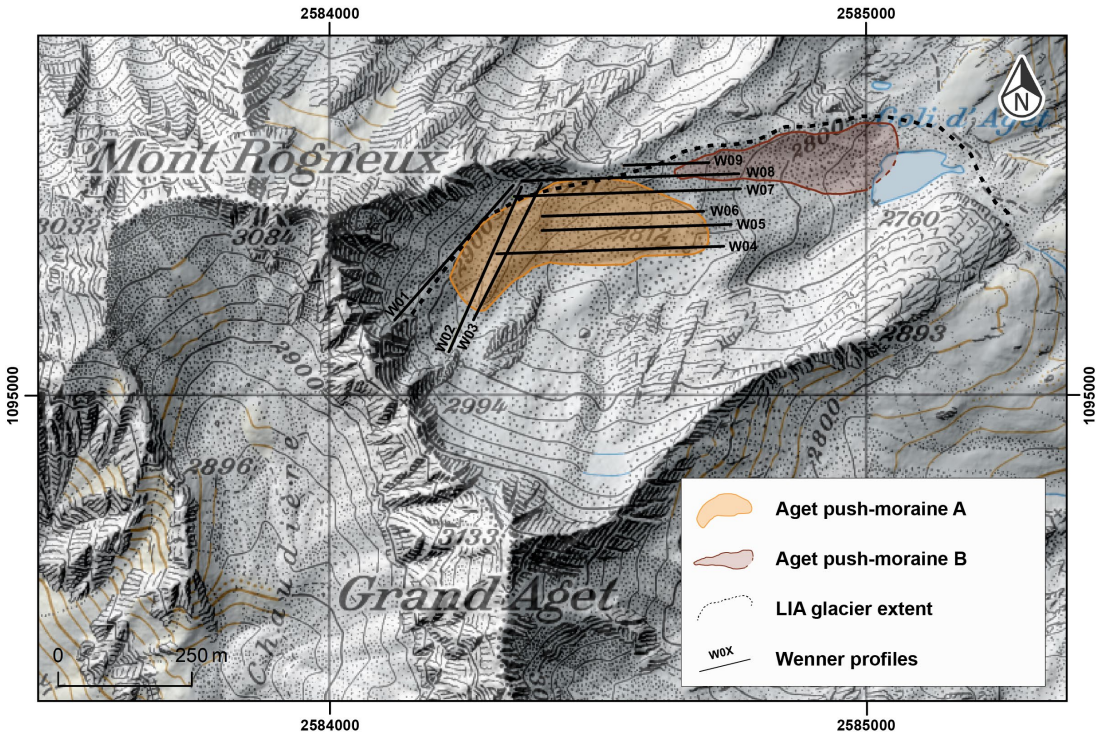

Figure 44: Location of the Aget push-moraine complex within the LIA glacier forefield and the location of the repeated Wenner profiles.

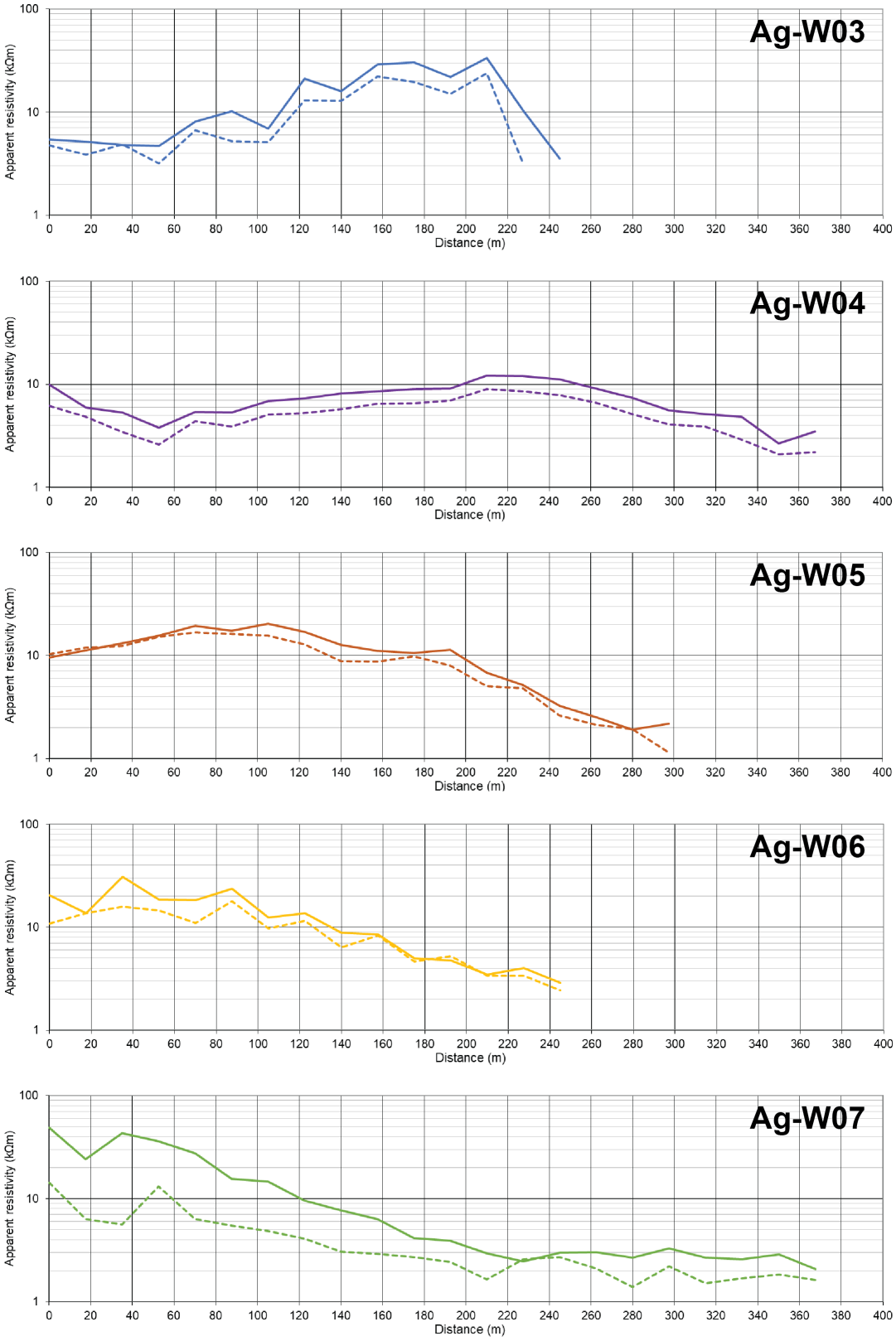

Figure 45: Change in apparent resistivity from 1998 (solid line) to 2017 (dashed line) of the selected Wenner profiles.

Nine geoelectrical profiles with a set distance of 17.5 m between each electrode (Wenner array) allowed the **investigation of the spatial distribution of ground ice at a constant pseudo-depth of 10 m**. The measurements performed in September 1998 revealed lateral variations of resistivity in the push-moraine complex (Devaud, 1999). The values obtained for the apparent resistivity mainly ranged between 3 to 10 kΩm in the margins of the push-moraine A (cf. Appendix Figure 63). Patches of frozen material with resistivity values ranging from 10 to 30 kΩm were observed in the actively back-creeping part of the push-moraine, with a peak of resistivity values in the centre of this zone (ρa > 30 kΩm) (Figure 46).

The surveys conducted by Devaud (1999) in 1998 revealed that **conductive materials (ρa ≤ 3 kΩm) dominate the margins of the push-moraine complex**, confirming the results obtained from the soundings Ag-S03 and Ag-S04. In the centre of the **actively back-creeping zone** of the push-moraine A (at the intersection between Ag-W03 and Ag-W07), apparent resistivity values reaching up to **50 kΩm** were measured in 1998, which corroborates with the **high resistivity values of the sounding Ag-S08**, as well as the WEqT of **-1.7°C** measured in this zone.

The geoelectrical profiles (Wenner mapping) repeated in August 2017 yielded **lower resistivity values throughout the push-moraine complex** (Figure 45). The maximal decrease of resistivity (> -20 kΩm) was observed in the zone where the highest resistivity values were measured in 1998 (cf. Ag-W07; Figure 46).

Minor increases in resistivity were observed punctually. This can be due to the geometrical configuration of the electrodes (contact of electrodes with the ground), increasing the margin of error.

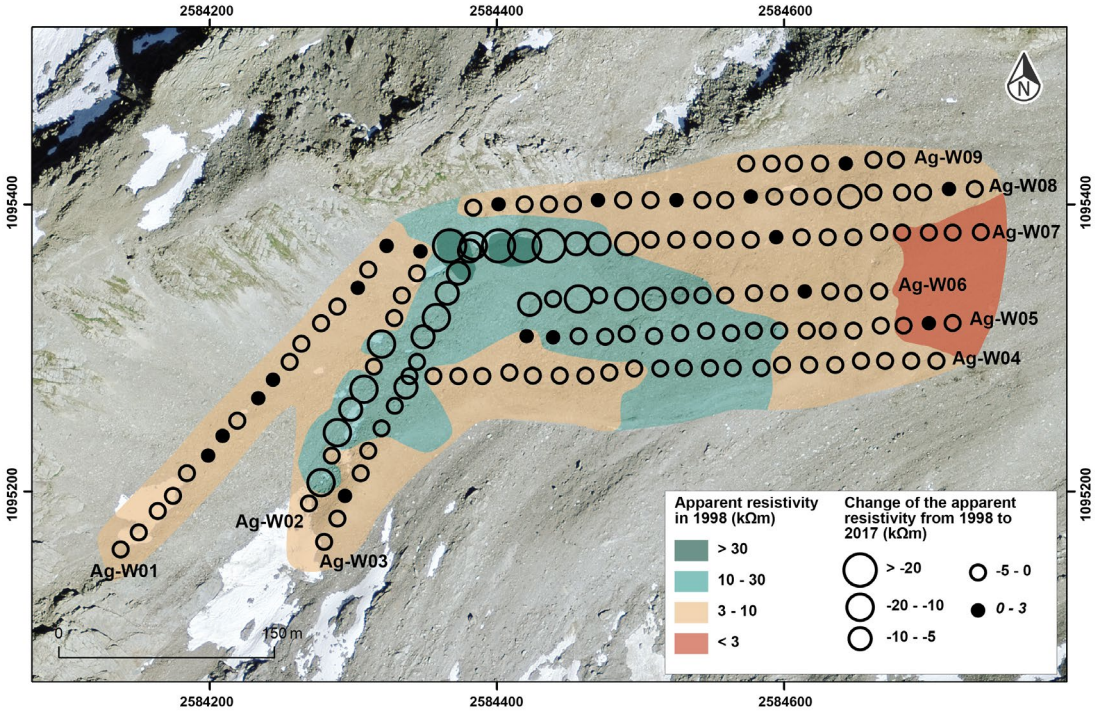

Figure 46: Interpolated (IDW) apparent resistivity values measured at a pseudo-depth of 10 m in 1998 and the absolute change of the apparent resistivity from 1998 to 2017.

4.2 Kinematic response

The kinematic behaviour of rock glaciers or back-creeping push-moraines can be used as a proxy for the response of permafrost to a warming climate, and consequently its thermal state (Staub, 2015). This subchapter will present the **thermo-mechanical** processes that affect the kinematic activity of the Aget push-moraine.

4.2.1 Surface displacement rates

In the central zone of the push-moraine A, surface displacements ranging from 0.15 to more than 0.20 m/y have been measured. Whereas only small surface movements (mainly between < 0.05 to 0.10 m/y) have been observed in the margins of the push-moraine (Figure 47). The direction of the surface movement follows the slope aspect, towards the SE (mean slope angle of 15). The slope angle decreases toward the frontal zone of the push-moraine (between 5° to 10°), inducing a geometrical adjustment, and consequently contributing to the smaller velocities. Close to the rooting

zone of the push-moraine (topographical rupture), the slope angle gradually changes from 15° to 40°, favouring faster velocities (> 0.20 m/y) in the area. However, the slope angle becomes rapidly less steep towards the SE. Displacements in the same range of velocities (> 0.20 m/y) have been observed in the central part of the push-moraine where the slope angle ranges from 15 to 20°.

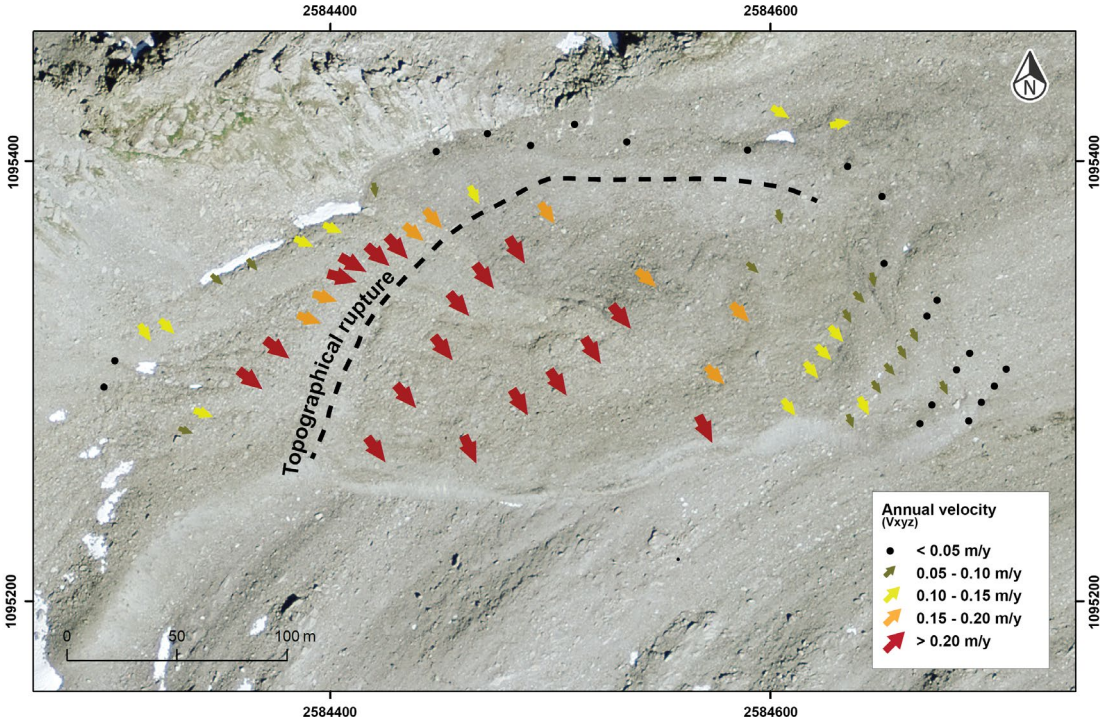

Figure 47: Mean annual horizontal surface displacement rate between 2001 and 2017 (v_{xyz}) in m/y.

Permafrost creep rates are considerably dependent of thermally induced processes. Generally, **creep velocities tend to increase exponentially with warming ground surface temperatures**, as a decrease of relative ice-water content ratio due to thawing favours ice deformation at the shear horizon (Delaloye et *al.*, 2008; Staub, 2015). The surface displacement velocities illustrated in Figure 47 coincide well with the distribution and thermal evolution of ground ice throughout the push-moraine presented in Figure 46.

The faster creep rates in the zone where (over)saturated frozen sediments (10 to > 30 kΩm) have been observed, may be explained by a decreased ice-water ratio content, which is expressed by the significant change in resistivity. Whereas, in the margins of the push-moraine, slower surface displacement rates (< 0.05 to 0.10 m/y) coincide quite well with the zone where conditions of subsaturated permafrost (or even no

permafrost) were found. Consequently, inferring an advanced state of ice melt, which causes an increase in friction at the shear horizon, hindering creep deformation.

4.2.2 Variations of ground surface elevation changes

To assess the **contribution of ice melt to the loss of surface elevation**, the slope angle of the surface movement was compared with the topographical slope, and with the extension and compression flow patterns (Figure 48). Following Lambiel and Delaloye (2004), it is assumed that 1% extension of a moving mass of 10 m thick generates a loss in surface elevation of 10 cm, which doubles if the moving mass is 20 m thick. For Aget, the mean thickness of the deforming terrain is estimated to be 20 m thick in the uppermost zone and 10 m thick in the eastern terminus of the push-moraine.

Flow pattern of the moving mass

Throughout the push-moraine, **the flow pattern is mainly extending**, especially in the **uppermost part of the moving terrain**, near the starting scar, where values up to **+12%** are found over a 17-year period (2001-2017). As for the rest of the surface, the extension rate remains relatively low with values ranging between **0%** and **+5%**. **Compression is restricted to the frontal zone of the push-moraine**, where the topography flattens. As a geometric response to **compressive flow**, a **gain in surface elevation** of 1 meter at the front is expected, whereas for the area concerned by an **extension flow**, a **decrease of the thickness** of more or less 2 meters of the moving mass is anticipated.

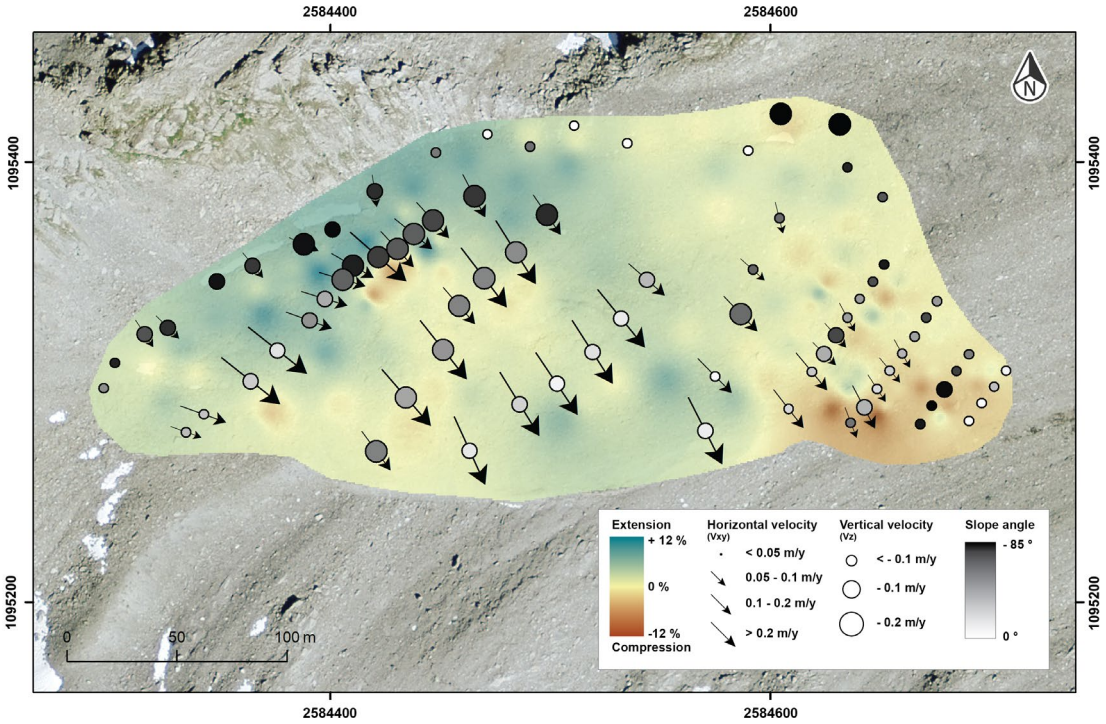

Figure 48: Interpolation (IDW) of the contribution of extension/compression flow patterns and surface displacements to thickness variations. The arrows show the annual horizontal velocity, the circles the annual vertical velocity and the different shades of grey indicate the displacement slope angle of each point.

Displacement slope angle and topographical slope

The slope angle of the surface movements was compared to the topographical slope of three longitudinal profiles (Figure 49). For most of the points taken into account in each profile, **the slope angle of the observed movement was steeper than the topographical slope**, suggesting a loss in surface elevation (subsidence). In some zones of the push-moraine, the extending flow pattern could explain this vertical loss. However, in some cases, the values of the vertical displacement (loss in elevation) are much greater than the ones estimated from the extension flow patterns as illustrated in Figure 48. For example, an estimated loss of elevation of -2.13 m was expected for point Ag-124, yet a decrease of elevation of -3.21 m was measured (Table 5). Furthermore, in zones where a gain in surface elevation is expected due to the compressing flow pattern, important losses in surface elevation have been observed, **suggesting subsidence driven by ice melt**.

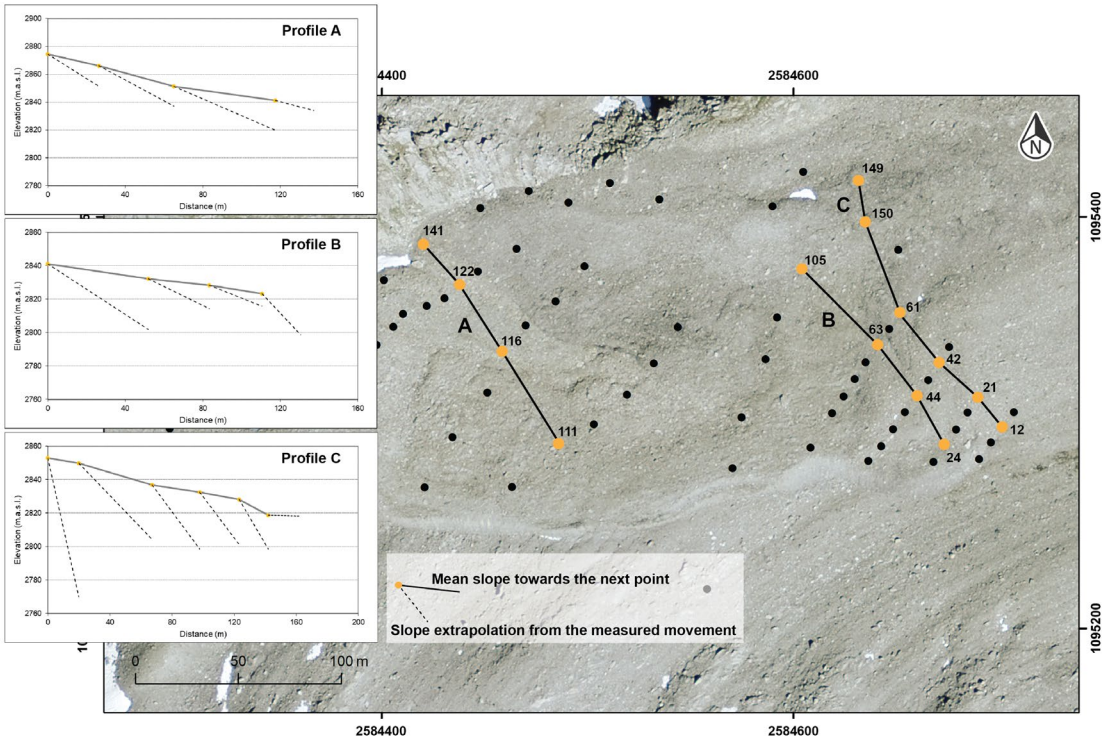

Figure 49: Comparison between estimated topographical slope and movement of single blocks along selected longitudinal profiles on the Aget site (modified after Lambiel and Delaloye, 2004).

Contribution of ice melt to surface elevation changes

Eighteen points were selected (Figure 50) – including six points (Ag-023, Ag-024, Ag-137, Ag-139, Ag-148 and Ag-149) that expressed an important slope angle anomaly[2] combined with **almost no** (or very little) **horizontal surface displacement yet significant vertical displacement** – to gain a better understanding of the processes involved in the loss in surface elevation observed on the push-moraine. Therefore, to assess the **extent to which ice melt contributes to the vertical displacement**, the contribution of the flow pattern to the point's position has to be taken into account. Hence, the estimated theoretical vertical position (which considers extension and compression flow patterns) was compared to the measured absolute vertical displacement (Table 5).

[2] The difference between the topographical slope angle and the point's displacement slope angle.

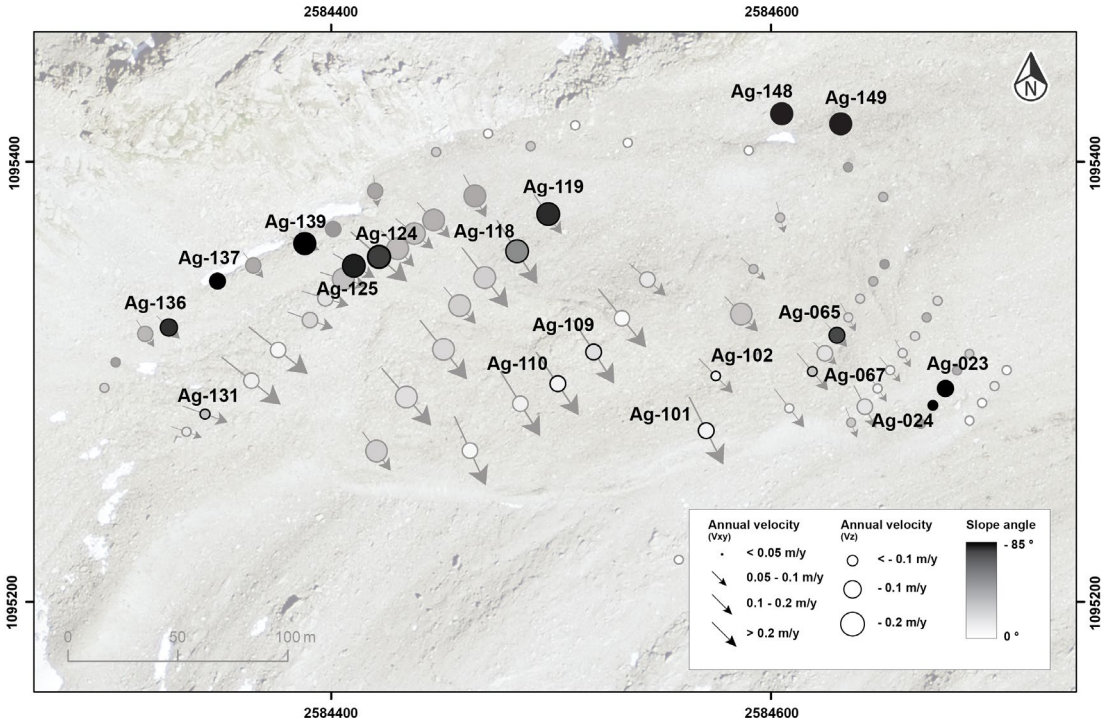

Figure 50: Horizontal and vertical surface displacements for selected points.

The results obtained from the comparison between the estimated theoretical vertical position and the absolute vertical position of the selected points (blocks) reveal that **for most of the selected points, ice melt contributes to the loss of surface elevation**. However, the extent to which ice melt contributes to surface lowering varies throughout the push-moraine. The vertical change in elevation of the points **Ag-023** and **Ag-024** located in the front of the push-moraine, where a concentrated compressive flow (-5% to -12%) is observed, is explained by thawing frozen sediments. Subsidence driven by ice melt contributes to **100%** and **93%** of the total surface elevation loss of the points **Ag-148** and **Ag-149** located in the margins of the push-moraine, expressed by a mean elevation loss of **-0.12 and -0.11 m/y**, respectively. The **loss in elevation** of point **Ag-065** due to **thawing of permafrost** account for **76%** of its total vertical loss. However, the mean vertical change driven by ice melt is **slower** (-0.04 m/y) than the above-mentioned points. A similar behaviour could be expected for its neighbouring point, **Ag-067**, yet the value obtained regarding the contribution of ice melt to surface lowering is of **22%**. Considering the displacement slope angle of the point Ag-067 and the topographical slope angle, it can be inferred that **the loss of surface elevation is mainly due to the downslope trajectory of the point**.

A **surface lowering of -0.05 m/y driven by ice melt** was estimated for points **Ag-118** and **Ag-119**, which accounts for respectively **37%** and **33%** of the total loss in elevation. For these two points, the **extension flow pattern** is a factor that has an important contribution to the vertical changes as an extension of **+3% to +5%** of the moving mass has been estimated (over a 17-year period), which generated a surface lowering of **-1.43 meters** and **-1.54 meters**, respectively. The points **Ag-124** and **Ag-125** are also located in a zone in which the **extension of the moving mass contributes significantly to the elevation change** observed, especially for point Ag-125 ice melt contributes to roughly **5%** of the decrease in surface elevation, which can be considered as negligible. Whereas for point Ag-124, the elevation loss due to thawing ground ice is estimated at **-0.06 m/y**, which accounts for **28%** of the total elevation loss. Point **Ag-102** has subsided **-0.62 meters** over a 17-year period. According to the estimated values, **26%** of this surface elevation change seems to have been caused by ice melt.

The elevation loss of eight of the selected points (Ag-101, Ag-109, Ag-110, Ag-125, Ag-131, Ag-136, Ag-137 and Ag-139) do not seem to be affected by a subsidence process, as the values expressing the extent to which ice melt contributes to the latter range between 0% and 5%. The downslope displacement and the extension flow pattern of the moving mass explain the elevation change of these points, as it induces a geometric thinning.

Table 5 : Parameters contributing to the estimation of the contribution of ice melt to vertical displacement.

Point ID	Displacement slope angle (°)	Topographical slope angle (°)	Slope angle anomaly (°)	Absolute vertical displacement to origin (m)	Absolute horizontal displacement to origin (m)	Theoretical vertical position without considering ext./comp. (m)	Contribution of extension/compression to the vertical position (m)	Theoretical vertical position considering ext./comp. (m)	Total contribution of ice melt for vertical displacement (m)	Annual contribution of ice melt for vertical displacement (m/y)	Contribution of ice melt to vertical displacement (%)
Ag-023	-60	-18	-42	-0.82	0.48	-0.16	0.5[1]	0.34	-1.16	-0.07	129.76
Ag-024	-68	-12	-56	-0.55	0.22	-0.05	0.5[1]	0.45	-1.00	-0.06	164.23
Ag-137	-55	-11	-44	-0.83	0.58	-0.11	-0.75[2]	-0.86	0.00	0.00	0.00
Ag-139	-59	-19	-40	-1.65	0.99	-0.34	-1.4[2]	-1.74	0.00	0.00	0.00
Ag-148	-73	-14	-58	-1.88	0.59	-0.15	0.15[1]	0.00	-1.88	**-0.12**	100.15
Ag-149	-85	-9	-76	-1.89	0.18	-0.03	0.1[1]	0.07	-1.96	**-0.11**	92.67
Ag-065	-23	-9	-14	-0.76	1.78	-0.28	0.1[1]	-0.18	-0.57	-0.04	75.74
Ag-067	-20	-18	-2	-0.76	2.11	-0.70	0.1[1]	-0.60	-0.16	-0.01	21.60
Ag-101	-17	-14	-3	-1.33	4.49	-1.12	-0.2[1]	-1.32	-0.01	0.00	0.96
Ag-102	-11	-3	-8	-0.62	3.12	-0.16	-0.3[1]	-0.46	-0.16	-0.01	26.29
Ag-109	-19	-13	-6	-1.38	4.05	-0.93	-0.4[2]	-1.33	-0.05	0.00	3.86
Ag-110	-16	-15	-1	-1.09	3.75	-1.01	-0.4[2]	-1.41	0.00	0.00	0.00
Ag-118	-33	-13	-20	-2.29	3.52	-0.83	-0.6[2]	-1.43	-0.85	-0.05	37.36
Ag-119	-49	-15	-34	-2.30	1.99	-0.54	-1[2]	-1.54	-0.76	-0.05	33.12
Ag-124	-45	-25	-20	-3.21	3.23	-1.53	-0.6[2]	-2.13	-1.08	-0.06	27.50
Ag-125	-51	-33	-18	-3.27	2.68	-1.71	-1.4[2]	-3.11	-0.16	-0.01	4.78
Ag-131	-23	-18	-5	-0.72	1.70	-0.55	-0.4[2]	-0.95	0.00	0.00	0.00
Ag-136	-46	-27	-20	-1.54	1.48	-0.74	-0.8[2]	-1.54	0.00	0.00	0.00
10 m thick layer[1] and 20 m thick layer[2]											

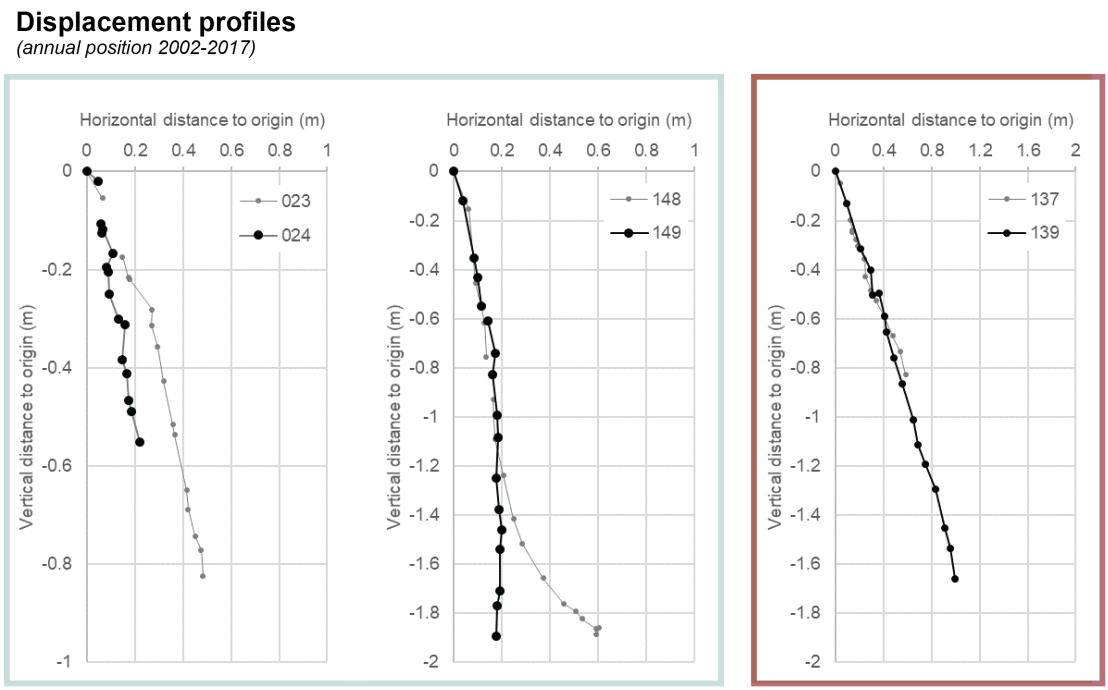

Figure 51: Displacement profiles (annual position 2002-2017) for points Ag-023 and Ag-024, Ag-148 and Ag-149 and, Ag-137 and Ag-139 showing a significant vertical displacement.

Although the displacement profiles of the points presented in Figure 51 express a similar kinematic behaviour, it has been shown by the values obtained in Table 5 that the vertical displacement of these points are caused by different processes. The higher conductivity of the frozen sediments in the margins of the push-moraine infer that permafrost is in a degraded thermal state, allowing efficient ice melt. The melting of ground ice at the permafrost table induced the subsidence of the ground surface elevation (Lugon et *al*., 2004). The **volume loss due to melting underlying ground ice** is well illustrated by the displacement profile of point **Ag-148**, as no movement occurred for the last three years, implying a complete degradation of permafrost. The displacement profile of point **Ag-149** and the terrain's morphology (Figure 52) show signs of subsidence, however, the degradation of ground ice does not appear to be complete, which also seems to be the case for points **Ag-023** and **Ag-024**.

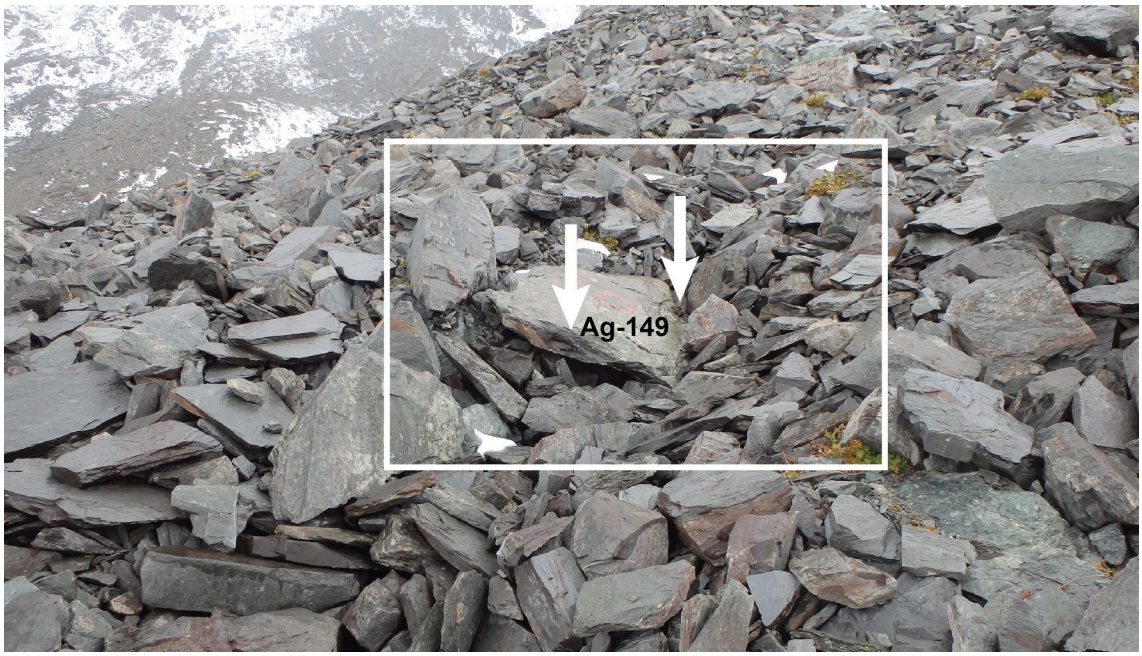

Figure 52: Subsidence of the ground surface represented by block Ag-149 (October 7 2018).

The significant vertical change of points **Ag-137** and **Ag-139** is essentially due to an **important extension flow pattern** of the zone in which these two points are located. “Besides inducing a geometric thinning of the moving mass, extending flow is usually assumed to cause melting processes in the active layer: a thinning of the covering materials occurs, which leads to a **deepening of the permafrost table as a thermal response**” (Haeberli and Vonder Mühll, 1996 in Lambiel and Delaloye, 2004: 239). In this case, the thermal response to the thinning of the moving mass is expressed by decreased resistivity values.

4.2.3 Thermal influence on ground surface changes

Displacement profiles established for each monitored point show that the annual displacement rate is not always constant (Figure 53) which could partly imply the influence of thermally driven processes occurring at the permafrost table. Therefore, it can be inferred that **when temperatures are warmer a more important loss in surface elevation** due to subsidence (ice melt) or downslope displacement (increased creep velocities) should be observed.

Displacement profiles

(annual position 2002-2017)

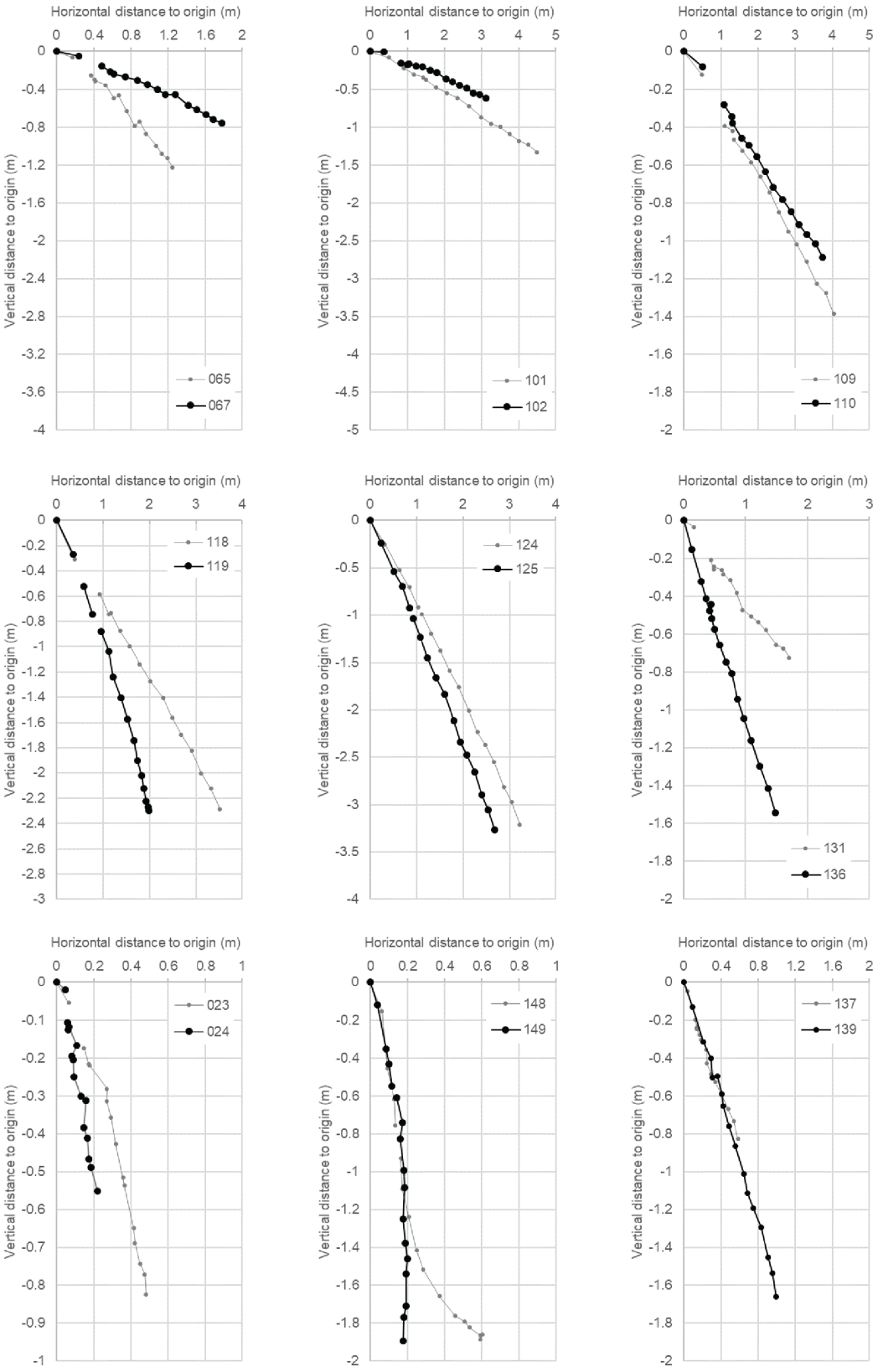

Figure 53: Displacement profiles (annual position 2002-2017) for all selected points.

To assess the extent to which ground surface temperatures contribute to the vertical displacement rate of the selected points, the annual ground thawing index[3] (GTI) was plotted against the annual vertical displacement. The GTI of seven different locations on the push-moraine was obtained. This allowed the attribution of an approximate index for the different zones. The vertical displacement rate values of each point was compared to the GTI measured by the temperature logger station located closest to the point.

As illustrated by Figure 54 and Figure 55, the relationship between vertical displacement and the GTI varied, but was generally weak. Only four of the eighteen analysed points showed a relatively good linear relation with R^2 ranging between 0.7 and 0.9. Whereas, for the rest of the points, weak or no relationship was observed. Indeed, scatter was shown in the majority of the relations. This is likely due to the singularity and heterogeneity of each of the site-specific parameters influencing the behaviour of each block, but also to the site-specific topo-climatic conditions of the location of each temperature monitoring site. Indeed, the variability of GTI is high as it is greatly influenced by variable ground surface conditions. The examples demonstrate that the kinematic response of each block to the ground thermal regime differs from one another, which is likely due to the site-specific conditions of each point.

[3] The cumulative number of degree-days above 0°C for a given time period.

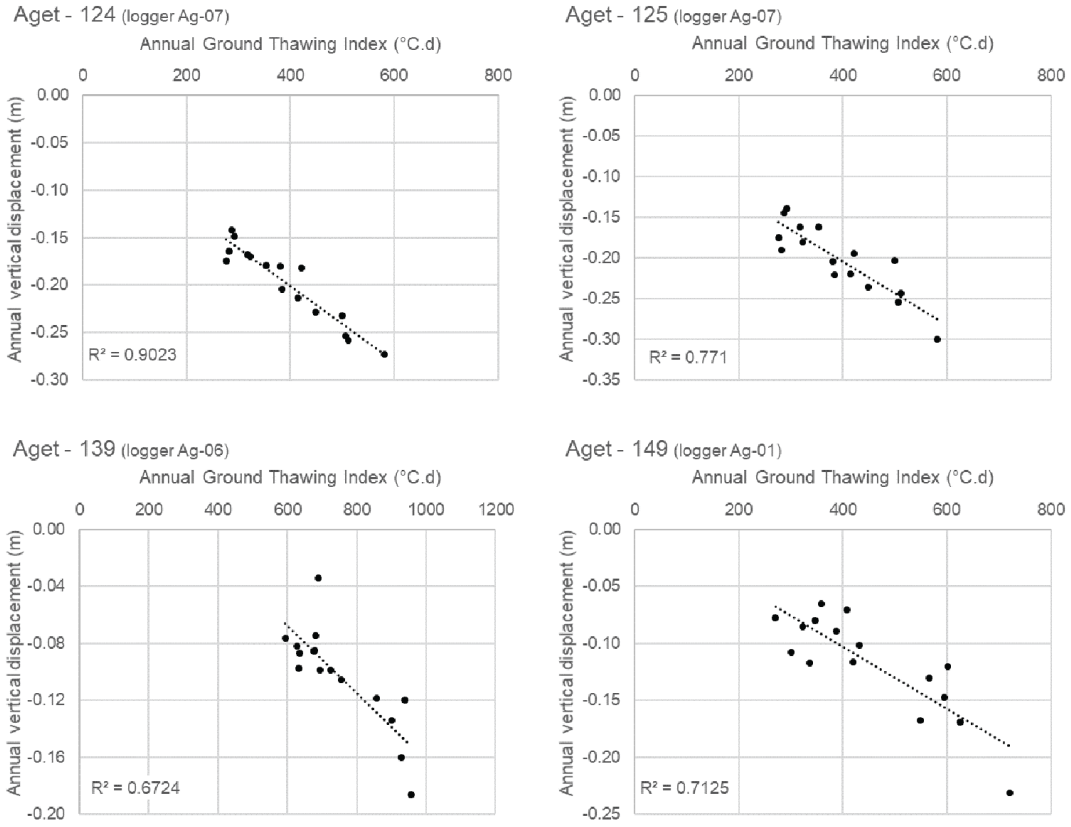

Figure 54: Relationship between the annual GTI and the annual vertical displacement rate expressed by a relatively good R^2.

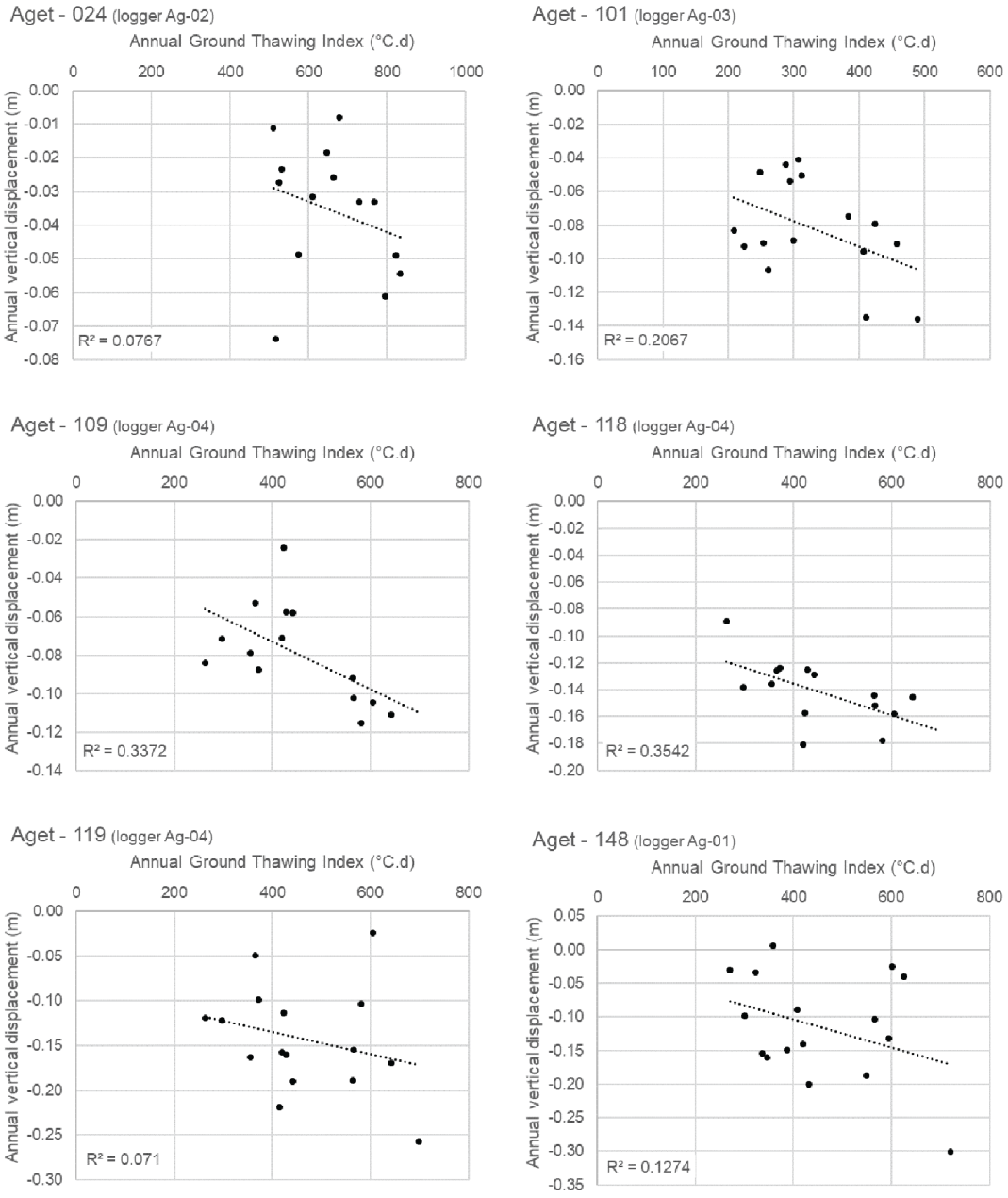

Figure 55: Weak relationship between the annual GTI and the annual vertical displacement expressed by a poor R^2.

4.3 Synthesis

Considering the resistivity changes observed throughout the push-moraine an **overall thermal degradation** can be attested. VES surveys showed stronger decreases in resistivity values were observed in some parts of the push-moraine. Indeed, thawing of permafrost was indeed expressed in the margins through the subsidence of the ground surface in zones where a gain in elevation was expected due to the compressive flow pattern. Extensive flow patterns were concentrated in the steeper zones of the push-moraine (upper and central parts) and contributed to surface elevation in these areas (e.g. point Ag-137 and Ag-139). Indeed, extension flow contributes to the geometrical thinning of the moving mass, which favours the thermal degradation of underlying ground ice. Resistivity changes and the kinematic behaviour of the push-moraine both express the occurrence of **mass-wasting processes**.

5 Discussion

This chapter proposes to discuss the main findings of this study and their interpretation. The presentation of the current state of ground ice in the Aget glacier forefield (5.1) will be followed by a discussion on the evolution of ground ice from 1998 to 2017 (5.2), and by a section assessing the influence of the latter on the dynamics of the push-moraine (5.3).

5.1 Current state of ground ice in the Aget glacier forefield

The analysis of the geoelectrical profiles and geomorphological indicators enabled the definition and characterization of the spatial distribution and the current state of ground ice within the Aget glacier forefield. Indeed, the resistivity values obtained during the 2017 field campaign allowed to highlight a heterogeneous distribution of ground ice throughout the glacier forefield and to assess its thermal state.

The distribution of ground ice within the Aget glacier forefield is **sparse** and **concentrated in its lateral margin**. Such distribution has also been observed in other glacier forefield systems such as the Becca d'Agè and the La Chaux glacier forefields in the Bagnes valley, the Creux de la Lé glacier forefield north of the Rhone valley, and the Muragl glacier forefield in Upper-Engadine (Reynard et *al*., 2003; Delaloye, 2004; Kneisel et *al*., 2000). This configuration of ground ice distribution is largely due to glacier fluctuations throughout the Holocene, which contributed to the development and evolution of the sedimentary cover of the glacier forefield. However, the main features observed today are essentially results of the impact of the dynamics and thermal regime of the Aget glacier during the LIA.

Geomorphological indicators characterized the south-eastern zone of the glacier forefield as deprived of ground ice. Indeed, the presence of fluted moraines suggests that the glacier was temperate at its base, as they indicate the flow direction of the glacier induced by basal sliding. Hence, the presence of water between the glacier's base and the ground surface, as well as geothermal heat flux would have contributed to the thawing pre-existing frozen sediments.

The morphology of the north-western margin of the glacier forefield is characterized by the combined results obtained regarding glacial and periglacial processes. According to the observations made, during its LIA advance, the Aget glacier displaced pre-existing frozen sediments towards the margins of its forefield, forming a push-moraine complex consisting of an actively back-creeping push-moraine (A) and a fossil push-moraine (B). The interstitial ice found in the actively back-creeping push-moraine suggests that the LIA glacier was **cold in its margins**, which allowed the **displacement of frozen sediments** and the **preservation of their thermal state**. The spatial distribution of permafrost implies that the glacier was polythermal, which is a common thermal state for small glacier within the belt of discontinuous permafrost (Etzelmüller and Hagen, 2005; Bosson et *al*., 2014). According to Gilbert et *al.* (2012), the presence of cold ice in the glacier's ablation zone is essentially due to the absence of snow at the glacier's surface; therefore, the meltwater cannot be trapped and is directly evacuated by surface runoff, which hinders the release of latent heat by refreezing. Whereas in the accumulation zone, meltwater is trapped in the snow/firn layer and latent heat is released when it refreezes, warming the glacier.

5.2 Evolution of ground ice from 1998 to 2017

The repetition of both vertical electrical soundings and Wenner profiles allowed the assessment of the evolution of ground ice in the Aget glacier forefield over a period of almost two decades, which is rare in the permafrost literature. Overall, all apparent resistivity profiles revealed similar structures, but a significant decrease of resistivity values has been systematically observed where permafrost conditions were present in 1998, implying its degradation. The **increased conductivity** of the frozen ground measured in 2017 infers a warmer state of ground ice, which suggests a **decrease of the relative ice-water content ratio**. Moreover, the combination of a MAGST of 0.6°C measured on the Aget push-moraine and a warming trend of GST of +0.14°C per decade sets favourable conditions for the thermal degradation of ground ice. Due to the complementarity of resistivity and temperature, the combined analysis of the latter would provide interesting information regarding the evolution of the thermal state of ground ice (measured at larger depths).

The decrease of resistivity generates changes of the properties of ground ice, which can be expressed by thermo-mechanical adjustments, such as thaw settlement. The

latter is likely to be observed in (over)saturated permafrost conditions, when the ice content exceeds the ice-free porosity of the granular material. Consequently, the ice volume loss would contribute to the surface volume loss, causing a geometrical adjustment (subsidence). Whereas in subsaturated permafrost conditions, the ice volume loss is less and/or sometimes not perceived as the ice content does not exceed the pore space. The loss in surface elevation of points located in zones of compressive flow, markedly expressed subsidence driven by ice melt, explained by an advanced and ongoing thermal degradation of ground ice. Indeed, the kinematic behaviour combined with the resistivity change observed in the margins of the push-moraine A (points Ag-023, Ag-024, Ag-148 and Ag-149) clearly expose the occurrence of thawing of an (over)saturated frozen layer whose thermal state ((semi)temperate) measured in 1998 inferred conditions favourable for degradation.

Moreover, the resistivity values obtained from the VES allowed the identification of the thickening of the active layer, and consequently a deepening of the permafrost table. Increased conductivity at greater depths suggests an increase of water content within the frozen layer, as illustrated by Figure 56.

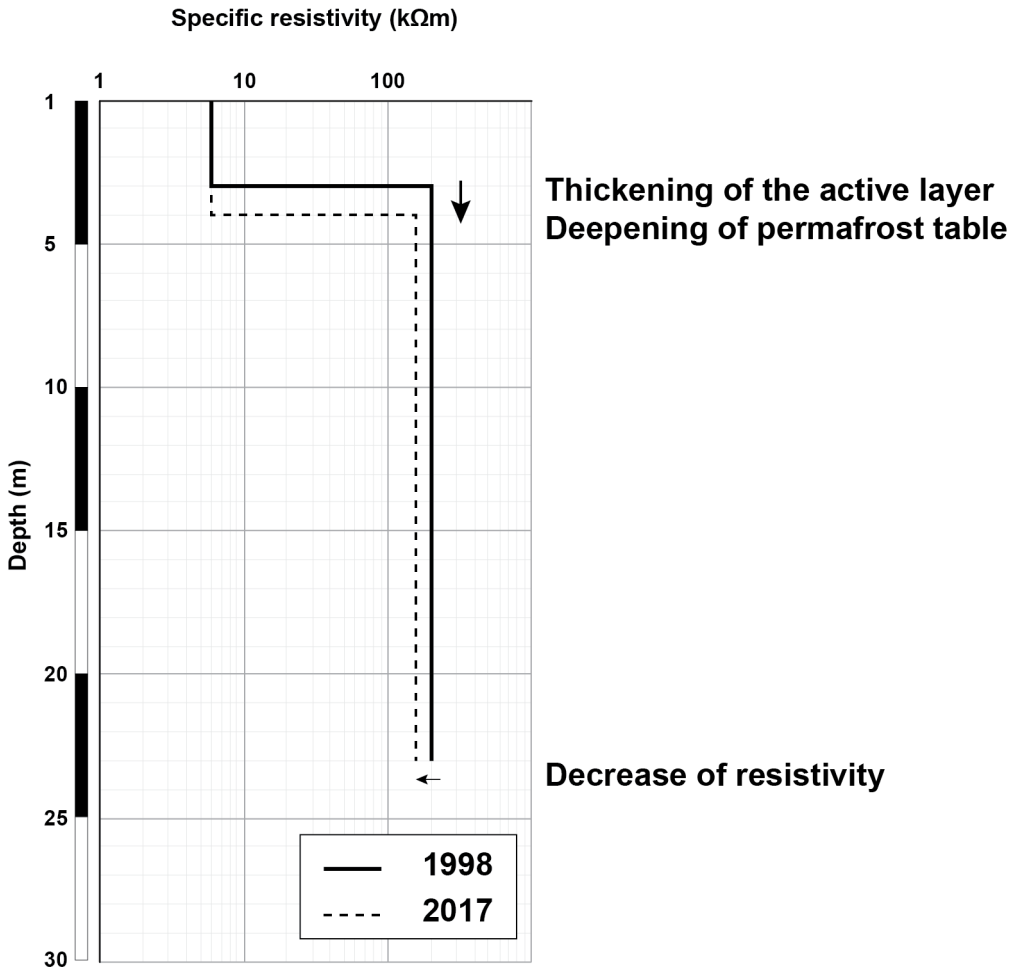

Figure 56: Thickening of the active layer and the deepening of the permafrost table due to a decrease in resistivity between 1998 and 2017 (sounding Ag-S08).

The suggested increase in water content in the frozen layers of the push-moraine can be considered as a direct consequence of ground ice degradation, which is expressed by a decrease in apparent resistivity values ranging between **-7.5% to -34%** from 1998 to 2017. The section of the push-moraine whose apparent resistivity has decreased the most (profile Ag-S07) corresponds to areas where an important subsidence has been observed, **reflecting a significant melt of the underlying ground ice**. The smaller changes in apparent resistivity values (-7.5% for Ag-S08) can be explained by an initially thick, (over)saturated and very resistive frozen layer, hindering important ice melt and water to be stored in pores.

As exposed previously, the ground surface thermal regime of the Aget push-moraine is currently undergoing an increase in temperatures. This warming trend does not impact the push-moraine's ground ice thermal state uniformly, as revealed by the results

obtained from geoelectrical surveys. This is due to the occurrence of the **large variability of permafrost properties within the push-moraine**. Consequently, the response of ground ice to thermal changes is greatly dependent of its intrinsic properties.

Through the geoelectrical monitoring of different high-mountain permafrost sites, Mollaret et *al*. (in prep.) revealed a large variability of permafrost conditions in the Swiss Alps (Figure 57) ranging from fine-grained surface debris layer and weathered bedrock at Schilthorn (SCH) to massive ice in a coarse-blocky crystalline rock glacier at Murtèl-Corvatsch (MCO). The response of each of the monitored sites to the ongoing warming trend in mountainous regions varies as a function of their site-specific properties, as shown by Figure 58. Indeed, it has been demonstrated in terms of change in resistivity that the evolution of permafrost is highly dependent of site-specific conditions.

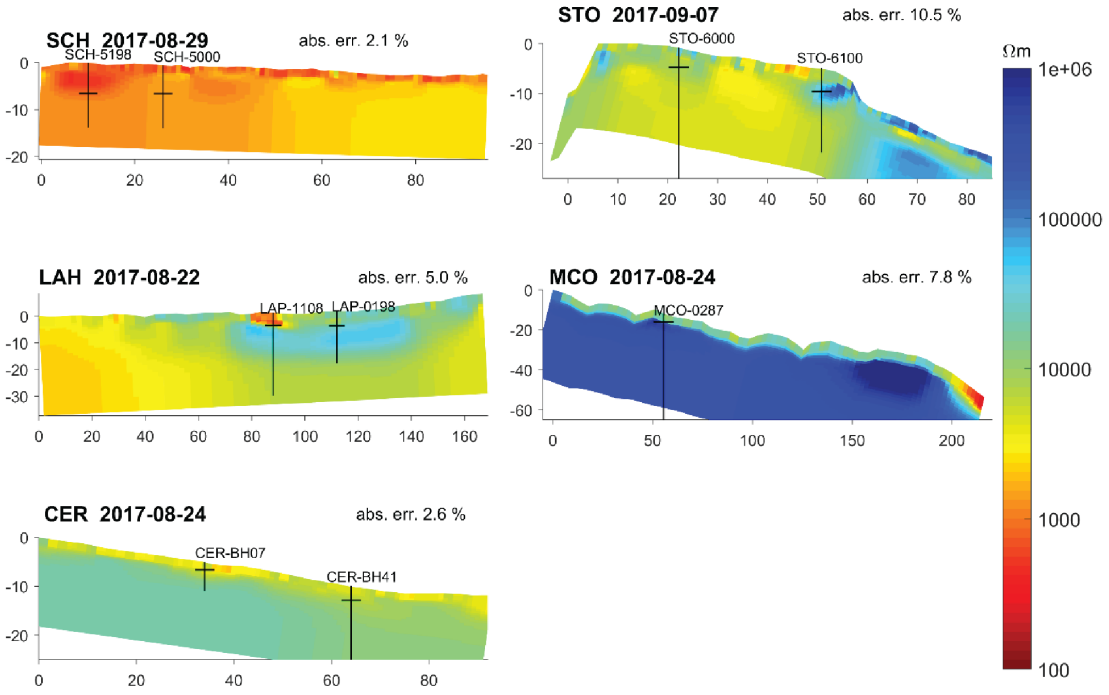

Figure 57: Representative end-of-summer tomograms for each site (modified after Mollaret et *al*., in prep).

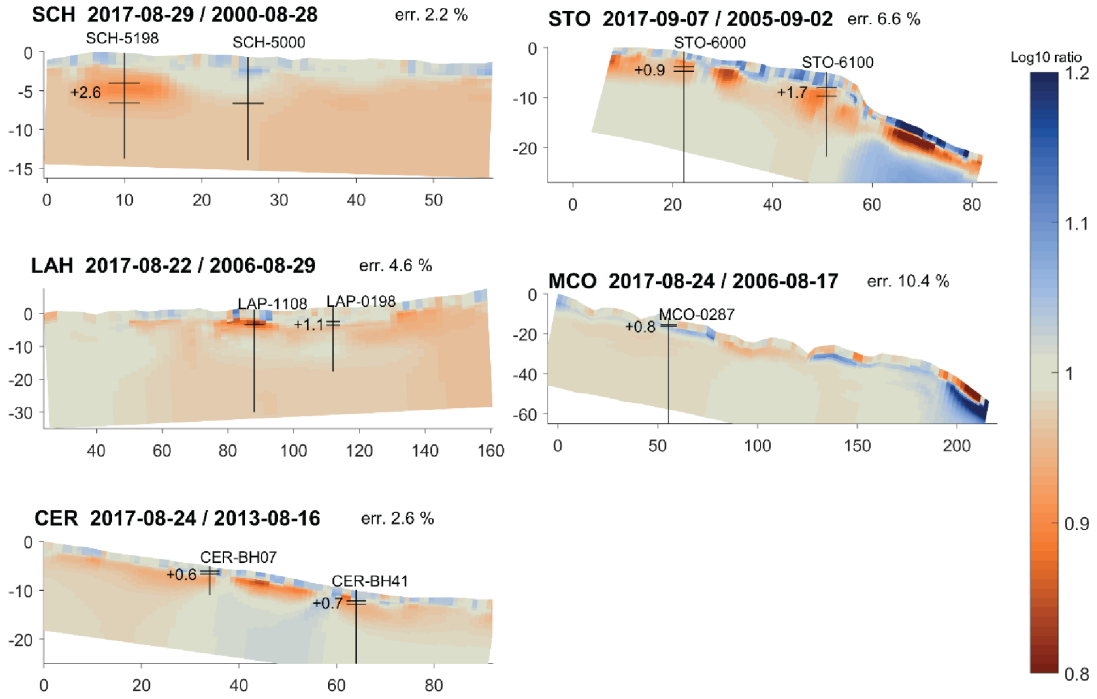

Figure 58: Resistivity change tomograms showing the longest term resistivity change for comparable dates at the end of summer in the first and last year of the time series for each site (modified after Mollaret et *al.*, in prep.).

Amongst all sites, a marked decrease in resistivity occurs at Schilthorn (SCH) and Lapires (LAH). The recorded borehole temperature at 10-meter depth display negative temperatures close to the melting point (Mollaret et *al.*, in prep.), which implies (semi)temperate permafrost conditions, consequently favouring permafrost thermal degradation. Similar results of resistivity change were observed for most geoelectrical surveys carried out on the Aget push-moraine, except for Ag-S08 that expressed a behaviour comparable to Murtèl-Corvatsch (MCO). Indeed, only a small decrease of resistivity values was expected considering the initially high resistivity of the ice-rich and cold permafrost layer measured at Ag-S08 and MCO.

Moreover, in the scope of a parallel project, geoelectrical investigations have been carried out in the Creux de la Lé LIA glacier forefield, north of the Rhone valley. The data obtained yielded similar values of resistivity changes for the same time-period (Figure 59), implying a thermal degradation of permafrost.

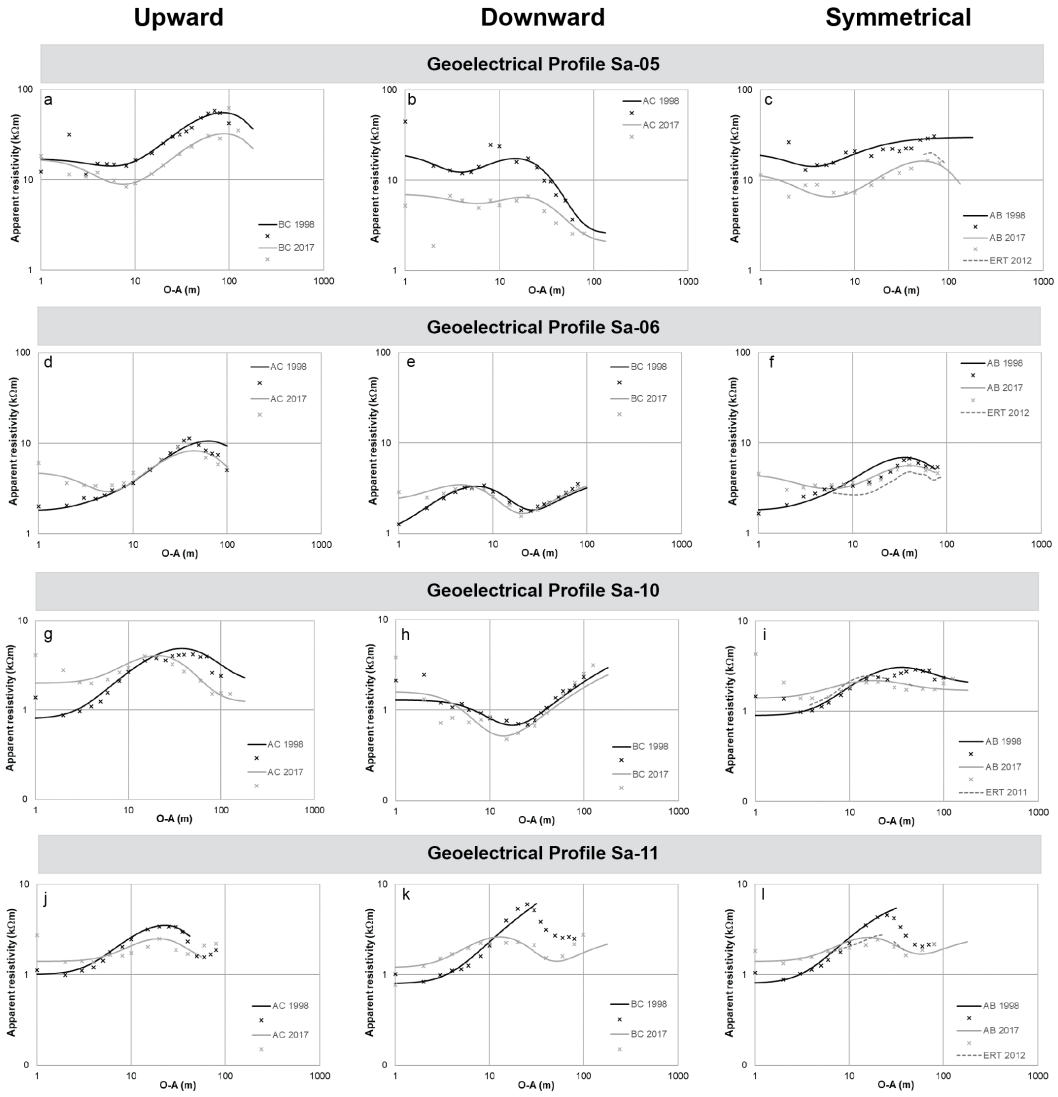

Figure 59: Comparison between resistivity profiles from the 1998 VES (black curve) and the resistivity profiles from the 2017 VES (grey curve).

5.3 Dynamics and response of the Aget push-moraine to the thermal degradation of permafrost

Glacier forefields have been characterized as **transient systems** pursuing a state of equilibrium by adjusting to non-glacial conditions (Lane et *al.*, 2016 in Carrivick and Heckmann, 2017; Figure 60). In this context, temporality is a component that is strongly linked to spatial scale, as the intensity of geomorphic processes (adjustment) of proglacial systems is conditioned by the environment in which they occur (Carrivick and

Heckmann, 2017). Bosson et *al*. (2014) stressed that glacier forefields that lie within the belt of discontinuous permafrost and that have been deglaciated since the end of the LIA are subject to **intense geomorphological activity**, especially under the current conditions of a warming climate. Such transient systems set a stage for highly dynamic paraglacial and periglacial processes, in sight of a state of equilibrium.

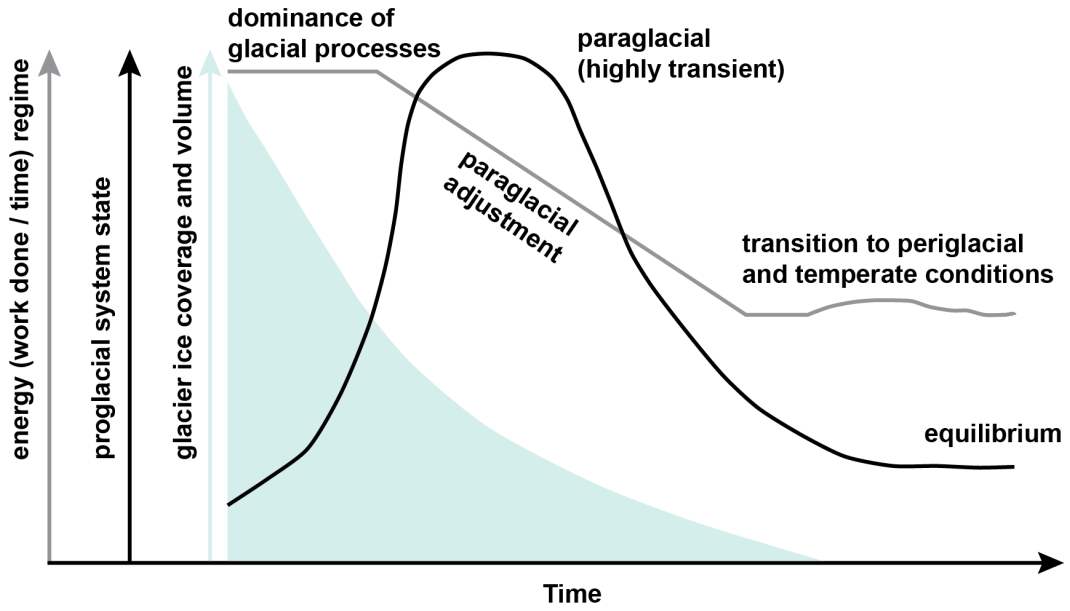

Figure 60: Conceptual model of a proglacial system transition from domination by glacial processes, through a paraglacial period towards a periglacial and ultimately a temperature landscape (modified after Carrivick and Heckmann, 2017).

Until 2009, the kinematic behaviour of the Aget push-moraine followed the regional trend of accelerating surface velocities. Since then, a clear deceleration of surface velocities has been observed. This shift in dynamics could reflect the intensity of the adjustment of the push-moraine within its proglacial systems. Indeed, the actual kinematic behaviour of the Ager push-moraine expresses a state of near-stabilisation and suggests that it has reached and surpasses its peak activity, and is now entering new processes.

In such systems, the rate of geomorphological processes and changes are largely dependent of the ground surface temperatures, the thermal state of ground ice and the topographical setting. The topo-climatic conditions found at Aget reflect a transition stage approaching periglacial and temperate conditions (Figure 60), which are in turn expressed by the degraded thermal state of ground ice and decelerating surface

velocities. Indeed, the latter reflect “a common thermo-hydro-mechanical reaction to changes of the surface energy balance” (Staub et *al*., 2016: 96).

As the warming of ground ice induces a decrease of the relative ice to water content ratio, which favours internal creep deformation, an acceleration of the moving mass should be expected, as illustrated by Figure 61 (Staub et *al*., 2016). However, the observations made at Aget, express a reverse reaction to warming permafrost.

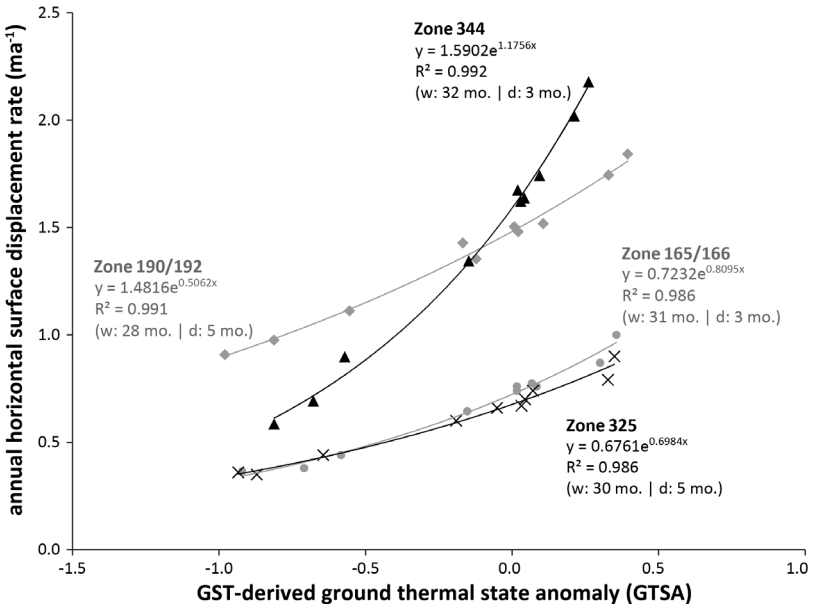

Figure 61: The influence of the ground thermal state on mean annual permafrost creep velocities illustrated using GPS and ground surface temperature (GST) monitoring data from the Becs-de-Bsson rock glacier in the Valais Alps measured between 2004 and 2014 (Staub et *al*., 2016).

Due to the highly heterogeneous and complex distribution and evolution of ground ice throughout the Aget push-moraine, and to the topographical setting in which the landform evolves, different processes contribute to its decelerating behaviour. Amongst the processes involved in the decelerating dynamic of the push-moraine, the occurrence of geometrically (topography) and thermally induced processes can be observed in its frontal margins. Indeed, the frontal zone of the push-moraine, where displacement rates are the slowest, is advancing towards a flatter topography, gradually braking its displacement rate. Moreover, the decrease in resistivity of this frontal zone expressed by the subsidence of the ground surface attest an advanced state of permafrost degradation. The ongoing thermal degradation of ground ice leads to changes in friction at the shear horizon. Indeed, in advanced states of ice melt, the shear resistance is expected to increase (Staub et *al*., 2016). Ice melt also contributes to the deepening to the active layer which supposedly reduces the water column within

the frozen ground above the shear horizon, causing decelerating creep rates (Figure 62). As mentioned in a previous chapter (5.2) and illustrated by Figure 56, the change in resistivity attest the deepening of the active layer. Therefore, the proposed hypothesis of a reduced water column within the frozen layer causing a negative pore-water pressure could contribute to the gradual decrease of creep rates.

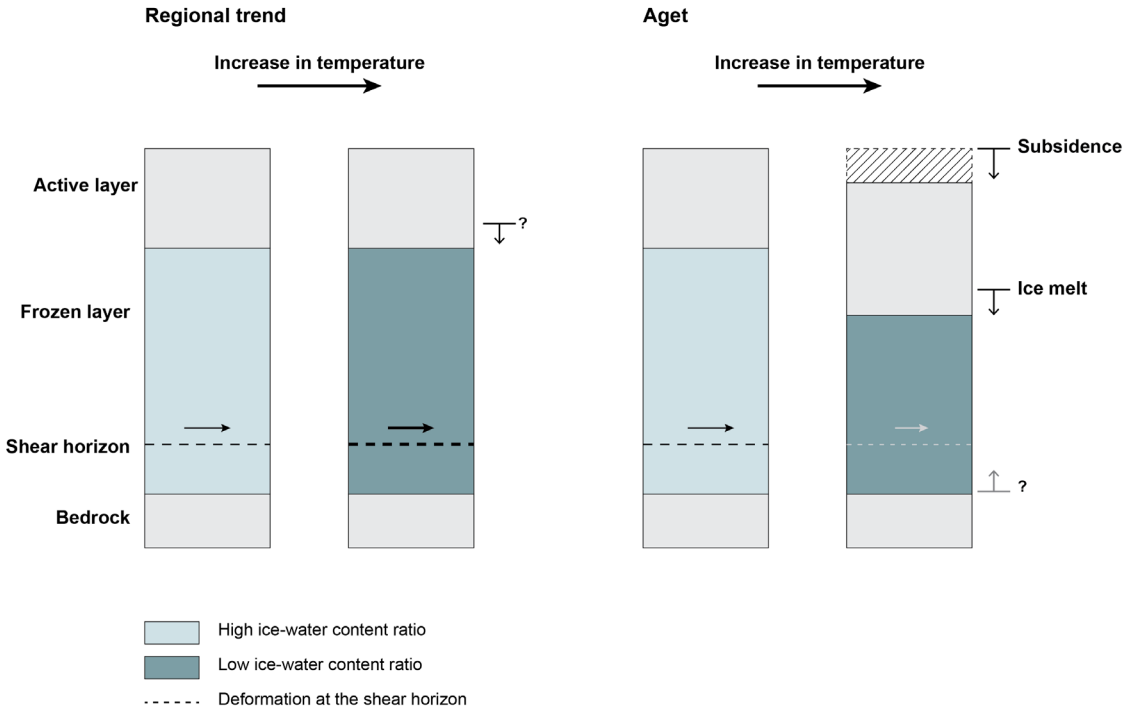

Figure 62: Increase in temperature between T_0 and T_1, which changes in the portion of ground ice and water within creeping landforms. The decrease ice-water content ratio influences the internal structure of frozen landforms, which can alter the pore-water pressure and consecutively the friction at the shear horizon.

Although a decrease in resistivity has been observed in the upper and central parts of the push-moraine, the measured values do not necessarily express an advanced thermal degradation of ground ice (e.g. Ag-S06 and Ag-S08). Therefore, it can be inferred that the kinematic behaviour of this zone of the push-moraine is a response to the strong deceleration of the frontal zone, which brakes the inertia of the mass as a whole. This would imply that the decelerating behaviour of the push-moraine stems from a *cascade reaction* of the upper zone to the frontal zone, which is entering into a flatter topographical setting but also into an advanced state of thermal degradation, both hinder faster creep rates.

6 Conclusion and perspectives

6.1 General conclusion

This study gathers and synthesizes nearly twenty years of research on the Aget glacier forefield, a complex system located within the boundaries of glacier and permafrost interactions. A literature review and the collection of a large dataset provided material with which to improve the knowledge of these systems sitting astride the frontier of one another. The focus of this study is set on the understanding of the evolution of the dynamics of the Aget back-creeping push-moraine, which is a witness of glacier and permafrost interactions.

The data used in this study was collected over a period of twenty years. The **past** and **current** internal structure of the push-moraine was investigated with vertical electrical soundings and Wenner profiles in 1998 and 2017. Surface dynamics are monitored since 2001 (ongoing monitoring) with differential GPS measurements. The joint analysis of repeated geoelectrical measurement and surface displacements highlighted the main processes that control the behaviour of the Aget push-moraine. The comparative analysis of electrical resistivity values asserts a **twenty-year degradation of permafrost**, in response to warmer ground surface temperatures. Furthermore, the verticality of surface displacements observed in the margins of the push-moraine reflects a rapid and advanced downwasting of ground ice, consequently leading to a complete degradation of permafrost. These observations could explain the decelerating behaviour of the push-moraine. However, this relationship is discussable as lower resistivity means higher relative water content favouring faster creep rates. Conversely, the deepening of the active layer has supposedly reduced the water column within the frozen ground above the shear horizon, contributing to lower the creep rate. Moreover, the dynamics of the back-creeping push-moraine is also constrained by its flow pattern, which is not uniformly distributed throughout the moving mass. Indeed, important extensive flow pattern can also explain the strong vertical displacements observed in the upper part of the push-moraine (points Ag-137 and Ag-139), as it contributes to a thinning of the covering material.

The current internal structure of the Aget push-moraine and associated dynamics reflect the complex glacier-permafrost interrelations throughout the Holocene – but particularly the Little Ice Age – where glacial and periglacial processes interacted and succeeded one another, allowing the accumulation and displacement of frozen debris within this glacier forefield. The deglaciation of the glacier forefield illustrate the transition from a glacial to periglacial system, where thermo-morphodynamic readjustments occur as a reaction to changes of the surface energy balance.

6.2 Research perspectives

This study attempted to bring light to the understanding of the behaviour of the Aget push-moraine. However, further development and exploration on this research topic would complete and deepen the knowledge on these complex systems. Being confined between two separate disciplines, such systems have to be studied through a multidisciplinary approach, in order to overcome the barrier between glacial and periglacial research.

Even if the combined analysis of geoelectrical and surface displacement measurements established in the scope of this study brought new elements to the understanding of the dynamics of the push-moraine, further investigations could be developed.

- ***Development of knowledge on the internal structure***: further investigations regarding the repartition of ground ice and its nature would determine the amount of ice and water present in these systems. This would contribute to the understanding of the thermal regime of these systems and their response to a warming climate. The combined use of geophysical methods such as ERT and seismic refraction would bring elements to complete the description of these systems. Moreover, the development of a network of long-term monitoring-sites (Hilbich et *al*., 2008) focused on proglacial systems would contribute to detailed information about the spatio-temporal evolution of permafrost in these complex systems.

- ***Development of knowledge on the kinematic behaviour***: the identification and the understanding of the processes driving the current dynamics of the push-moraine could be enhanced by pursuing field monitoring and by

developing remote monitoring. For instance, terrestrial laser scanning (LiDAR measurements) would generate data to build digital elevation models (DEM), and consequently to quantify surface volume changes. This method would allow detailed surface processes to be captured and linked to sub-surface processes (e.g. ice melt). Interferometric synthetic aperture radar (InSAR) monitoring would be complementary to terrestrial geodetic surveys and would allow a greater spatial coverage of surface movements.

– ***Integration of other systems where similar processes are observed***: to test the hypothesis that intense geomorphic processes induce rapid changes within proglacial systems. Therefore, a comparison of the rates of change *within* proglacial systems to those *beyond* proglacial areas would contribute to the understanding of the temporal component which is strongly influenced by the spatial scale (e.g. climatic and topographic settings) (Carrivick and Heckmann, 2017).

– ***Integration of more study sites***: to improve the knowledge on these systems, similar investigations should be applied to other glacier forefields in periglacial environments (ideally, whose ice content has already been investigated in the past). For example, the glacier forefields of Ritord and Pro, in the Entremont valley, or the complex proglacial system of Tsarmine, in the Hérens valley would be interesting investigation sites. Moreover, potential investigation sites could be detected using InSAR method.

  The development of geoelectrical monitoring combined to geodetic monitoring would provide interesting information regarding the dynamics of glacier forefields. Moreover, as resistivity and temperature datasets are highly complementary, the integration of borehole temperature data in proglacial systems would complete and shed light on certain processes occurring in these systems.

– ***Integration of the study of all the different components found in proglacial systems*** (at a *larger scale*): to assess their internal structure, in order to understand the transience of these complex systems, as well as their reaction to climatic variation and the processes involved (e.g. Bosson and Lambiel, 2016).

7 References

Bhattacharya, P. and Patra. H. (1968). Direct Current Geoelectric Sounding: Principles and Interpretation. Amsterdam, Elsevier.

Berthling, I., Schomacker, A. and Benediktsson, I.-O. (2013). The Glacier and Periglacial Research Frontier: Where from Here?, *in* Schroder, J. (ed) *Treatise on Geomorphology*. San Diego: Academic Press, 8: 479-499.

Bosson, J.-B., Lambiel, C., Deline, P., Bodin, X., Schoeneich, P., Baron, L. and Gardent, M. (2014). The influence of ground ice distribution on geomorphic dynamics since the Little Ice Age in proglacial areas of two cirque glacier systems. *Earth Surface Processes and Landforms*, 40, 666-800.

Bosson, J.-B. (2016). *Internal structure, dynamics and genesis of small debris-covered glacier systems located in alpine permafrost environments*. Thesis, Lausanne, Faculty of Geosciences and Environment, University of Lausanne.

Bosson, J.-B. and Lambiel, C. (2016). Internal Structure and Current Evolution of Very Small Debris-Covered Glacier Systems Located in Alpine Permafrost Environments. *Frontiers in Earth Science*, 4: 1-17.

Carrivick, J. and Hackmann, T. (2017). Short-term geomorphological evolution of proglacial systems. *Geomorphology*, 287: 3-28.

Cuffey, K.M. and Paterson, W.S. (2010). *The physics of glaciers*. Elsevier.

Delaloye, R. and Devaud, G. (2000). La distribution du pergélisol dans les marges proglaciaires des glaciers de Challand, d'Aget et du Sanetschhorn (Valais, Alpes suisses). Hegg, Ch., Vonder Mühll, D. (Hrsg.): *Beiträge zur Geomorphologie. Proceedings der Fachtagung der Schweizerischen Geomorphologischen Gesellschaft vom 8.-10. Juli in Bramois (Kt. Wallis)*. Birmensdorf, Eidgenössischen Forschungsanstalt WSL, 89-96.

Delaloye, R. (2004). *Contribution à l'étude du pergélisol de montagne en zone marginale.* GeoFocus vol. 10, Thesis, Fribourg, Department of Geosciences – Geography, University of Fribourg.

Delaloye, R. and Lambiel, C. (2008) Typology of vertical electrical soundings for permafrost/ground ice investigation in the forefields of small alpine glaciers, *in* Hauck, C. and Kneisel, C. (eds) *Applied Geophysics in Periglacial Environments*. Cambridge, Cambridge University Press: 101-108.

Delaloye, R., Perruchoud, E., Avian, M., Bodin, X., Hausmann, H., Ikeda, A., Kääb, A., Kellerer-Pirklbauer, A., Krainer, K., Lambiel, C., Mihajlovic, D., Staub, B., Roer, I. and Thiebert, E. (2008): Recent interannual variations of rock glacier creep in the European Alps, in *Proceedings of the 9th International Conference on Permafrost,* 29 June – 03 July 2008, Fairbanks, Alaska, pages 343-348.

Devaud, G. (1999). *Etude de la distribution du pergélisol dans les marges proglaciaires. L'exemple des marges proglaciaires des glaciers d'Aget et du Sanetschhorn, VS*. Master thesis, Department of Geosciences – Geography, University of Fribourg

Etzelmüller B. and Hagen, J.-O. (2005). Glacier-permafrost interaction in Arctic and alpine mountain environments with examples from southern Norway and Svalbard, *in* Harris, C. and Murton, J.B. (eds) *Cryospheric systems: Glaciers and Permafrost.* London, The Geological Society, Special Publications, 242: 11-27.

Evin, M. (1992). Les relations existant entre la moraine de refoulement, le glacier rocheux et le glacier du Petit Age Glaciaire dans le Haut Vallon d'Asti (Queyras, Alpes du Sud, France). *Geografia Fisica e Dinamica Quaternaria*, 15: 101-105.

Gilbert, A., Vincent, C., Wagnon, P., Thiebert, E. and Rabatel, A. (2012). The influence of snow cover thickness on the thermal regime of Tête Rousse Glacier (Mont Blanc range, 3200 m a.s.l.): Consequences for outburst flood hazards and glacier response to climate change. *Journal of Geophysical Research*, 117: 1-17.

Haeberli, W. (1979). Holocene Push-Moraines in Alpine Permafrost. *Geografiska Annaler*, 61:43-48.

Haeberli, W., (1981). Ice motion on deformable sediments. *Journal of Glaciology*, 27: 365-366.

Haeberli, W. and Beniston, M. (1998). Climate Change and Its Impacts on Glaciers and Permafrost in the Alps. *Ambio*, 27(4), 258-265.

Haeberli, W. (2005). Investigating glacier-permafrost relationships in high-mountain areas: historical background, selected examples and research needs. *Cryospheric Systems: Glaciers and Permafrost*, 242: 29-37.

Haeberli, W. (2013). Mountain permafrost – research frontiers and a special long-term challenge. *Cold Regions Science and Technology*, 96: 71-76.

Hilbich, C., Hauck, C., Hoelzle, M., Scherler, M., Schudel, L., Völksch, I., Vonder Mühll, D. and Mäusbacher, R. (2008). Monitoring mountain permafrost evolution using electrical resistivity tomography: A 7-year study of seasonal, annual, and long-term variations at Schilthorn, Swiss Alps. *Journal of Geophysysical Research*, 113: 1-12.

Hilger, L. (2017). *Quantification and regionalization of geomorphic processes using spatial models and high-resolution topographic data: A sediment budget of the Upper Kauner Valley, Ötztal Alps*. Thesis, Faculty of Mathematics and Geography, Catholic University of Eichstätt-Ingolstadt.

Hoppe, G. and Schytt, V. (1953). Some Observations on Fluted Moraine Surfaces. *Geografiska Annaler*, 35(2): 105-115.

Huss, M. and Fischer, M. (2016). Sensitivity of Very Small Glaciers in the Swiss Alps to Future Climate Change. *Frontiers in Earth Science*, 4: 1-17.

Ivy-Ochs, I., Kerschner, H., Maisch, M., Christl, M., Kubik, P. and Schlüchter, C. (2009). Latest Pleistocene and Holocene glacier variations in the European Alps. *Quaternary Science Reviews*, 28: 2137-2149.

Kneisel, C. (1998). Occurrence of surface ice and ground ice/permafrost in recently deglaciated glacier forefields, St. Moritz area, eastern Swiss Alps. *Proceedings of the Seventh International Conference on Permafrost,* Yellowknife, Canada: 575-581.

Kneisel, C. (1999). *Permafrost in Gletschervorfeldern. Eine vergleichende Untersuchung in den Ostschweizer Alpen und Nordschweden*. Thesis. Trier, Trierer Geographischen Studien.

Kneisel, C., Haeberli, W. and Baumhauer, R. (2000). Comparison of spatial modelling and field evidence of glacier/permafrost relations in an Alpine permafrost environment. *Annals of Glaciology*, 30: 269-274.

Kneisel, C. (2003). Permafrost in recently deglaciated glacier forefields – measurements and observations in the eastern Swiss Alps and northern Sweden. *Zeitschrift für Geomorphologie*, 47(3): 289-305.

Kneisel, C. and Kääb, A. (2007). Mountain permafrost dynamics within a recently exposed glacier forefield inferred by a combined geomorphological, geophysical and photogrammetrical approach. *Earth Surface Processes and Landforms*, 32: 1797-1810.

Kneisel, C., Hauck, C., Fortier, R. and Moorman, B. (2008). Advances in Geophysical Methods for Permafrost Investigations. *Permafrost and Periglacial Processes*, 19: 157-178.

Lambiel, C. and Delaloye. R. (2004). Contribution of Real-time Kinematic GPS in the Study of Creeping Mountain Permafrost: Examples from the Western Swiss Alps. *Permafrost and Periglacial Processes*, 15:229-241.

Lugon, R., Delaloye, R., Serrano, E., Reynard, E., Lambiel, C. and González-Trueba, J.J. (2004). Permafrost and Little Ice Age Glacier Relationships, Posets Massif, Central Pyrenees, Spain. *Permafrost and Periglacial Processes*, 15: 207-220.

Maisch, M., Haeberli, W., Frauenfelder, R. and Kääb, A. (2003). Lateglacial and Holocene evolution of glaciers and permafrost in the Val Muragl, Upper Engadin, Swiss Alps. *Swets & Zeitlinger*, 717-722.

MétéoSuisse, Office fédéral de météorologie et de climatologie (2018). https://www.meteosuisse.admin.ch/home/climat/le-climat-suisse-en-detail/donnees-homogeneisees-depuis-1864.html?station=gsb [visited on the 02.08.2018].

Mollaret, C., Hilbich, C., Pellet, C., Flores-Orozco, A., Delaloye, R. and Hauck. C. (In prep.). Monitoring of Long-term Mountain Permafrost Degradation using an Electrical Resistivity Tomography Network.

PERMOS. 'Permafrost in Switzerland 2010/2011 to 2013/2014'. Glaciological Report (Permafrost) of the Cryospheric Commission of the Swiss Academy of Sciences. Fribourg, 2016.

Pfeffer, W., Arendt, A., Bliss, A. and Bolch, T. (2014). The Randolph Glacier Inventory: a globally complete inventory of glaciers. *Journal of Glaciology*, 60(221): 537-552.

Reynard, E., Lambiel, C., Delaloye, R., Devaud, G., Baron, L., Chapellier, D., Marescot, L. and Monnet, R. (2003). Glacier/permafrost relationships in forefield of small glaciers (Swiss Alps). *Swets & Zeitlinger*, 947-952.

Reynolds, J. (2011). An Introduction to Applied and Environmental Geophysics. Chichester, Wiley-Blackwell.

Scapozza, C. (2012). *Stratigraphie, morphodynamique, paléoenvironments des terrains sédimentaires à forte déclivité du domaine périglaciaire alpin*. Thesis, Lausanne, Faculty of Geosciences and Environment, University of Lausanne.

Serrano, E. and Martín-Moreno, R. (2018). Surge glaciers during the Little Ice Age in the Pyrenees. *Cuadernos de Investigación Geográfica – Geographical Research Letters*, 44(1): 213-244.

Staub, B. (2015). *The evolution of mountain permafrost in the context of climate change: towards a comprehensive analysis of permafrost monitoring data in the Swiss Alps*. Thesis, Fribourg, Department of Geosciences – Geography, University of Fribourg.

Staub, B.; Lambiel, C. and Delaloye, R. (2016): Rock glacier creep as a thermally-driven phenomenon: a decade of inter-annual observations from the Swiss Alps, *in* Günther, F. and Morgenstern, A. (eds.) *XI. International Conference on Permafrost – Book of Abstracts*, 20–24 June 2016, Potsdam, Germany. Bibliothek Wissenschaftspark Albert Einstein, pages 96–97.

Vonder Mühll, D. (1993). *Geophysikalische Untersuchungen im Permafrost des Oberengadins*. Thesis, Zurich, VAW/ETH Zürich.

Zemp, M. (2006). *Glaciers and climate change: spatio-temporal analysis of glacier fluctuations in the European Alps after 1850*. University of Zurich, Faculty of Science.

Zemp, M., Paul, F., Hoelze, M. and Haeberli, W. (2008). Glacier Fluctuations in the European Alps, 1850–2000. An overview and a spatiotemporal analysis of available data. *Trends in natural landscapes*, 11: 152-167.

8 Appendix

Table 6 : Change in % of the apparent resitivity between 1998 and 2017 of the profile Ag-S07.

		Upward	Downward	Symmetrical
OA (m)		AC (kΩm)	BC (kΩm)	AB (kΩm)
10	1998	5.16	4.30	5.05
	2017	3.63	3.85	3.78
	1998-2017 change (%)	**-29.55**	**-10.59**	**-25.25**
15	1998	6.81	4.92	5.93
	2017	3.98	4.04	4.03
	1998-2017 change (%)	**-41.51**	**-17.88**	**-32.08**
20	1998	8.02	5.27	6.66
	2017	3.60	4.06	3.85
	1998-2017 change (%)	**-55.14**	**-23.01**	**-42.19**
30	1998	6.76	4.86	5.85
	2017	3.98	3.90	3.97
	1998-2017 change (%)	**-41.16**	**-19.59**	**-32.16**
40	1998	6.12	4.49	5.32
	2017	4.04	3.67	3.86
	1998-2017 change (%)	**-34.04**	**-18.20**	**-27.43**
60	1998	5.77	3.68	4.73
	2017	4.71	3.45	4.07
	1998-2017 change (%)	**-18.41**	**-6.11**	**-13.89**
80	1998	5.65	3.45	4.57
	2017	4.67	3.43	4.04
	1998-2017 change (%)	**-17.27**	**-0.67**	**-11.57**

Table 7 : Change in % of the apparent resistivity between 1998 and 2017 of the profile Ag-S09.

		Upward	Downward	Symmetrical
OA (m)		AC (kΩm)	BC (kΩm)	AB (kΩm)
10	1998	7.43	5.17	6.46
	2017	5.58	3.32	4.57
	1998-2017 change (%)	**-24.89**	**-35.73**	**-29.22**
15	1998	9.38	4.46	6.79
	2017	6.84	3.55	5.24
	1998-2017 change (%)	**-27.04**	**-20.39**	**-22.90**
20	1998	10.51	4.98	7.55
	2017	8.26	3.73	6.00
	1998-2017 change (%)	**-21.39**	**-25.02**	**-20.46**
30	1998	7.42	4.50	5.98
	2017	5.84	3.51	4.66
	1998-2017 change (%)	**-21.29**	**-22.00**	**-22.06**
40	1998	4.98	2.35	3.60
	2017	3.91	2.23	3.05
	1998-2017 change (%)	**-21.55**	**-5.04**	**-15.48**
60	1998	2.46	1.62	2.04
	2017	1.98	1.52	1.49
	1998-2017 change (%)	**-19.53**	**-6.29**	**-27.31**

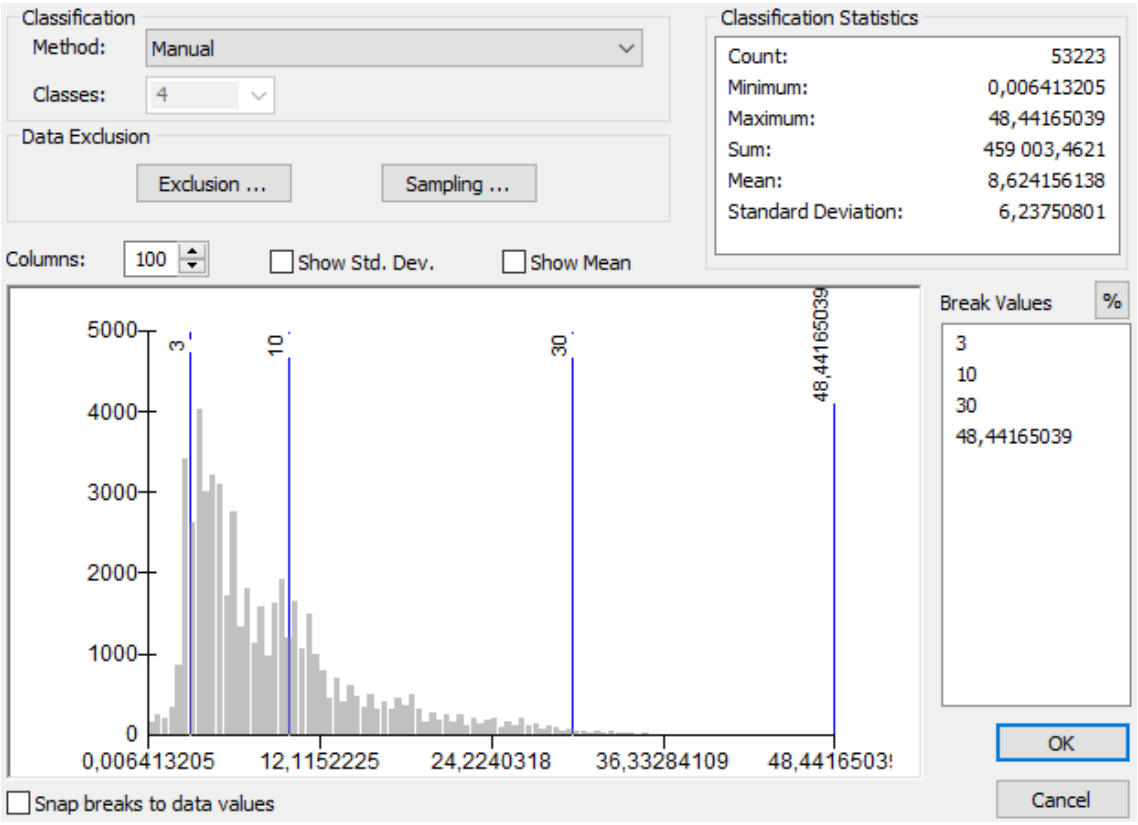

Figure 63 : Distribution of apparent resistivity values